FABRICATION AND APPLICATIONS OF FIBRE BRAGG GRATINGS

KATE SUGDEN

Doctor of Philosophy

THE UNIVERSITY OF ASTON IN BIRMINGHAM

January 1996

THE UNIVERSITY OF ASTON IN BIRMINGHAM

FABRICATION AND APPLICATIONS OF FIBRE BRAGG GRATINGS

Kate Sugden

Doctor of Philosophy

1996

Abstract

This thesis presents details on the fabrication and properties of fibre Bragg gratings, a variety of applications is also demonstrated.

The consequences of fabricating Bragg gratings in various fibres, with or without hydrogen loading, and with varying laser power levels are explored. Three new techniques for fabricating chirped gratings are presented. Beams with dissimilar wavefront curvatures are interfered to give chirped gratings. With the same aim techniques of writing gratings on tapered fibres and on deformed fibres are also covered. With these techniques, a wide variety of gratings has been fabricated from the 'superbroad' (with bandwidths of up to 180nm), small to medium bandwidth gratings with linear chirp profiles and quadratic chirped gratings.

It is demonstrated that chirped grating can be concatenated to form all-fibre Fabry-Perot and Moiré resonators. These are further concatenated with chirped gratings to produce filters with narrow passbands and very broad stopbands.

A number of other applications are also addressed. The use of chirped fibre gratings for dispersion compensation and femtosecond chirped pulse amplification is demonstrated. Chirped gratings are used as dispersive elements in modelocked fibre lasers producing ultrashort pulses. A chirped fibre grating Fabry-Perot transmission filter is used in a continuous wave laser that exhibits eleven simultaneously lasing wavelengths. Finally, the use of grating-coupler devices as variable reflectivity mirrors for laser optimisation and gain clamping is considered.

Key words: Optical fibre; Bragg grating; chirped grating; optical fibre filters; fibre optic resonators.

Acknowledgements

I must particularly acknowledge the help of my supervisor Ian Bennion for his continuous support, encouragement and enthusiasm, and Kevin Byron for helpful discussions and encouragement throughout the work.

I would like to thank Lin Zhang and to John Williams for their help and support. Acknowledgement is due to Graham Town, Martin Fermann, Manfred Ober and Martin Hofer for interesting collaborations, especially in reference to the work contained in Chapter 6. Thanks to Doug Reid for sharing his invaluable experimental experience. I would also like to acknowledge the help of BNR Europe Ltd in supporting my work and providing fibres and equipment.

Lastly, my thanks to Kyla and everyone else who kept me going and inserted the commas.

Contents

Table of Figures

1. Overview

1.1 Introduction

Since the first demonstration of side-written gratings by Meltz *et al*[1] in 1989 there has been a proliferation of studies on fibre Bragg gratings and applications. Fibre Bragg gratings are mirror-like reflectors that are formed in the cores of fibres by inducing a periodic modulation of the refractive index. In the last three years gratings have moved from being a research-based interest into the market place where they command industrial investment and an ever expanding range of possible applications.

One of the proposed applications for the use of fibre gratings is as a possible means of dispersion compensation[2,3] in long haul systems. There are also other applications that have been proposed such as pulse compression[4,5,6], sensors[2,7], noise reduction[8,9] and gain flattening[10] in erbium fibre amplifiers, as high reflectors for tuneable rare earth doped lasers[11,12] and as linewidth narrowing elements in semiconductor lasers[13]. Several of these applications have yet to be demonstrated experimentally and are part of a rapidly expanding and challenging field.

1.2 Fibre Bragg Gratings

When light travelling down a fibre core meets a periodic modulation of the refractive index a narrowband of wavelengths centred around the Bragg resonance wavelength will be reflected. The Bragg resonance wavelength, λ_B, is related to the periodicity of the modulation such that

$$\lambda_B = n_{eff} \Lambda_B$$

Equation 1

where n_{eff} is the effective refractive index of the fibre core and Λ_B is the grating pitch or spacing.

The grating length and the amplitude of the modulation determine the response profile of the grating. Generally, the longer the grating is the narrower the wavelength band that is reflected. Likewise, the higher the modulation of the refractive index modulation the stronger the grating response. This means that the parameters of a grating can be selected to give a variety of responses and the gratings can then be used to replace basic optical components such as mirrors, wavelength filters and partial reflectors. It then becomes possible to use these new grating components to design all-fibre integrated systems that completely avoid the use of bulk optics. This option is ideal for telecommunication, laser and sensor systems where long term, low maintenance operation is required.

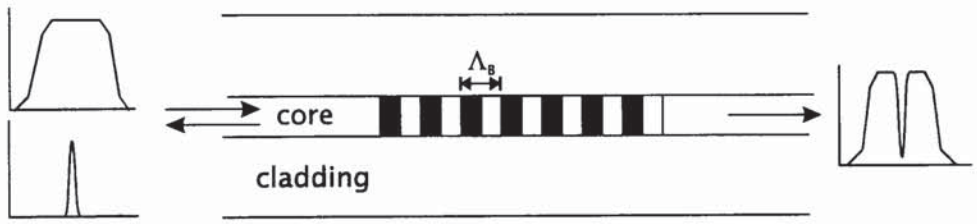

Figure 1-1 Schematic representation of a uniform-period fibre Bragg grating illustrating the transmission and reflection spectrum response.

Bragg gratings are usually defined by the grating pitch (the spacing of the amplitude modulation) or the tilt of the grating planes relative to the fibre axis. Gratings that have a constant pitch and grating planes that are normal to the fibre axis, Figure 1-1, are referred to as *uniform-period* or *linear gratings*. The reflection bandwidth of such gratings is determined by the length of the grating and the strength of the index modulation. Typically these gratings reflect a narrow bandwidth of wavelengths. Consequently they act as good wavelength selection elements that can be used for strain and temperature sensors or as tuning elements for fibre and semiconductor lasers.

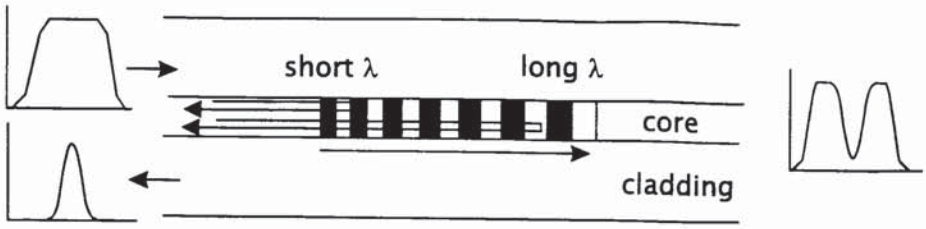

Figure 1-2 Schematic representation of a chirped fibre Bragg grating. A variation in the pitch of the modulated refractive index alters the reflected wavelength as a function of position along the grating.

It is possible to vary the reflected Bragg wavelength along the length of the grating. When this occurs the gratings are known as *chirped* or *aperiodic gratings*. By considering Equation 1 it can be seen that the wavelength reflected can be altered by incorporating a spatial dependence of either the grating period, or the effective refractive index, or both, Equation 2.

$$\lambda_B(z) = n_{eff}(z)\Lambda(z)$$

Equation 2

where z gives the distance along the fibre axis. Introducing chirp increases the reflection bandwidth of a grating by increasing the number of reflected wavelengths. Since it is difficult to vary the effective refractive index by large amounts this is used only to produce relatively small changes in the reflected wavelength whereas changes to the periodicity of the grating can be used to produce small or large changes in the reflected wavelength. Since chirped gratings exhibit a distributed reflection they can be used to impart a dispersion on the reflected wavelengths *i.e.* they introduce a time delay that is frequency dependent. This effect can be used for the dispersion compensation of pulses broadened by chromatic dispersion; for pulse compression; and for modelocking fibre lasers. Chirped gratings with bandwidths of up to 170nm have been demonstrated.

For some applications, where it is desirable that there is no reflection back down the fibre, gratings can be used as loss elements. If the grating planes are tilted, light can be outcoupled into lossy cladding modes and in this case the gratings are called *blazed gratings*. This is illustrated by

Figure 1-3. The tilt of the grating planes and the coupling strength of the grating determine the efficiency of the outcoupling. Blazed gratings have been used to outcouple excess pump laser wavelengths from systems[14] and have also been demonstrated in the gain flattening of erbium amplifiers.

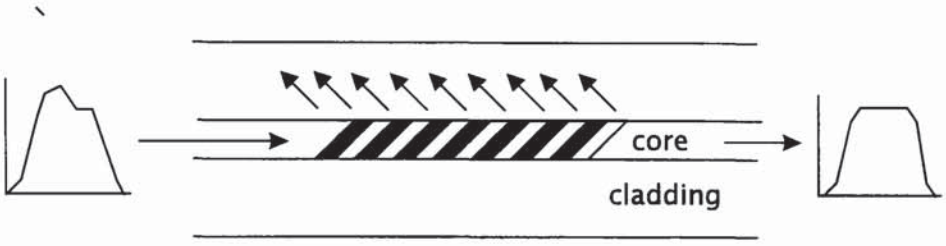

Figure 1-3 Schematic diagram of blazed fibre Bragg grating illustrating the use of radiation outcoupling to flatten an input spectrum.

Gratings are also described by the mechanism by which they are formed. There are three types of grating that are written directly into the fibre core without etching. The gratings that are considered here, known as Type I gratings, are permanently written into the core of the fibre. This is made possible by the fact that certain fibres are photosensitive; they exhibit a change in refractive index which increases (up to a saturation point) with the length of exposure to ultraviolet light.

Type II gratings are sometimes known as *damage gratings*. These structures are usually formed when using high power excimer lasers. The high absorption band of germania in the UV coupled with very high peak powers produces a periodic structure of expansion induced damage. There is a third type of grating which is known as Type IIA. This type of grating has only recently been proposed and may be a misnamed since it appears to have more in common with the properties of Type I gratings. It is thought that these gratings are formed after the fibre has been irradiated in the fabrication of Type I gratings by a similar process involving different colour-centres.

1.3 Historical Perspective

The first work on photorefractive gratings was published by K O Hill *et al*[15,16] in 1978. Long gratings were formed in the core of germanosilicate fibre during an experiment that involved the fibre core being exposed to an interference pattern set up between counter-propagating modes of 488 or 514.5nm radiation from an argon ion laser. This produced what are now known as *Hill gratings*. The exact mechanism behind this effect remains slightly unclear but an interference pattern is set up in the core originating from a Fresnel reflection off the fibre end. This results in a periodic change in the refractive index. Hill gratings can reach lengths of 1m and as a consequence the reflection profile can be very narrow, ~1.5 x 10^{-4}nm. One disadvantage of gratings formed in this way is that the reflected wavelength is tied to the wavelength of the writing source available resulting in very little flexibility. Although this effect caused a lot of interest at the time the subject was not extensively pursued until over a decade later when another method of writing gratings was demonstrated by Meltz *et al*[1] in 1989.

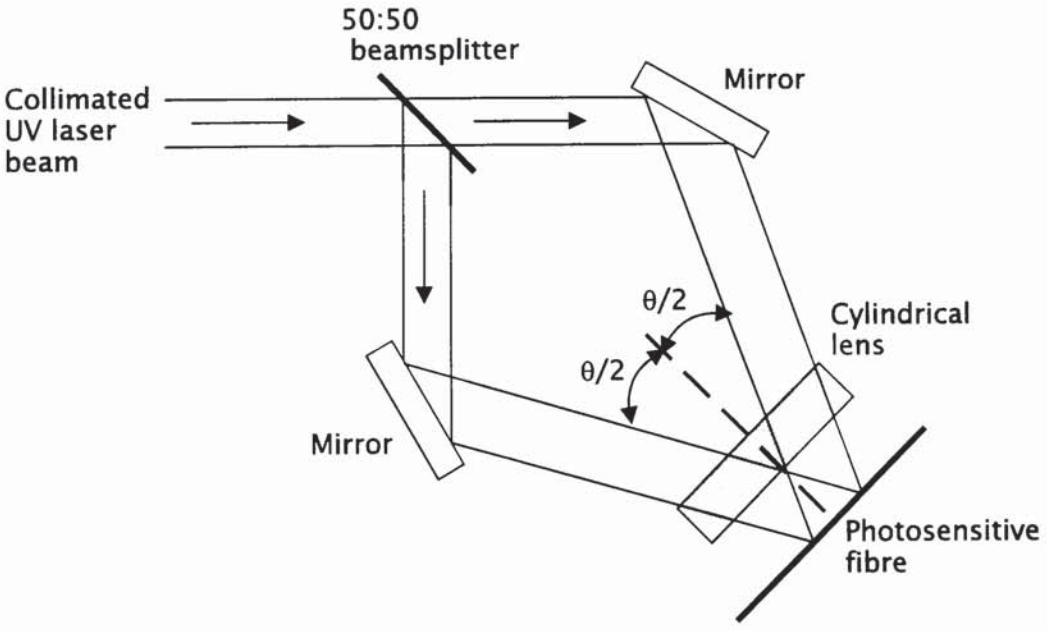

Figure 1-4 Arrangement for transverse two-beam interferometric exposure of a fibre to write uniform-period gratings.

Meltz *et al* used a traditional interferometer which enabled gratings to be side-written into fibres, Figure 1-4. A beamsplitter splits a collimated UV laser beam into two and the resulting beams are directed by mirrors so that they interfere where the fibre is held by a mount. The reflection wavelength of the fabricated grating is selected by changing the angle between the two arms of the interferometer. The interferometer must be highly stable to allow long writing times. This technique forms the basis of the technique used in the work described herein.

Various prism arrangements[17,18,19,20] have been used as an alternative to the kite-shaped interferometer. In the arrangement illustrated in Figure 1-5, where a beam, incident on the hypotenuse face, is internally incident on the apex angle of the prism. Half the beam is reflected from the side face to interfere with the side that was incident on the back face. Since the beam is effectively folded over on itself this arrangement requires a beam that is spatially coherent. The set-up is intrinsically very stable and exposure times of up to eight hours have been reported. Gains over the kite-shaped interferometer in simplicity and stability are made at the cost of losing control and flexibility which becomes more important when fabricating aperiodic gratings.

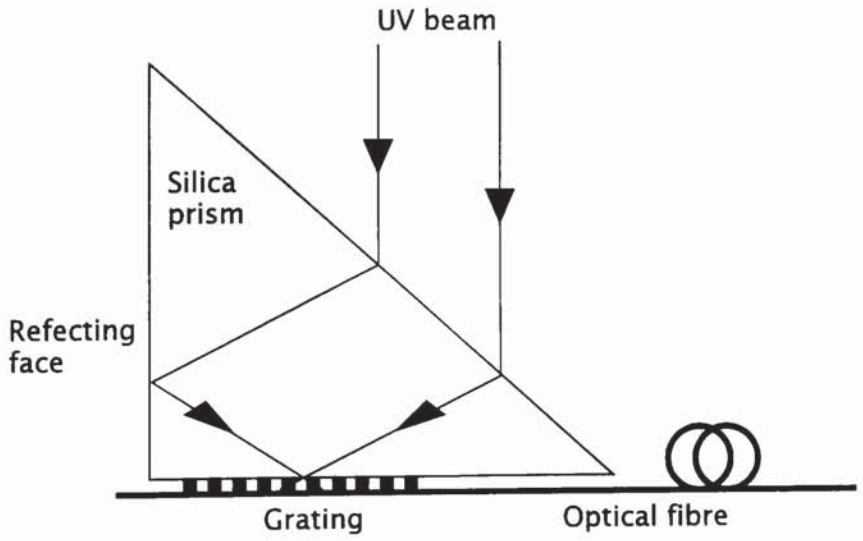

Figure 1-5 Prism-based interferometer for writing uniform-period gratings.

Prior to direct-write interferometric techniques, periodic filter devices were written using photoresists and surface relief etching[21,22]. The fabrication process involved mounting the fibre in a glass block and polishing the cladding down to give a flat surface, overlaying a patterned photoresist, and then etching through the photoresist into the fibre. Using this technique high reflectivity gratings (>90%) can be fabricated. The gratings have a reflection profile that is similar to that of the photorefractive gratings but in transmission they introduce losses at wavelengths below the reflection peak by way of modal outcoupling. The advantage of the direct-write interferometer approach was that it avoided both the wavelength inflexibility of the Hill gratings and the multi-stage, labour intensive process associated with side-etching.

The side-writing approach was limited in the maximum reflectivity that could be achieved by the photosensivity of the fibres available in the early 1990s. Two important advances occurred in 1993 that meant that side-written gratings could exceed the efficiencies of the side-etched gratings. The first was the fabrication of boron-germania co-doped fibres. The addition of boron as a co-dopant enhanced the photosensitivity of the fibres by a factor of ten and increased the intensity of the search for highly photosensitive fibres that were compatible with telecommunication systems. The second advance was the publication of results which showed that hydrogen loading fibres, under high pressures, dramatically increased the photosensitivity of all germania based fibres by several orders of magnitude. It then became possible to write gratings that reflected ~100% of the power at the Bragg wavelength over sub-mm distances.

Over the same period several other techniques for fabricating uniform-period gratings were developed. Most notably, the last two years have seen the emergence of phase mask based methods, Figure 1-6. Phase masks are diffractive elements that split an incident beam into various diffraction orders and were first used to fabricate UV written gratings in fibre by Hill[23] in 1993. The pattern on the mask, written either holographically or by electron-beam lithography, is etched to a depth $d=\lambda_{UV}/2(n_{UV}-1)$ where λ_{UV} is the wavelength of the write beam and n_{UV} is the refractive index at the write wavelength of fused silica. This depth is

chosen because it causes the maximum suppression of the zero order for a normally incident beam and it also maximises the power in the plus and minus first orders.

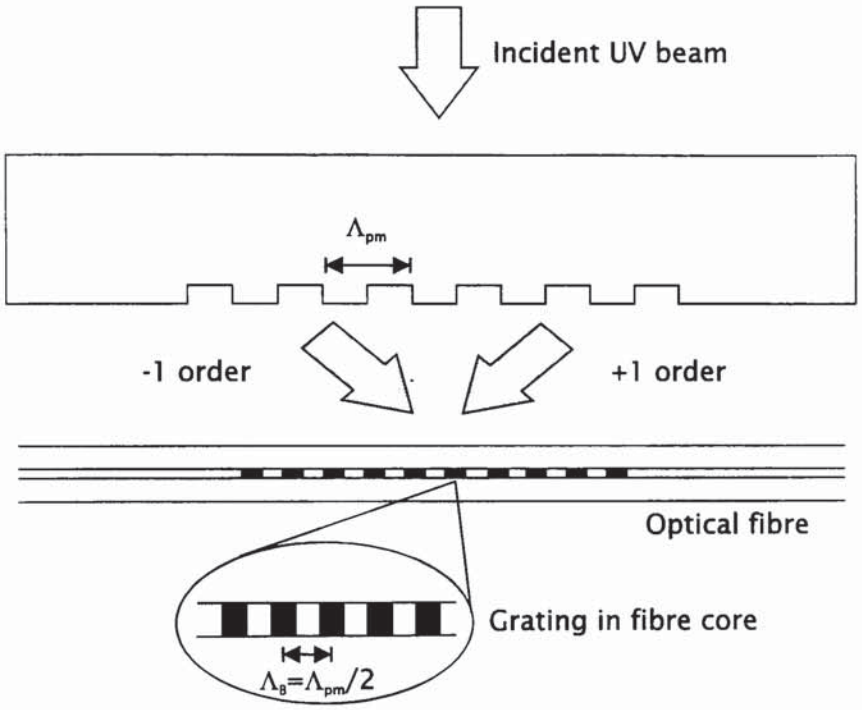

Figure 1-6 Arrangement used for writing Bragg gratings using a phase mask.

The fibre is placed in near-contact directly behind the phase mask so that the fibre axis is normal to the grooves in the phase mask. The diffracted plus and minus first order beams interfere in the near field producing a fringe pattern which photoimprints a refractive index modulation in the fibre core. The period of the interference fringes (Λ_B) is half that of the phase mask (Λ_{pm}).

Another phase mask arrangement used a silica block placed behind the phase mask to direct the plus and minus first orders to a fibre on the other side of the block[24]. This meant that the fibre did not need to be placed in contact with the mask thus avoiding possible damage. An arrangement interfering the zero and -1 diffracted orders to write a grating with a period equal to the phase mask period has also been demonstrated[25].

The phase mask method allows the production of a large number of gratings with excellent reproducibility between them and relaxation of the temporal and spatial coherence requirements of the write source. Since the phase of the interference pattern is insensitive to the position of the write beam very long gratings can be fabricated by translating either the beam or the phase mask and fibre. Martin *et al* [26] made a 15mm long grating by translating the phase mask and fibre in contact and keeping the write beam stationery. Rourke *et al* [27] took the alternative approach and translated the write beam across a static phase mask to fabricate a 50mm grating. The length of the grating is then only dependent on the length of the phase mask.

This technique is still limited by the periodicity of the phase mask; a change in wavelength requires a new phase mask to be made. Some variation in the wavelength can be obtained by stretching the fibre during fabrication[28,29]. It has also been shown that placing a magnifying lens in front of the phase mask varies the Bragg wavelength[30]. However, these two methods give only a few nanometres flexibility. Recently, another technique was proposed where both the phase mask and write beam are translated at different speeds in opposite directions where the achieved period is then some function of the relative velocity between the two.

Two non-interferometric techniques for fabricating in-core gratings have been proposed. 360μm gratings have been written fringe by fringe with periods of ~1 and ~1.5μm by a step and repeat technique[31]. A pulsed excimer laser was used and the fibre was exposed to an image of a slit where the fibre was moved a set distance in between each laser pulse. Because of diffraction limits the image was not small enough to write the fundamental Bragg period but it was demonstrated that the 2nd and 3rd Bragg orders could achieve up to 70% reflectivity.

A second technique used high resolution imaging to project a condensed image of a multi-slit periodic amplitude mask onto the photosensitive fibre[32]. Using a lens with a field size of the order of 10mm gratings have been fabricated with periods in the range 1 to 6μm. A 3mm period grating exhibited a 1.44μm 6th Bragg order that was 72%

reflecting and had a full-width half-maximum (FWHM) reflection bandwidth of 1.5nm. The disadvantage of this technique is that the UV transmission imaging lens required to achieve the necessary resolution are expensive.

Remarkably, it was only as recently as 1992 that the first chirped fibre gratings were fabricated[9]. The concept and practical realisation of chirped gratings in slab waveguide structures appeared in the 1970s[33,34], but could only be realised in optical fibres with the development of highly photosensitive fibres. The first chirped fibre gratings were side-etched into the cladding of fibre[9] and were used for residual pump laser rejection at 980nm and 1480nm. There are many ways in which chirp can be realised in a fibre grating, either by axially varying the grating period[35,36,37] or by varying the effective refractive index[38,39,9].

One of the proposed applications for the use of chirped fibre gratings is as a possible means of dispersion compensation in long haul systems. Increasingly chirped fibre gratings were being viewed as a possible solution to mounting concerns over chromatic dispersion in telecommunication systems[2,5]. There was also interest in pulse compression and the need for broadband reflectors in sensor work and filters for noise suppression. However, any increase in the bandwidth of the optically made gratings was at the expense of a lowered reflection efficiency; the strength of the grating was photosensitivity limited. Again it was the increase in fibre photosensitivity due to boron doping and hydrogen loading that allowed this limitation to be overcome. It then became possible to increase the bandwidth of the gratings whilst keeping the same grating length and yet not incur a rapid decrease in the reflectivity. At this point the progression of chirped grating technology split into two main directions that were applications driven and can probably best be classified by the dispersion constraints on the gratings required.

Highly dispersive gratings were required by those parties that were interested in dispersion compensation, pulse compression and in using dispersive elements for modelocking fibre lasers. The gratings need to be long (>1cm) and have a fairly narrow bandwidth (<5nm) with a high

degree of control over the chirp rate. Sensor applications and filtering systems tend not to rely on the dispersive qualities of the gratings and are concerned primarily with the resultant bandwidth so have different constraints on the grating parameters.

Several different fabrication technique for chirped fibre gratings have been proposed. The use of phase masks has been shown to be effective for fabricating gratings for dispersion compensation demonstrations[40], as has the interferometric technique of interfering beams with different beam curvatures[35,41] and that of sampled gratings[37]. Other techniques for fabricating chirped gratings have included imposing variable strain on a linear grating by the addition of two weights[42] or by mounting the grating on a tapered cantilever where strain is applied[43]; gratings written in tapered fibre[38]; graded pre-exposure of the fibre before exposure to a uniform interference pattern; the use of the shading in half gaussian beams[44], and fibre deformation[36]. Three of these techniques - tapers, fibre deformation and dissimilar wavefronts - will be discussed in detail in Chapter 4.

Two of the techniques mentioned above are also valid for the fabrication of large chirps: that of fibre deformation and techniques using dissimilar wavefronts. The latter case is more useful. Using various lens arrangements to produce dissimilar wavefronts it is possible to fabricate chirped gratings from the very small (<5nm) to the very large (>170nm). Three optical arrangements will be discussed within the section on dissimilar wavefronts.

1.4 Thesis Summary

This chapter has provided an introduction to the field of fibre Bragg gratings and to the historical context in which the work described herein is set. Chapter 2 details the basic information required to understand the concepts of fibre gratings and photosensitivity. Modelling techniques that are used to characterise experimental results are described. The concept of fibre dispersion is briefly discussed since it is important to many of the considered grating applications. The

current knowledge of fibre photosensitivity in fibres is summarised, as is the work to date on grating stability.

Uniform-period gratings are discussed in Chapter 3. The fibres used are summarised in terms of the magnitude of the refractive index modulation achieved. The interferometer used to fabricate uniform-period gratings is described. The evolution of gratings with respect to power and time and the wavelength stability due to hydrogen outdiffusion are also discussed.

Chapters 4, 5 and 6 form the main body of novel work in the thesis. Chapter 4 describes three new techniques for fabricating chirped fibre gratings, including the first direct-write technique that was published. Three different lens arrangements, using beams with dissimilar wavefront curvatures to produce superbroad, linear and quadratic chirped gratings are considered. Resonator structures comprising pairs of chirped fibre gratings are discussed in Chapter 5. From this work came the first published demonstrations of chirped fibre grating resonators as Fabry-Perot structures and Moiré resonators.

The number of applications proposed for fibre gratings has rapidly increased over the last couple of years. Chapter 6 highlights a range of chosen applications and illustrates well the greater breadth of potential applications. The chapter includes sections on the first published demonstrations of fibre gratings dispersion compensation and femtosecond chirped pulse amplification. Three different laser systems are presented. The first two use the dispersive properties of chirped gratings to modelock fibre lasers to generate ultrashort pulses; the third system uses a chirped grating Fabry-Perot as a transmission filter in a continuous wave (CW) laser that exhibits eleven simultaneously lasing wavelengths. Finally, the use of grating-coupler devices as variable reflectivity mirrors for laser optimisation and gain clamping is considered.

Chapter 7 summarises the work presented in this thesis and highlights possible areas for future work. Chapter 8 documents the publications associated with this body of work.

2. Background

2.1 Introduction

This chapter is designed to introduce the reader to some of the modelling techniques used for predicting grating. The subject of photosensitivity will be discussed briefly to give some background on the type of fibres used. This will include information on the absorption profiles of silica fibre and the choice of laser sources for grating fabrication. The techniques used to characterise will be discussed in this chapter. Lastly, issues that have arisen regarding grating stability and low wavelength loss will be summarised.

2.2 Modelling Fibre Gratings

There are two main approaches for modelling the response of a grating. By far the most commonly used and referenced technique for modelling uniform-period gratings is based on coupled mode theory.

For a uniform sinusoidal modulation with a refractive index profile described by $n(z) = n_{core} + \delta n\left[1 + \cos\left(\frac{2\pi z}{\Lambda}\right)\right]$ where δn is the amplitude of the refractive index modulation, then coupled mode theory uses a pair of first-order differential equations to describe the amplitudes of forward (incident) and backward (reflected) travelling modes. The grating provides a coupling mechanism between the two modes so that energy can be transferred from the incident to the reflected mode. The formation of and solution to these equations is well documented elsewhere[45,46] and involves finding the ideal eigenmodes in a uniform fibre and then using them to represent the perturbed fields in a grating. From this the reflectance R(L,λ) as a function of wavelength and filter length is given by

$$R(L,\lambda) = \frac{\kappa^2 \sinh(SL)}{\delta\beta^2 \sinh^2(SL) + S^2 \cosh^2(SL)} \qquad \text{for } \kappa^2 > \delta\beta^2$$

$$= \frac{\kappa^2 \sin^2(QL)}{\delta\beta^2 - \kappa^2 \cos^2(QL)} \qquad \text{for } \kappa^2 < \delta\beta^2$$

Equation 3

L is the grating length, κ is the coupling coefficient, $\beta = 2n_{eff} / \lambda$ is the mode propagation constant and Λ is the perturbation period. The variable δβ=β-(pπ/Λ), p=1 for the fundamental mode, $S = (\kappa^2-\delta\beta^2)^{1/2}$ and $Q = (\delta\beta^2-\kappa^2)^{1/2} = \iota S$. Assuming no loss then the normalised transmission T=1-R.

Varying the term δβL gives an amount of detuning from the central Bragg wavelength of the grating and so can be used to explore the reflection profile of a grating. Figure 2-1 shows the reflectance R plotted against δβL for a periodic grating for values of κL=0.5, 1, 2, 3 and 4. As κL increases the grating becomes more strongly reflecting and the central peak starts to broaden. For strong gratings the bandwidth becomes highly dependent on κ as a consequence these gratings exhibit broader bandwidths.

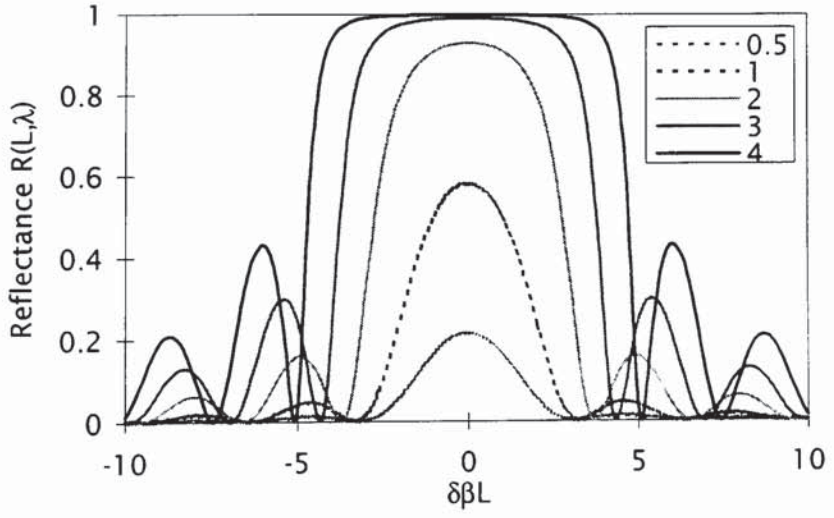

Figure 2-1 Reflectance R(L,λ) plotted against δβL for a periodic grating with values of κL =0.5, 1, 2, 3, 4.

The maximum reflectivity across the bandwidth of a uniform grating occurs when $\delta\beta=0$, *i.e.* when the Bragg condition is met so that

$$p\lambda = 2n_{eff}\Lambda \equiv \lambda_B$$

Again, p is the diffractive order and, for the fundamental Bragg order when the reflection is strongest, p=1. For $\delta\beta=0$ Equation 3 can be simplified to give the peak reflectivity R_{max} such that

$$R_{\max} = \tanh^2(\kappa L).$$

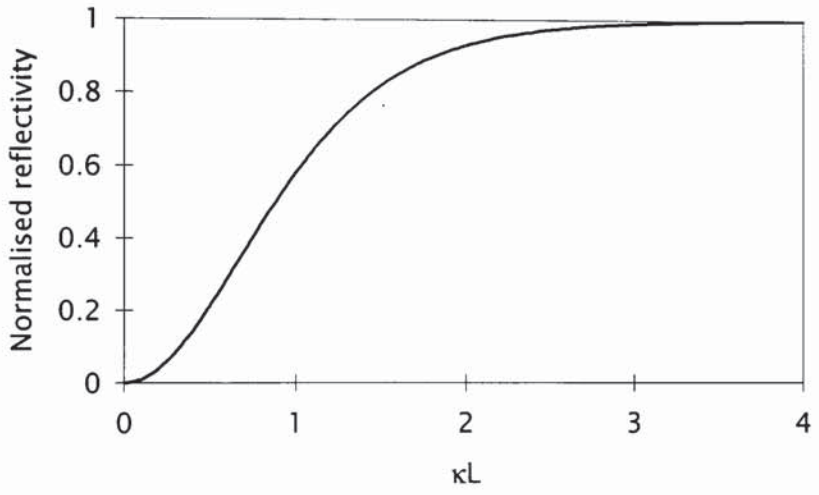

Figure 2-2 Normalised reflectivity as a function of κL.

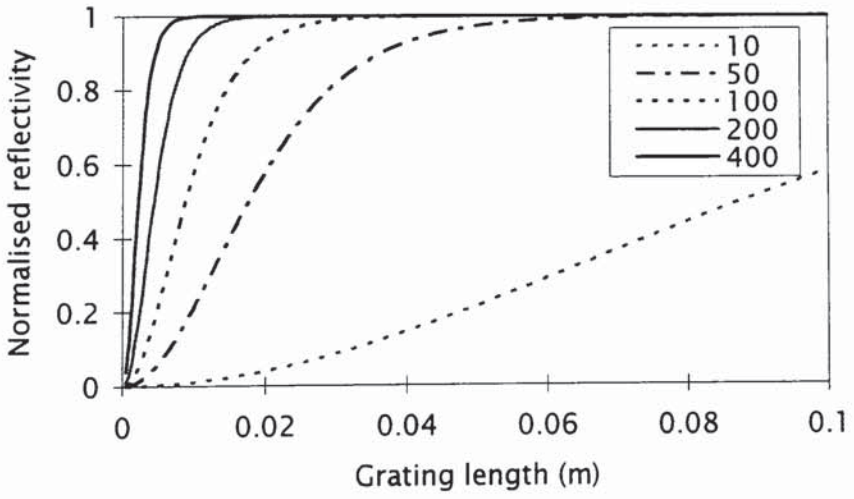

Figure 2-3 Peak normalised grating reflectivity for grating lengths between 0 and 0.1m for five coupling coefficients of values 10, 50, 100, 200, 400 m^{-1}.

Figure 2-2 plots the peak normalised reflectivity as a function of κL. However to design a grating it is sometimes easier to separate κ from L. Figure 2-3 illustrates this by showing how the reflectivity varies as a function of grating length for κ=10, 50, 100, 200, 400. The plot shows how for a fixed value of κ the reflectivity increases as the length of the grating increases.

In order to select the parameters required to give a grating with a set bandwidth and reflectivity it is helpful to consider Figure 2-4. From Equation 3 the full bandwidth measured between the two zeroes on either side of R_{max} is given by

$$\Delta\lambda = \frac{\lambda_B^2}{\pi n_{eff} L}\left[(\kappa L)^2 + \pi^2\right]^{1/2}$$

Equation 4

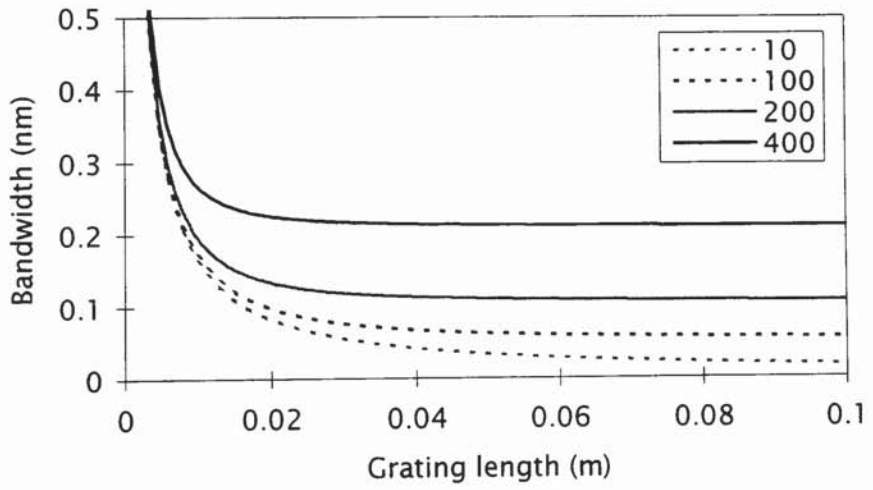

Figure 2-4 Variation in grating bandwidth with respect to increasing grating length for four coupling coefficients of values 10, 50, 100, 200, 400 m^{-1}.

Figure 2-4 plots this relationship between bandwidth and grating length for different values of κ. Where Figure 2-3 shows how for large values of κ the reflectivity tends towards 100% for only a short length of grating, it can be seen from Figure 2-4 that, for the same value of κ, the bandwidth of the grating does not narrow greatly with increasing

length. This is because the grating is so strong that most of the light does not see the full length of the grating before being reflected. Consequently, to obtain narrow bandwidth gratings it is necessary to fabricate very long, weak gratings.

For a uniform-period sinusoidal modulation of the refractive index, amplitude Δn, throughout the core, the coupling coefficient κ can be expressed as

$$\kappa = \frac{\pi \Delta n}{\lambda_B} \eta$$

where η is the fraction of the normalised mode power that exists within the fibre core and so can interact with the grating. If the grating is written uniformly across the whole of the core then, for a fibre with a V-value of V, $\eta \approx 1 - V^{-2}$.

There are limitations to this model in that it tackles a simplification of the experimental situation and does not allow for a variation of the period or coupling coefficient along the length of the fibre. It is possible to describe a more general case and solve numerically either by iterating a pair of coupled mode equations[47,48,49] or by reducing the coupled mode equations to a single Riccati differential equation[34].

Another approach to modelling aperiodic gratings is to use the transfer matrix approach[50,51]. This technique deals with a complex structure by sub-dividing it into a large number of thin sections and then assuming that within each section the medium is homogeneous. The effect that each section in turn has on the optical field is then considered and expressed as a 2x2 transfer matrix. To obtain the overall grating response the transfer matrices of all the sections are then multiplied together. This method will be used later in this thesis to predict responses for chirped gratings.

2.3 Dispersion Compensation

Group velocity dispersion (GVD) causes a pulse containing a band of frequencies to spread out as it travels along a fibre. This dispersion degrades the system performance either by limiting the maximum data rate that can be used, so the neighbouring pulses do not merge, or by decreasing the distance between repeaters where the signal is decoded and then re-encoded. By introducing components into a system which exhibit a dispersive effect equal in magnitude but opposite in sign to the fibre GVD the fibre dispersion can be cancelled, see Figure 2-5, and the original pulse retrieved. This approach is known as dispersion compensation. For successful dispersion compensation the induced time delay between the different wavelengths within the pulse should be equal to the initial time delay caused by the fibre dispersion. There have been several different methods proposed for this purpose[52,53,54] one of them being the introduction of chirped fibre Bragg gratings. The resonant wavelength of the grating is a function of the position along the grating. The different wavelengths within the pulse are reflected at different points and at different times relative to each other. This introduces either a positive or negative dispersion depending on grating orientation. The sign of the grating introduced dispersion can therefore be changed just by physically reversing the grating.

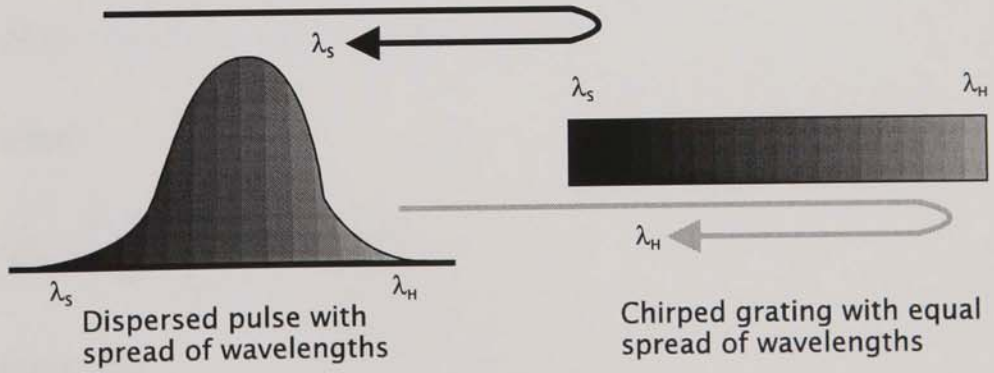

Figure 2-5 Schematic of dispersion compensation. The trailing edge of the pulse is reflected from the front edge of the grating and the leading egde of the pulse from the back edge of the grating.

2.3.1 Origins of dispersion

A pulse of light which contains a finite bandwidth of frequencies is temporally broadened as it travels down a fibre. In single mode fibre there are two dominant processes responsible for this broadening.

· *Material Dispersion.* This occurs because the refractive index of the fibre is wavelength dependent. The different frequencies contained in the pulse will therefore travel with different phase velocities and take slightly different times to travel the length of the fibre.

· *Waveguide Dispersion.* This less dominant process originates from the variation of mode field diameter with wavelength. The average refractive index experienced by each spectral component is dependent on how much travels in the core and how much in the cladding.

It is usual to consider dispersion in terms of the mode propagation constant β where

$$\beta(\omega) = n(\omega)\frac{\omega}{c}$$

n(ω) is the refractive index at frequency ω and c is the free-space velocity of light.

This can be expanded in the form of a Taylor's series about a central frequency ω_0 such that

$$\beta(\omega) = \beta_0 + \beta_1(\omega - \omega_0) + \frac{1}{2}\beta_2(\omega - \omega_0)^2 + \ldots.$$

where

$$\beta_m = \left[\frac{\partial^m \beta}{\partial \omega^m}\right]_{\omega=\omega_0} \qquad m = 0,1,2.....$$

From this

$$\beta_1 = \frac{1}{c}\left[n + \omega\frac{\partial n}{\partial \omega}\right] = \frac{1}{v_g} \qquad \beta_2 = \frac{1}{c}\left[2\frac{\partial n}{\partial \omega} + \omega\frac{\partial^2 n}{\partial \omega^2}\right] = \frac{\lambda^3}{2\pi c^2}\frac{\partial^2 n}{\partial \lambda^2}$$

where v_g is the *group velocity* of the pulse, and β_2 is known as the *group velocity dispersion* (GVD).

The GVD is zero around 1.3μm for standard fibre although in this area third and forth order terms must be taken into account. Altering the material composition of the fibre has only a small effect on the zero dispersion wavelength. It is however possible to move this wavelength by altering the dimensions of the fibre and hence the waveguide dispersion. The move tends to be towards the 1.55μm window in order to exploit the erbium fibre amplifier systems. This fibre is said to be dispersion shifted.

There exists another parameter that is often used in connection with this subject, this is the group delay dispersion D (ps nm^{-1} km^{-1}). This is connected to the group velocity dispersion by the expression

$$D = -\frac{2\pi c}{\lambda^2}\beta_2$$

When D is positive the system is said to be operating in the anomalous dispersion region, a negative D relates to the normal dispersion region.

Since broadening is independent of the sign of the GVD it occurs in both dispersion regions. Where $\beta_2>0$ (normal) the lower frequencies travel faster than the higher ones, this gives a pulse with a frequency distribution across its profile that by convention is known as a negative chirp. The sign indicates the direction of increasing frequency. Conversely, where $\beta_2<0$ in the anomalous dispersion region, the pulse acquires a positive chirp where the higher frequencies are found at the leading edge of the pulse and the lower frequencies at the trailing edge. The difference in speed between the frequencies contained in a pulse causes the pulses to widen. It is this effect that the process of dispersion compensation seeks to reverse by introducing an opposing chirp.

The grating group delay dispersion (ps nm^{-1}) is determined by the bandwidth and length, assuming that the dispersion is linear it is given by

$$D = \frac{2Ln}{c\Delta\lambda}\cdot 10^3$$

Equation 5

For example, a 5mm grating that has a bandwidth of 2nm the dispersion ~24ps nm^{-1}. Grating dispersions are sometimes quoted in units of ps^2, to convert from D(ps nm^{-1}) to D(ps^2) multiply D(ps nm^{-1}) by a factor of $\frac{\lambda^2}{2\pi c}\cdot 10^{21}$.

2.4 Characterisation of Gratings

2.4.1 In-situ measurements

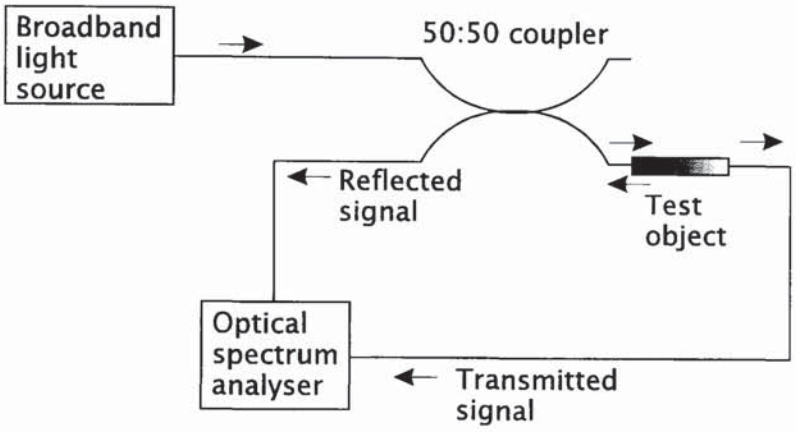

Figure 2-6 In-situ characterisation of fibre Bragg gratings.

During exposure it is important to be able to monitor the grating growth in situ. This is done using the set-up shown in Figure 2-6. The output of a broadband source that covers the appropriate wavelength region enters a 50:50 fibre coupler. The fibre in which the grating is being fabricated is attached to one of the output ports of the coupler and 50% of the light from the broadband source then interacts with the grating. The grating can be monitored using an optical spectrum analyser either in transmission, looking at the spectrum that exits the fibre with the grating in, or in reflection looking at the output of the opposite port of the coupler.

Figure 2-7 shows the transmitted and reflected spectrum from a 0.37mm grating fabricated in a hydrogenated boron-doped fibre. The

smooth line shows the theoretical fit calculated from Equation 3. The experimental and theoretical plots are well matched but there is a discrepancy in the transmission plots on the low wavelength side of the grating. This is a consequence of modal outcoupling due to the strength of the grating as discussed in Section 2.7. Figure 2-8 shows the evolution of a grating over time. The grating was 5mm long and was fabricated in hydrogen-loaded boron doped fibre. As the exposure time increases the grating response strengthens and broadens.

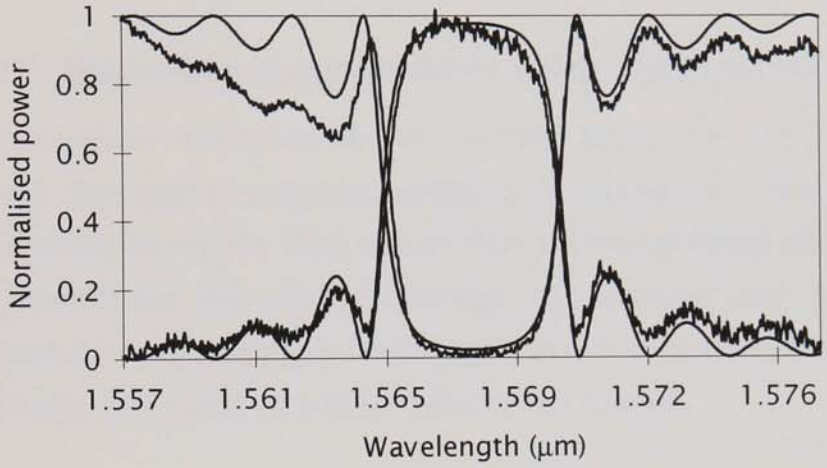

Figure 2-7 Transmitted (dip) and reflected response (peak) of a 0.37mm grating fabricated in boron-doped fibre. The smooth line shows a theoretical fit.

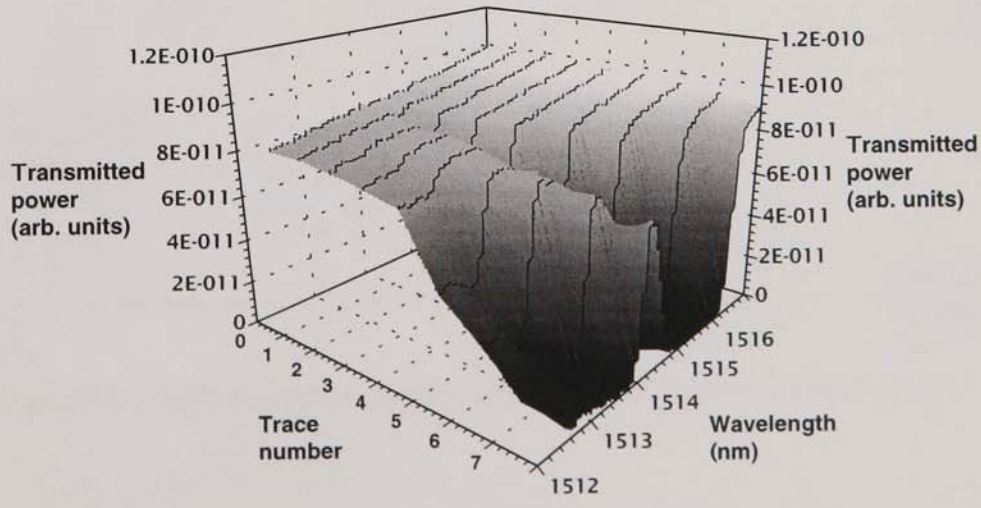

Figure 2-8 Evolution of a 5mm grating fabricated in boron-doped fibre.

The choice of broadband source depends on the grating wavelength. For gratings in the region of 1450-1650nm it is convenient use the fluorescence from a 3m length of erbium fibre pumped by the unconverted 488nm beam from the frequency doubled laser. For other wavelength regions diodes are used if they are available or if not a white light source. Lamp sources have the advantage of covering a wide range of wavelengths but tend to be of very low power at any one wavelength and limit the measurement accuracy. The reflectivity of a grating is deduced from the loss in transmission. This assumes that no absorption or outcoupling occurs which is not true for strong gratings, refer to Section 2.8.

2.4.2 Dispersion measurements using a microwave technique

The method described in the section above has certain limitations. Firstly the optical spectrum analyser is limited to a maximum spectral resolution of 0.1nm. This means that narrow gratings are not measured accurately and, for chirped gratings, substructure may be there but not observable. Secondly, for some applications it is necessary to be able to measure accurately the dispersion of the grating.

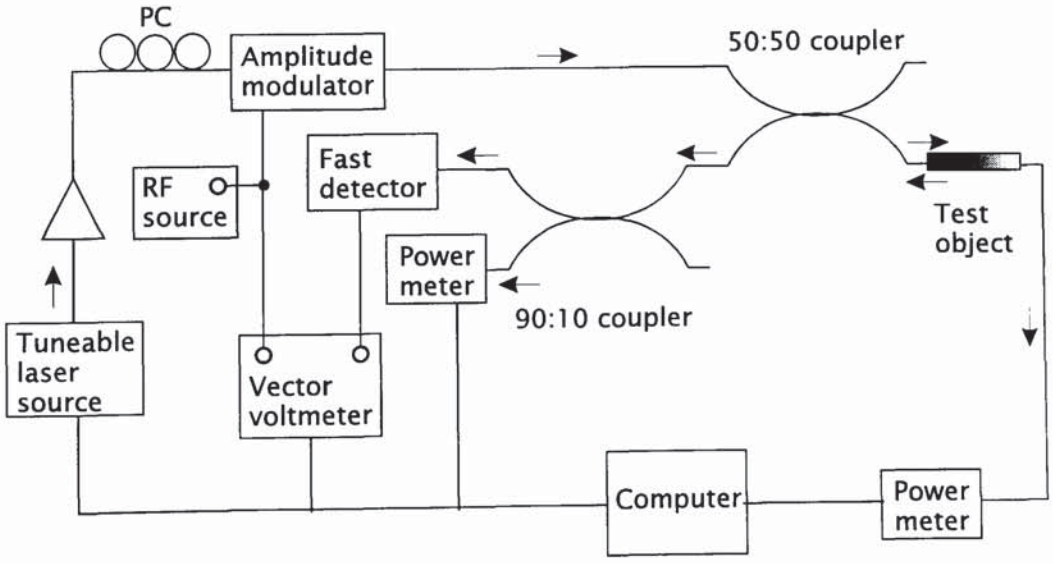

Figure 2-9 High resolution grating dispersion and profile measurements.

Figure 2-9 shows a set-up for making high resolution measurements for both the transmission and reflection responses and the grating dispersion. A tuneable wavelength laser is used that has a linewidth of less than 0.001nm. The laser tunes across the wavelength range that is required. The light goes into an amplitude modulator, is modulated with an RF source, and continues through to a 50:50 coupler and on to the grating. Light reflected from the grating is split through a 90:10 coupler. 90% goes to the fast detector, the phase of the signal is then compared to the RF source signal to give a measure of electrical delay which is related to the grating dispersion via the modulation frequency (to give optical delay) and the grating bandwidth. The remaining 10% goes to a power meter and monitors the reflectivity. The transmitted signal through the grating is also measured using a power meter.

2.5 Material Aspects of Photosensitivity in Fibres

The fibres used in the fabrication of in-core fibre gratings are said to be photosensitive, i.e. they exhibit a permanent change in core refractive index when exposed to ultra violet or deep blue light. The exact mechanisms behind this effect remain unclear but there is general agreement that in germanium doped fibres the effect derives from chemical reactions involving oxygen deficient sites.

Spectroscopic studies have shown that there is a germanium oxide (GeO) defect present that has a strong absorption band at 242nm[55] that is bleached during exposure to ultra violet light[59,56,57], Figure 2-10. Russell and Hand[58] suggested that this was caused by the GeO bonds being broken to form colour centres (GeE') with the subsequent emission of a free electron, Figure 2-11. This free electron is then at some point trapped at another site in the glass matrix forming a permanent charge separation. The presence of the colour centres causes the change in the UV absorption spectrum and the concurrent change in the refractive index.

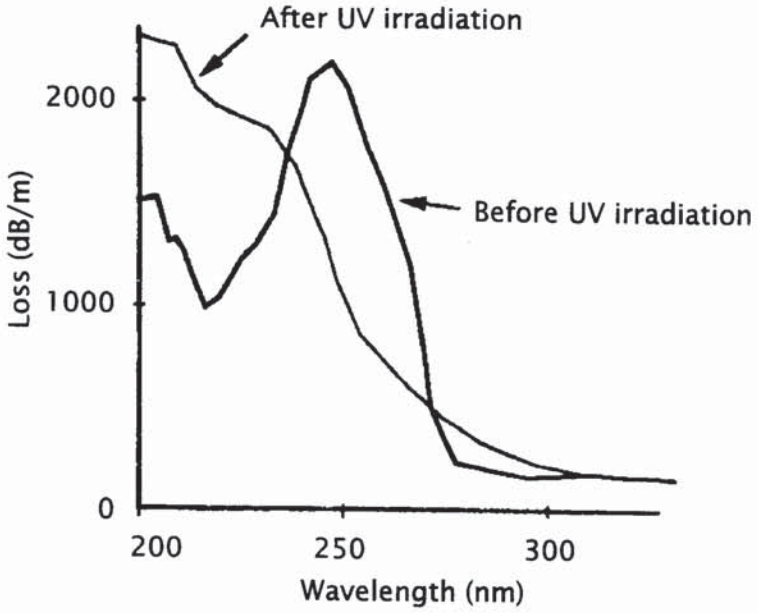

Figure 2-10 Transmission loss spectrum of a 15mm thick germania doped preform[59].

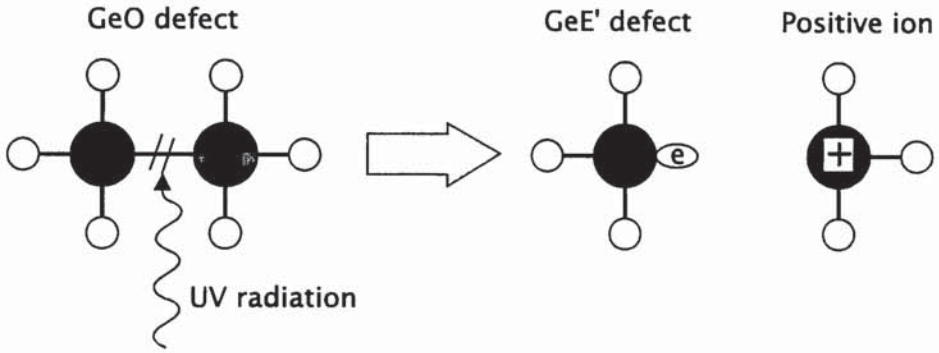

Figure 2-11 Illustaration of one of the reactions thought to be responsible for the photosensitive effect in germania-doped silica.

By modelling the expected change in the absorption spectrum using the Kramers-Kronig relationship[58] it is possible to predict the change in refractive index observed. The problem with this is that the values for the predicted change in refractive index predicted by using the 242nm absorption line are smaller than the experimentally measured values. It is thought that there are more changes occurring but that these take place at wavelengths below 200nm where it is experimentally very difficult to monitor.

Although there is a lot of experimental evidence in support of the GeO defect model[59,57,60,61,62] there is also a body of work[63,64,65] that suggests that

it is not the complete explanation. Xie *et al*[63] published results that indicate at least two processes occurring; one that is responsible for the initial grating where the reflectivity increases and then decreases due to saturation, and a second grating that grows on a slower time scale than the first after the initial grating has been erased. In the initial case the Bragg wavelength increases over time as the effective refractive index increases. For the second grating the Bragg wavelength decreases very slightly indicating a drop in the refractive index. This effect was not seen in all fibres, but was observed primarily in fibres with high germania concentrations (>16.5mol%) and only low quantities of other dopants. It has been suggested[61] that this effect is due to one- and two-photon absorption where the one-photon absorption is due to the photogeneration of GeE' centres and the two-photon absorption due to the photobleaching of the same centres. Glass densification induced by the photoionisation of the GeO defects has also been proposed[66] as an alternative model of lowering the refractive index at high intensity sites with some experimental support[67].

One of the most effective ways of enhancing the photosensitivity of a fibre is by hydrogenation. This idea in relation to fibre gratings was first proposed by Lemaire. Fibres were soaked at high pressure (20-750 atmospheres) and at temperatures between 20 and 70°C for several days. The length of time must be such that it allows the hydrogen to diffuse into the fibre core; being a diffusion process, a higher temperature and/or pressure decreases the time required. Hydrogen-loading can produce a factor of 100 change in the refractive index of a fibre from the non-hydrogenated case.

The exact reaction that occurs remains unclear but it appears that hydrogen allows every germania site, rather than just specific defect sites, to take part in the reactions that cause the refractive index change. It has been suggested that the UV photon causes a network bond to be excited at a dopant site. The excited bond then reacts with a nearby hydrogen molecule to cause the refractive index change.

Figure 2-12 illustrates the change in absorption that occurs with germano-silicate film and is taken from a paper by Maxwell[68]. The films

were heated in a hydrogen atmosphere for various lengths of time. At the start the absorption peaked at around 190nm and then decreased steadily as the wavelength moved towards 260nm. With increasing concentrations of hydrogen the 195nm peak increased but this was matched and then overtaken by a peak centred at 240nm.

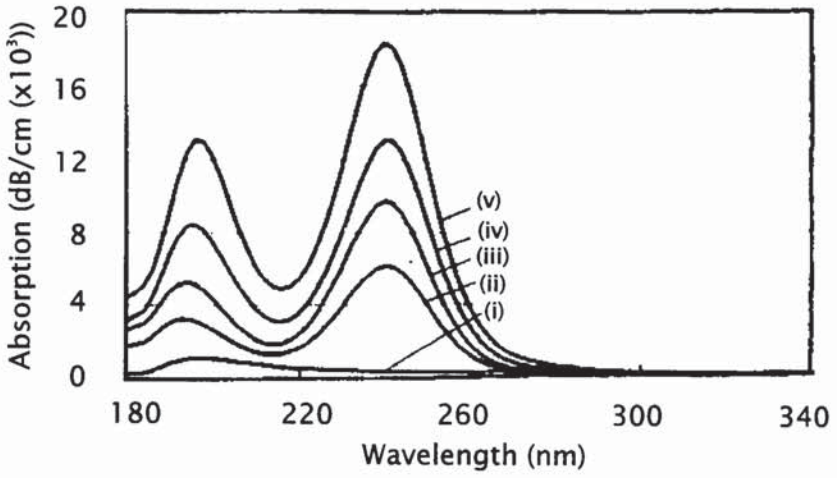

Figure 2-12 UV spectra[68] for GeO_2-SiO_2 films after annealing at 750°C in hydrogen for various times (i) 0 min, (ii) 10 min, (iii) 30 min, (iv) 60 min, (v) 120 min.

One of the consequences of using hydrogenated fibres is that an absorption loss[69] due to a Si-OH resonance occurs around 1390nm, Figure 2-13. For highly germania-doped fibres the tail end of this resonance can produce losses in a grating of ~1dB. This effect can be reduced by substituting deuterium in the loading process which shifts the resonance to longer wavelengths.

Germania silicate fibres have not been the only fibres to exhibit photosensitivity. High reflectivity gratings have been written in erbium doped fibres[70], but this is not unexpected since most erbium doped fibres also contain high concentrations of germania dopant. To a lesser extent photosensitivity has been observed in fibres doped with cerium[71] and europium[72] and gratings have been written in phosphorus doped fibres[73] but only with a lower write wavelength of 190nm.

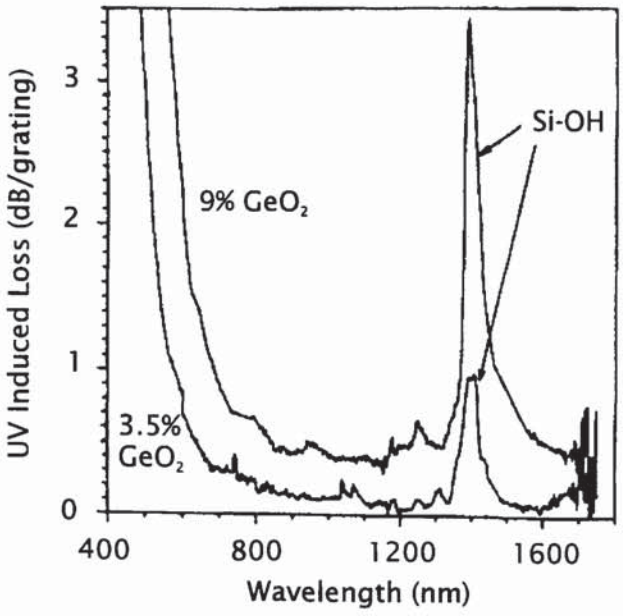

Figure 2-13 UV-induced loss changes in hydrogen-loaded fibres with 3.5- and 9-mol% GeO_2. Rising loss edged at short wavelengths are due to UV-created germania defects (Taken from reference 69).

2.6 Laser Sources

A laser source that is suitable for fabricating in-core Bragg gratings must have an output wavelength that falls within an absorption band of the germania oxide defect, Figure 2-10, and is not strongly absorbed by the cladding. Consequently, although several different laser sources have been used for fabricating side-written gratings they have all operated at wavelengths in the band ~190 to 280nm.

A wide variety of pulsed sources have been used, principally KrF (248nm) and ArF (193nm) excimer lasers with and without intracavity line-narrowing elements, and tuneable excimer-pumped frequency doubled dye lasers. The main disadvantage of using excimer lasers is that they exhibit low coherence and so are not ideal for complex holographic set-ups. Also pulsed, frequency quadrupled Nd:YAG[26] (266nm) and Nd:YLF[74] (262nm), have recently become popular; these lasers work well with hydrogenated fibres and exhibit very good coherence.

Since 1990 the CW frequency-doubled (BBO) argon-ion laser[17] has been used routinely at some institutions and was used for the devices presented in this thesis. With excellent beam quality and coherence this type of laser is good in situations where there are demanding holographic requirements. This source was more user friendly for holographic purposes than the excimer lasers since the coherence and beam quality were good and the output power was high enough to give reasonably short exposure times (a few minutes).

2.7 Grating Stability

If gratings are to fulfill their early promise as an important component in telecommunication and sensor systems then they must be stable in wavelength and reflectivity over a significant period. System lifetimes are generally required to be in excess of 25 years and a grating must not experience any significant decay during this time.

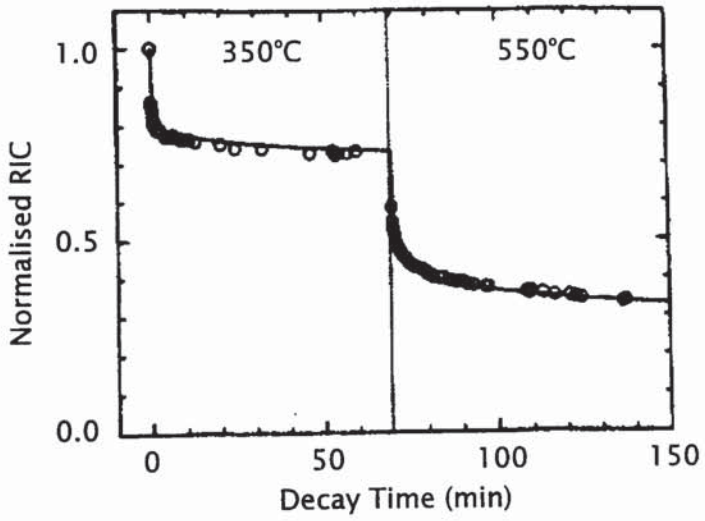

Figure 2-14 Decay curve for a single grating heated first to 350°C and then to 550°C. The graph plots the normalised refractive index change (RIC) against time. (From reference 79).

It has been shown that gratings decay when exposed to a uniform UV beam[75,76]. It appears that gratings also decay at a rate that is determined by the ambient temperature[77,78]. A representative decay curve is given by Figure 2-14 for a grating fabricated in a boron-germania doped fibre that

was isothermally annealed first at 350°C and then at 550°C. There is an initial rapid decay in the normalised refractive index change followed by a much slower decay rate that decreases with time. At the point where the temperature was increased a second rapid decay, the rate of which decreases with time, is observed. It is believed that this decay process is due to the thermal depopulation of trapped states that were created during the grating fabrication process. Erdogan *et al*[79] proposed the existence of traps with a broad distribution of activation energies that seems consistent with experimental results. They showed that this model predicts that for, a given temperature, a grating can be annealed to remove the portion of the traps that will decay quickly leaving behind the traps that will be stable over the long-term. They were able to fit this model to experimental data with very good agreement. There is a connection between the annealing time and the stability in years and the operating temperature. If the operating temperature or the lifetime requirement is increased the annealing temperature, which is calculated from experimental data, or the annealing time must also be increased. Using this model it is possible to predict post-annealing lifetimes in excess of 25 years.

It has also been observed[80] that the Bragg wavelength shows thermal hysteresis when heated in the temperature range 80°C to 425°C. The Bragg wavelength of a grating increases with temperature as the fibre expands and increases the separation of the grating fringes. However, when the grating is returned to its initial temperature, a permanent shift in the Bragg wavelength to shorter wavelengths is observed. The magnitude of the shift is dependent on the fibre and the exposure conditions but for one grating was as much as 0.35nm when the grating was heated to 230°C and then returned to room temperature[80]. Annealing at a temperature higher than the maximum operating temperature greatly reduces this effect.

2.8 Short Wavelength Loss

One important effect of introducing gratings with high refractive index modulation into the core of the fibre is that it induces short wavelength loss. Light is coupled into cladding and radiation modes instead of being reflected along the fibre core. This effect was first noted by Archambault *et al* [81] in the context of gratings made with very high power, single pulses from an excimer laser. Substantial loss was observed at wavelengths shorter than λ_B and the profiles looked similar to those obtained from side-etched gratings[21].

Subsequently, when gratings with high refractive index modulation were fabricated, similar results were obtained. Figure 2-15 shows the transmission and reflection profiles of a 5mm grating produced in hydrogen-loaded boron-germanium codoped fibre with a large Δn of approximately 2.2×10^{-3}. On the short wavelength side of λ_B the transmission profile exhibits a significant loss and superimposed on this are multiple sharp peaks. The reflection profile exhibits none of this structure and so it can be concluded that some loss process is occurring.

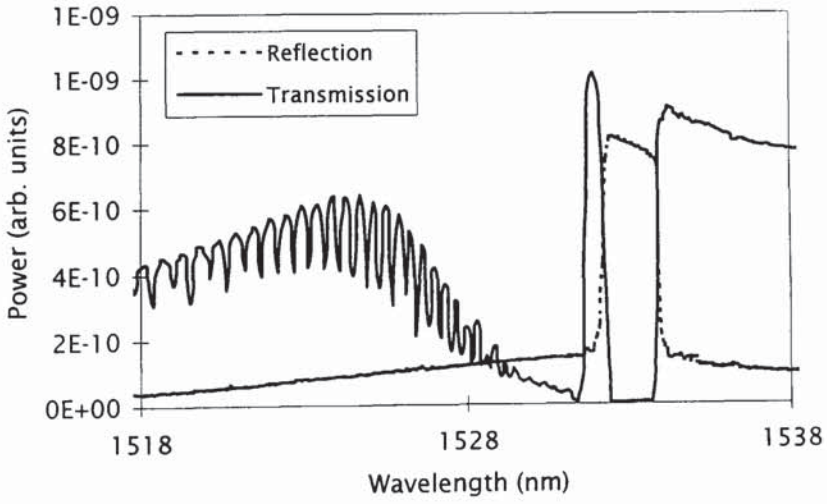

Figure 2-15 Measured transmitted and reflected profiles of a 5mm long uniform-period grating fabricated in hydrogen-loaded BT standard fibre.

The coupling to the cladding and radiation modes of the fibre has been characterised by Mizrahi and Sipe[82]. The radiation mode coupling efficiency is dependent on κ^2 and, therefore also of Δn^2; consequently it is more noticeable for strong gratings. If the fibre is submersed in index matching fluid the modal structure disappears leaving a broad loss spectrum.

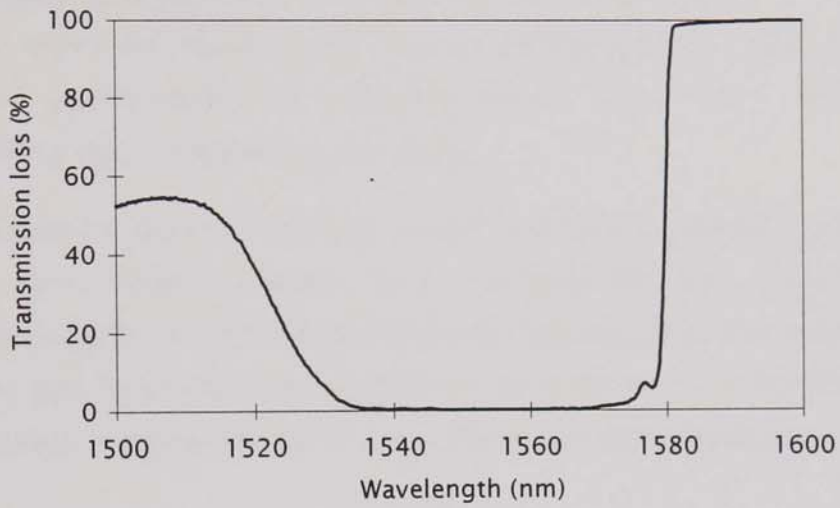

Figure 2-16 Transmission profile of a chirped grating.

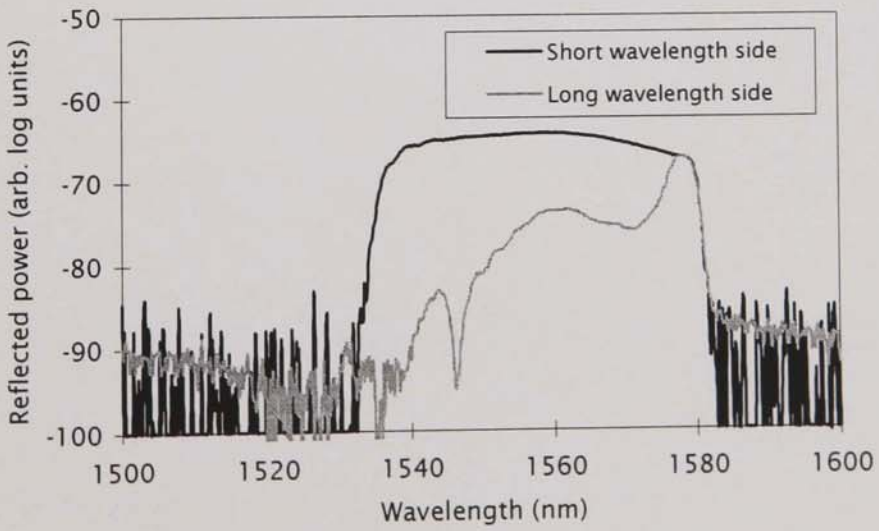

Figure 2-17 Reflection profile of a chirped grating obtained from the short wavelength and high wavelength sides of the grating.

Since strong gratings require very high changes in refractive index to achieve high reflectivities they are also affected by this outcoupling loss; however, the distributed nature of the reflected wavelength further complicates the situation. Figure 2-16 shows the transmission profile of a broadband grating. The reflection profiles obtained from both sides of the grating illustrate one of the problems associated with fabricating very strong gratings in that they exhibit a strong asymmetry in reflection due to the short wavelength loss, Figure 2-17. When the grating is orientated such that the low wavelengths are reflected first the short wavelength loss due to outcoupling is avoided because the short wavelengths are reflected before they contact the part of the grating that could outcouple them.

To reduce losses caused by modal outcoupling chirped gratings should be used, where possible, in a configuration that allows the shorter wavelengths to be reflected from the grating first. The short wavelength loss due to modal outcoupling can be reduced by using fibres with high numerical apertures since these fibres are more strongly guiding.

3. Uniform-Period Gratings

3.1 Introduction

The work described in this chapter forms the basis of all the grating and resonator fabrication work that follows. Holographic systems provide a highly flexible technique for fabricating gratings with the necessary finesse to produce a broad range of intricate structures. The different types of fibre used for fabricating gratings will be discussed in Section 3.2, along with some brief discussion of the hydrogen-loading process and a summary of the refractive index changes observed in the different fibres used. Section 3.3 provides details of the interferometer used for fabricating uniform-period gratings and shows examples of grating reflection and transmission in both hydrogenated and non-hydrogenated fibres. The time evolution of gratings during exposure is illustrated in Section 3.4; the effect of laser power on the exposure times is described in Section 3.5. Finally, Section 3.6 deals with the effect that hydrogen-loading has on the wavelength stability of gratings post-exposure.

3.2 Fibres and Photosensitivity

A wide range of different fibres with various germania dopant levels have been used for grating fabrication. Generally, consistent with Section 2.3, it has been found that the higher the concentration of germania the higher the level of photosensitivity. Fibres incorporating boron as a dopant have also been investigated. Contrary to almost all other dopants boron lowers the refractive index of the silicate[83]. Consequently boron doped fibres can have a much higher dopant concentration of germania than would otherwise be possible since the decrease in refractive index due to the boron balances the increase due to the germania and so the numerical aperture of the fibre is maintained at a value compatible with other fibres used in a system.

Hydrogen-loading was discussed in Chapter 2 as a technique for enhancing the photosensitivity of fibres. A hydrogen-loading chamber

was manufactured comprising a series of 10mm diameter steel tubes of length 2m. The tubes are filled with hydrogen from a high pressure cylinder to pressures of up to 100-150 atmospheres. The fibres remain in the hydrogen atmosphere at room temperature for 5-7 days to allow the hydrogen to diffuse into the core. When the fibres are removed from the hydrogen the hydrogen starts to diffuse out of the fibre at a rate that is temperature dependent. To increase the time at which the fibres remain at an elevated photosensitivity they can be stored at low temperatures. The percentage of out diffusion that takes place over one day at 21°C takes 75 days at -40°C[84]. Typically hydrogenation was found to enhance the photosensitivity of all the germania-doped fibres used by a factor of ~100.

Fibre type	Fibre source	Non-hydrogenated			Hydrogenated		
		R	Δλ (FWHM) (nm)	Δn	R	Δλ (FWHM) (nm)	Δn
York 800	York fibres	<5%	-	$x10^{-5}$	90%	0.25	$3x10^{-4}$
BT standard	BT labs	<5%	--	$x10^{-5}$	98%	0.61	$5.4x10^{-4}$
Erbium doped (Er/Ge)	BNR Europe Ltd research labs	--	--	--	100%	1.5	$1.2x10^{-3}$
Germania doped CA2114 (Ge)	as above	60%	0.3	$1x10^{-4}$	100%	2.35	$1.4x10^{-3}$
Germania doped CA3555 (Ge) cut-off 900nm	as above	76 %	0.16	$1.5x10^{-4}$	100%	1.62	$2.1x10^{-3}$
Boron doped CI (B/Ge)	as above	90%	0.42	$1.5x10^{-4}$	100%	3.0	$2.5x10^{-3}$
Boron doped CII (B/Ge)	as above	94%	0.40	$1.6x10^{-4}$	100%	3.5	$2.7x10^{-3}$
Boron doped CIII (B/Ge)	as above	95%	0.43	$1.7x10^{-4}$	100%	5	$3.3x10^{-3}$

Table 3-1 Summary of fibres used including fibre source, maximum obtained reflectivities (for grating lengths of 4-5mm), corresponding bandwidths and calculated values for the amplitude of refractive index modulation (Δn).

Table 3-1 summarises the fibres that were used for grating fabrication. Typical values for the non-hydrogenated and hydrogenated cases for the maximum achieved reflectivity and corresponding refractive index modulation (Δn) are given for ~4-5mm long gratings in eight different fibres. Also given are the approximate reflection bandwidths (Δλ FWHM)

that these figures correspond to. The values were obtained by fitting experimental data for the maximum reflectivity and the corresponding bandwidth (FWHM) to predicted values resulting from the coupled mode theory given in Chapter 2. Values for the reflectivity were derived from the loss in transmission observed using an optical spectrum analyser, Chapter 2.4.1.

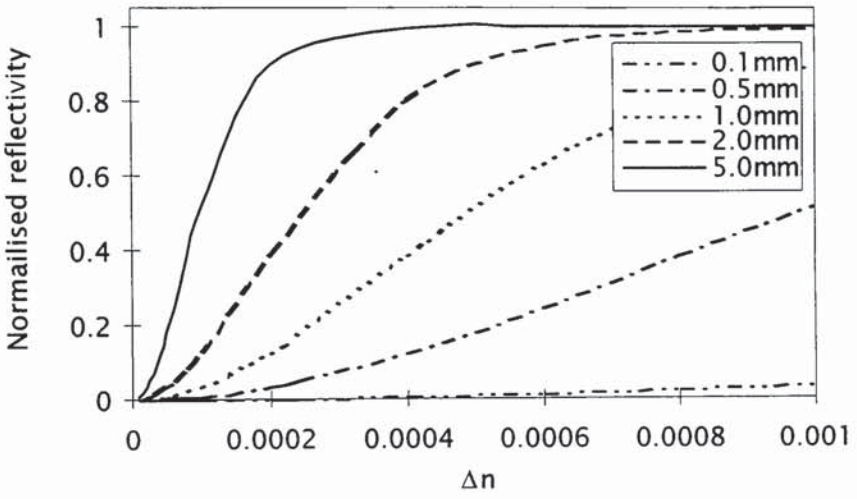

Figure 3-1 Normalised reflectivity as a function of the amplitude of refractive index modulation, Δn, for gratings of lengths 0.1, 0.5, 1.0, 2.0 and 5.0mm.

With reference to the values of Δn given in Table 3-1 these values can be related to the maximum values for the grating reflectivity predicted by the model in Chapter 2. Figure 3-1 plots the modelled normalised reflectivity for different grating lengths of 0.1, 0.5, 1.0, 2.0 and 5.0mm and for values of Δn up to $1x10^{-3}$ which is slightly above the current limit for non-hydrogenated fibre photosensitivity. The graph shows very clearly that even with heavily germania doped fibres gratings lengths approaching 5mm are required if reflectivity in excess of 80% are to be reached.

Figure 3-2 plots the same parameters as Figure 3-1 but encompasses the values attained by hydrogenated fibres. The hydrogenated standard fibres reach Δn values of $\sim 5x10^{-4}$ which means that for a 5mm grating the reflectivity has jumped from <5% in the non-hydrogenated case to

~100%. For the hydrogenated boron doped fibre 100% reflectivity can be obtained for gratings that are less than 0.5mm in length.

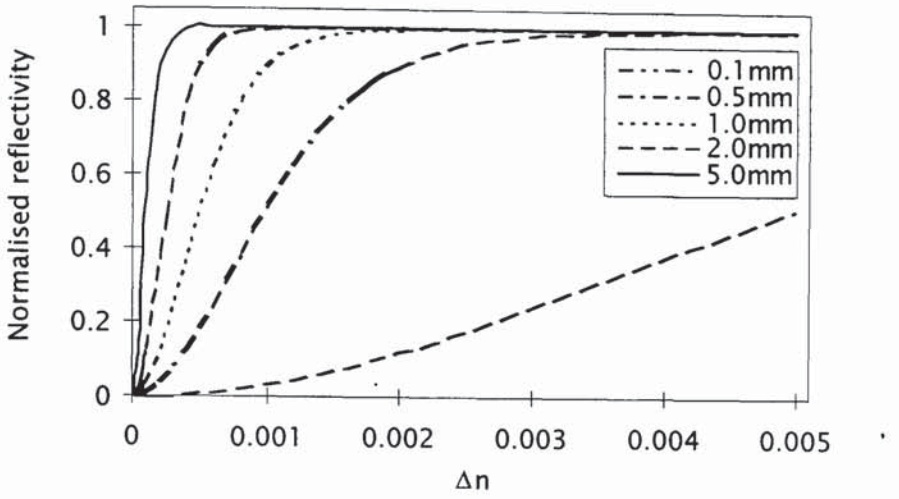

Figure 3-2 Normalised reflectivity as a function of change in refractive index for gratings of lengths 0.1, 0.5, 1.0, 2.0 and 5.0mm.

3.3 Fabrication of Uniform Gratings

Uniform gratings have been fabricated using the experimental arrangement shown in Figure 3-3. An additional mirror has been introduced by some other researchers to preserve the spatial parity of the interfering beams. This has been found unnecessary in the work here. However, it may be more important for excimer lasers where the beam quality and coherence are poor than for CW lasers. Where the two beams intersect an interference pattern is set up that gives fringes that are parallel to the kite bisector. A photosensitive fibre is placed at the point of intersection and exposed for a time that depends on the fibre photosensitivity. The induced refractive index follows the same periodicity as the interference fringes.

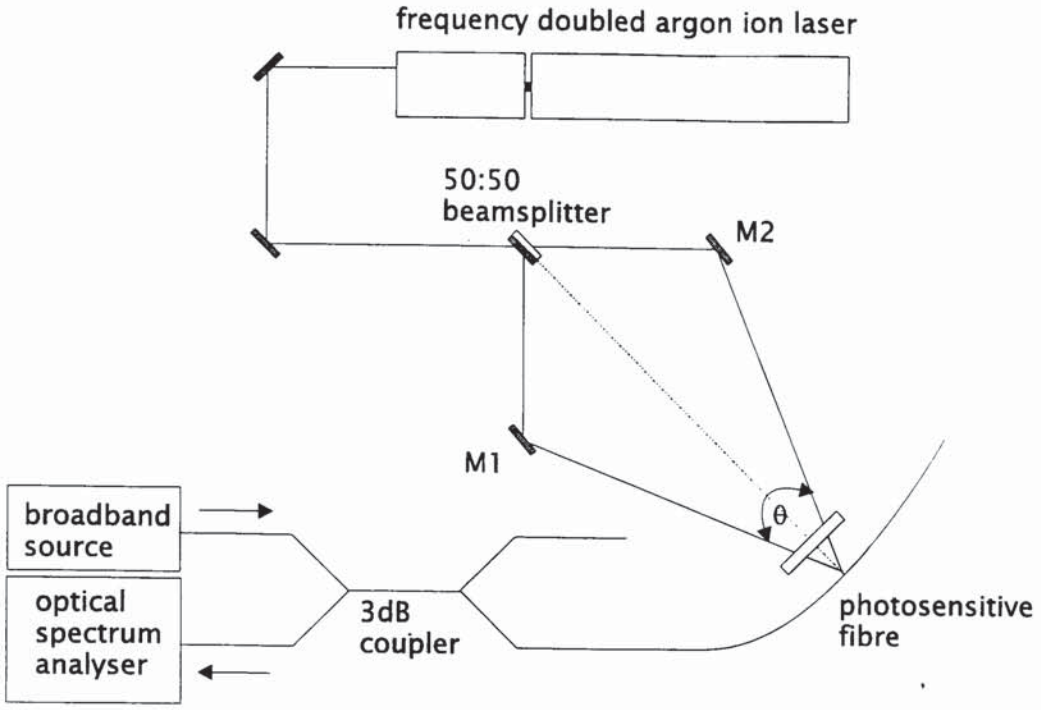

Figure 3-3 Kite-shaped interferometer for the fabrication of uniform-period gratings.

A frequency doubled argon ion laser is used to provide ultraviolet (UV) radiation at 244nm. The laser consists of a standard Spectra Physics 12W argon ion laser with the front reflector removed and a replacement output coupler that is situated on the far side of a frequency doubling BBO crystal and guiding and focusing optics. The optimised output power at 244nm is up to 200mW. In addition to the UV beam approximately 300mW of unconverted blue/green radiation at 488nm was available to pump an erbium fluorescence source used for in-situ monitoring of gratings in the 1450-1650nm range.

Beam steering optics were used to produce a horizontal beam at the correct height for the interferometer. An aperture was occasionally inserted to select the central portion of the beam to minimise the variation of intensity across its width. The linear output beam polarisation was rotated, using a half waveplate, to give vertically polarised light. The correct polarisation is achieved by rotating the half wave plate until the reflection from a glass plate set at Brewster's angle was minimised. Using vertical polarisation simplifies the interference conditions in the interferometer since the polarisation is not inverted on

every reflection and hence the number of reflections that each beam experiences need not be equal.

The Bragg wavelength of the grating produced is selected by altering the angle between the incident UV beams. This is done by changing the distance between mirrors M1 and M2 and the beamsplitter. Alternatively, to make small adjustments to the wavelength, the fibre holder can be moved backwards or forwards on a translational stage and then the mirrors rotated to optimise the beam overlap area.

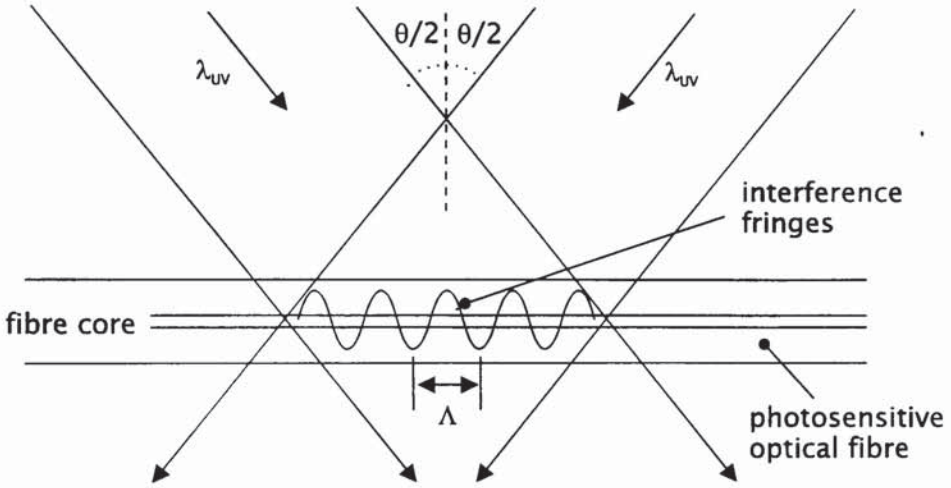

Figure 3-4 Interfering wavefronts resulting in a periodic intensity pattern coincident with the fibre core.

The grating spacing, Λ, is equal to the spacing of the interference fringes which is related to the fabrication wavelength, λ_{UV}, and the angle between the two beams, θ, such that

$$\Lambda = \frac{\lambda_{UV}}{2\sin\theta/2}$$

Equation 6

Light travelling down the fibre will interact with this refractive index modulation and will be reflected only if the Bragg condition for

constructive interference is met. For a fibre grating the first order Bragg condition can be expressed by

$$\lambda_B = 2n_{eff}\Lambda$$

Equation 7

i.e. the wavelength of the reflected light λ_B is determined by the grating spacing Λ. The value of n_{eff} is given by the average refractive index experienced by the mode travelling down the fibre. Figure 3-5 shows the variation in Bragg wavelength of the fabricated grating as the two mirrors are moved away from the beamsplitter. These values have been calculated by assuming the beamsplitter to be a constant distance, 20, 30 or 40cm, from the fibre. The fibre refractive index was taken to be 1.46.

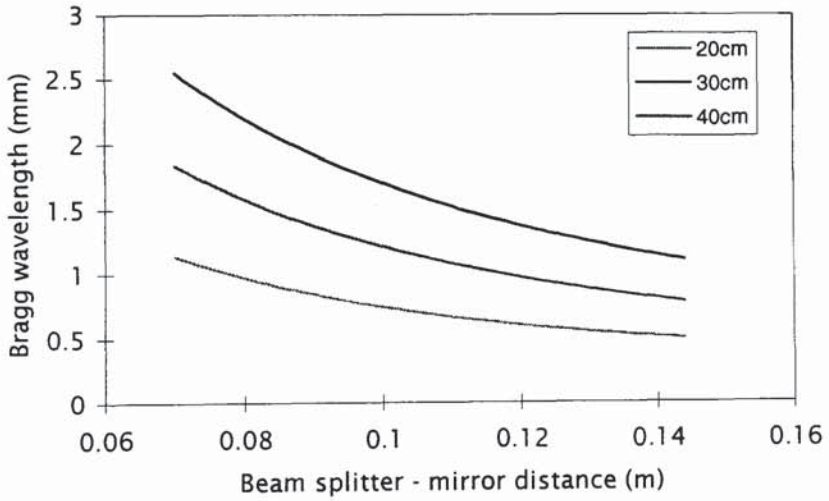

Figure 3-5 Calculated variation in the Bragg wavelength as the mirror positions are altered. The values were calculated for beamsplitter to fibre distances of 20, 30 and 40cm.

For fine-tuning the grating wavelength it was found that it was more accurate to move the fibre mount along the kite bisector and then rotate the mirrors to overlap the beams at the fibre. Figure 3-6 shows the Bragg wavelength shift achieved by moving the fibre mount along the kite bisector where the mirrors are positioned 8.3cm from the beamsplitter. For large shifts in wavelength this method of changing the wavelength is

generally avoided because it requires re-alignment of the focusing lenses.

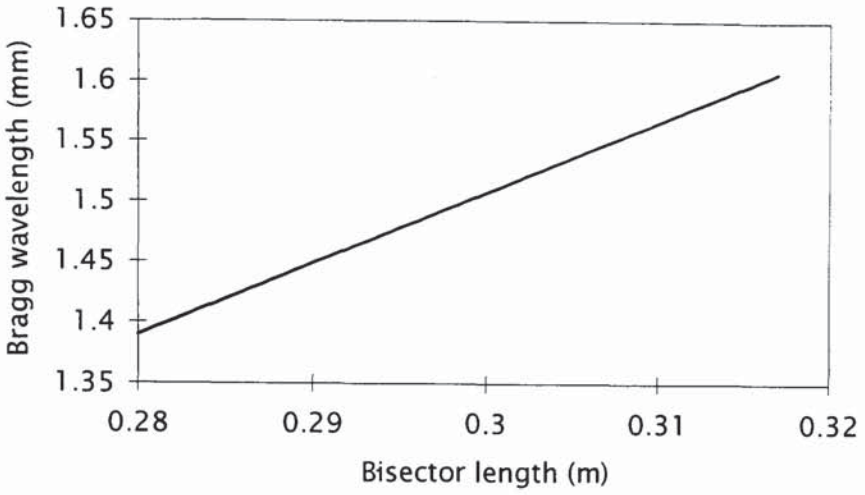

Figure 3-6 Calculated variation in the Bragg angle as the fibre mount is moved away from the beamsplitter. The mirrors were taken to be 8.3cm from the beamsplitter.

The alignment of the two UV write beams for the holographic formation of fibre gratings is critical. Good fringe visibility is required to maximise the strength of the grating; any decrease in the visibility will result in a decrease in the maximum refractive index modulation that is obtainable. In setting up the interferometer it is therefore vital to ensure that every component is correctly aligned and on-axis, this can be checked by using back reflections from each component as they are introduced. Also, the optical path lengths of each arm of the interferometer must be equalised to achieve good fringe visibility and to avoid chirping effects from the two beams having unmatched divergence.

To ascertain that the path lengths are equal the fibre mount was transversed in steps normal to the site bisector. When the mirrors were then rotated to give a good beam overlap the path length of each arm was changed very slightly. The average of the reflectivities of several gratings made at any one point was taken to provide a relative measure of the beam visibility. The interferometer should be then set to the position of gratings with maximum reflectivity.

The response of an ideal grating, i.e. one that is uniform in period and amplitude along the entire grating, should, from Chapter 2, show prominent sideband structure. In reality, holographic systems do not, in general, produce such gratings. The amplitude of the refractive index modulation is affected by the profile of the fabricating laser beam and a shading effect occurs which tapers the modulation profile towards the edges of the grating. This results in so-called uniform gratings being very slightly chirped with the result of suppressing the sidebands. Figure 3-7 shows the reflection and transmission profiles of two ~5mm long gratings fabricated in (a) boron doped fibre (CIII) and (b) germania doped fibre (CA2114) that are typical of uniform gratings from this set-up.

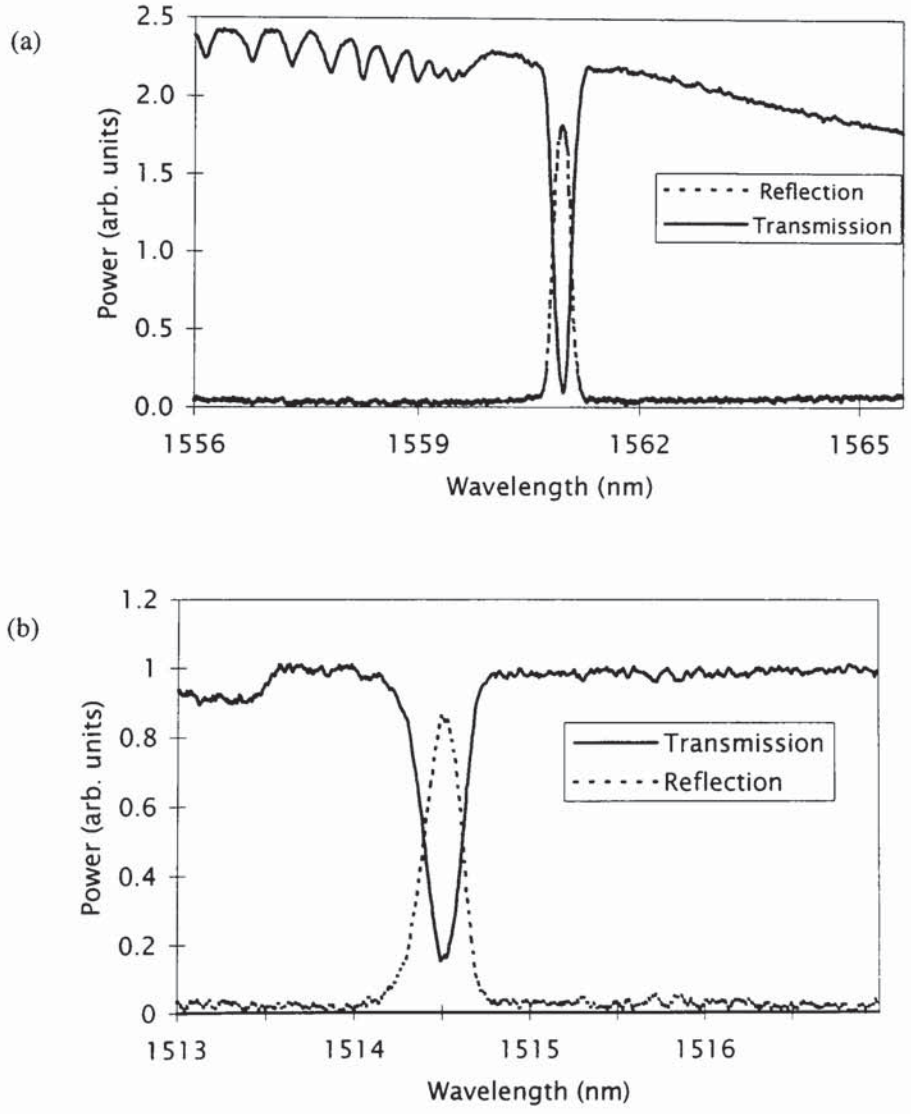

Figure 3-7 Uniform-period gratings ~5mm in length, fabricated in (a) boron doped fibre (CIII) and (b) germania doped fibre (CA2114).

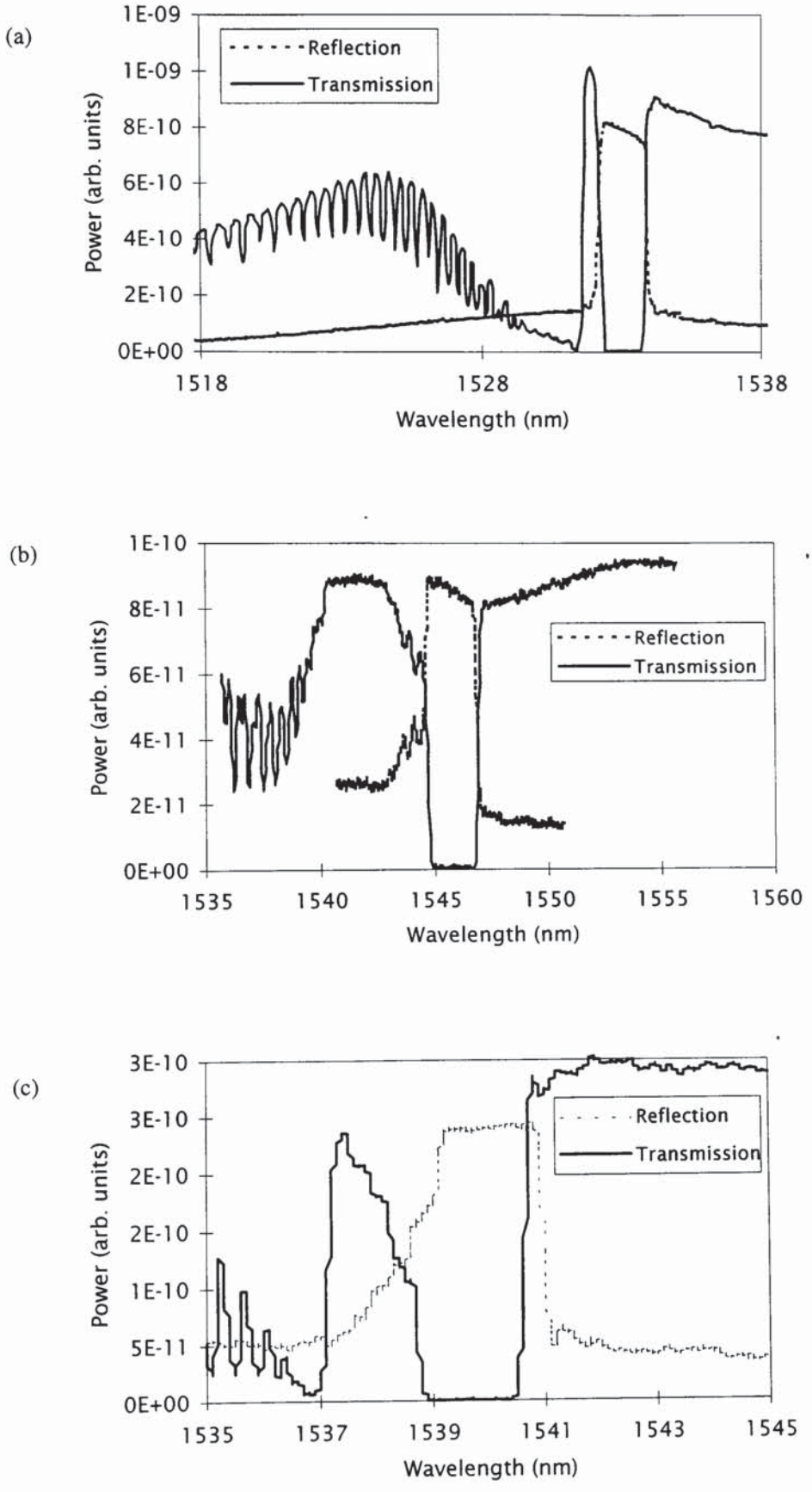

Figure 3-8 Reflection and transmission profiles of ~5mm gratings fabricated in hydrogen-loaded (a) BT standard fibre, (b) germania doped fibre (CA2114), (b) boron doped fibre (CIII).

As mentioned previously, hydrogen loading the fibres enhances the fibre photosensivity and enables ~100% reflecting gratings to be fabricated. Figure 3-8 shows the profiles of uniform gratings fabricated in hydrogen-loaded (a) BT standard fibre, (b) germania doped fibre (CA2114) and (c) boron doped fibre (CIII). Previous to the UV exposure the fibres were placed in a hydrogen at a pressure of 130 atmospheres and room temperature for six days, the gratings were ~5mm long. The gratings exhibit bandwidths of 1.65, 2.03, 2.42nm respectively. The increase in bandwidth is an indication of increasing fibre photosensivity.

The transmission plots show considerable short wavelength loss due to modal outcoupling. Grating (b), written in the germania doped fibre (CA2114) shows less short wavelength loss than grating (a), this is due to the fact that the fibre has a higher numerical aperture and so is more strongly guiding.

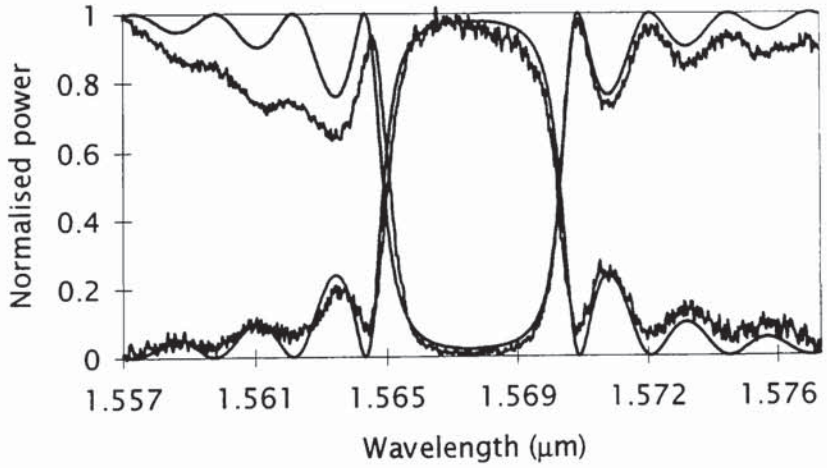

Figure 3-9 Transmission profile and reflection profile of a 0.37mm grating. The smooth black line is a theoretical fit.

Using an aperture to select only the centre of the laser beam decreases the shading effect and increases the visibility of the sidebands. Figure 3-9 shows the reflection and transmission profile of a much shorter grating ~0.4mm in length fabricated in hydrogen-loaded boron fibre (CIII). The grating reflectivity is approaching 100% and the bandwidth is much broader (~4.7nm FWHM) than the gratings shown in Figure 3-8 as

a consequence of the grating length. Since only the central portion of the beam was used to fabricate the grating there was no longer a significant amount of shading in the refractive index profile. Consequently, the sideband structure can be seen and this fits well with the modelled response from Chapter 2 shown by the smooth line on the graph.

Short gratings of reasonable strength can be fabricated by using hydrogenated boron doped fibre and the effect of grating length on the shape of the response can be illustrated. Three gratings of lengths 0.96, 0.37, 0.07mm were fabricated. The grating lengths were estimated by measuring the aperture width and then determined more accurately, using the results from the coupled mode theory given in Chapter 2, by matching the bandwidth and sideband positions of the grating response. The grating reflection profiles are shown in Figure 3-10. As the grating length decreases the response becomes progressively weaker and spreads over a broader bandwidth. The magnitude of the refractive index modulation was estimated from Chapter 2 to be in the region of 3-4x10^{-3}.

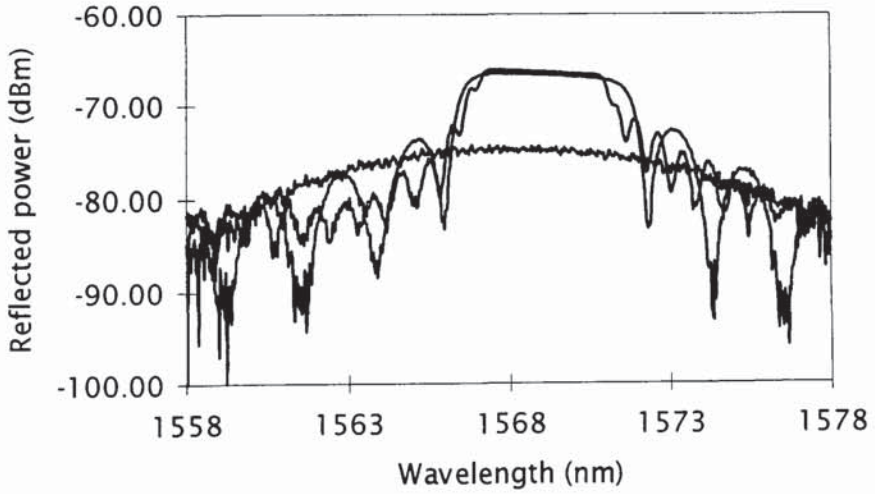

Figure 3-10 Reflection profiles of linear gratings of lengths 0.96 (narrowest), 0.37mm and 0.07 (widest). The sidebands for the 0.96mm grating are reduced in magnitude because of shading due to the UV laser beam profile.

3.4 Grating Evolution as a Function of Time

Figure 3-11 shows the evolution of the transmission spectrum of a grating fabricated in hydrogenated boron doped fibre. An increase with time of loss in the transmission profile due to the grating increasing in strength is seen towards the centre of the plot. On the left hand side of the plot there is an asymmetric loss profile which also increases with time and is due to modal outcoupling, (see Chapter 2.2).

It was found that the reflectivity evolution of gratings follows a general trend that is illustrated by Figure 3-12. Similar results were later published by Niay *et al*[65] and Xie *et al*[63]. The reflectivities of gratings written in boron doped fibre (CI) with exposure powers of 10, 20 and 60mW were recorded for a time period of 600s. After a rapid initial growth the increase in grating reflectivity slows and eventually reaches a maximum. The grating reflectivity then declines due to saturation of the photosensitivity. The speed of this process is determined primarily by the photosensitivity of the fibre but also by the alignment and stability of the interferometer.

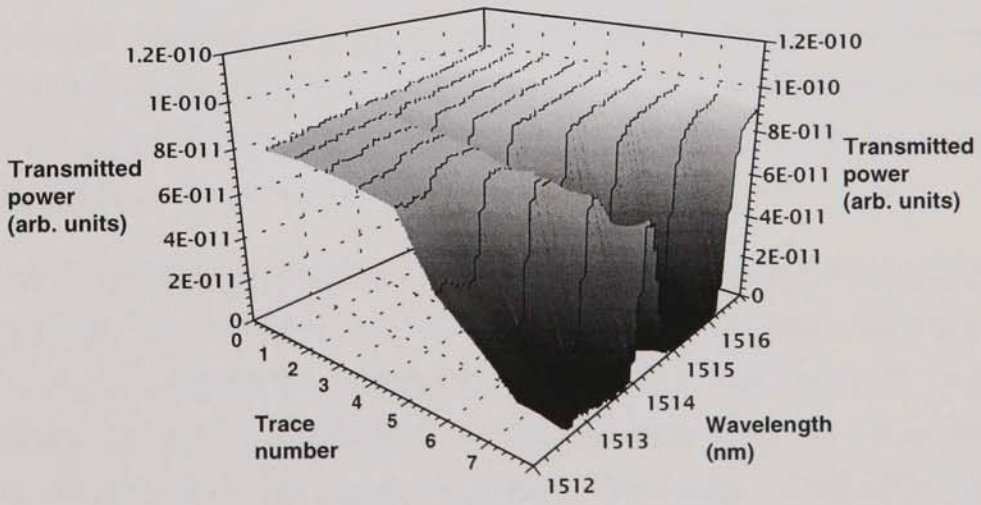

Figure 3-11 Evolution of the transmission spectrum during UV exposure of a grating fabricated in hydrogenated boron doped fibre. An increase in transmission loss due to reflection (symmetric dip) is accompanied by increasing short wavelength loss (asymmetric).

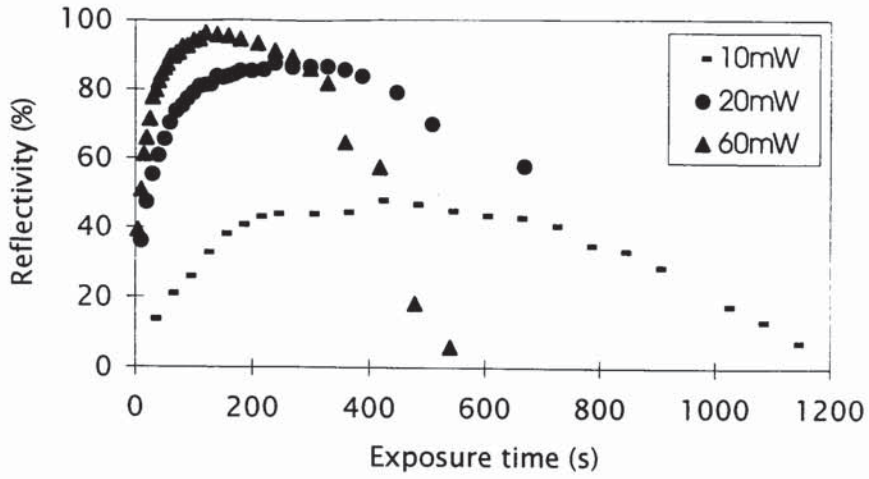

Figure 3-12 Reflectivity evolution of gratings written with exposure powers of 10, 20 and 60mW. The reflectivity grows as the refractive index modulation increases in amplitude and then falls as saturation occurs. The maximum reflectivity increases with exposure power.

The maximum achieved reflectivity has been found to vary with writing power. There are several possible reasons for this effect. There may be small instabilities within the interferometer but this is unlikely since exposure times in excess of 30 minutes have been successful in grating fabrication. Or, there may be a nonlinear process occurring; for example, a heating effect[85] that increases the rate of index growth at higher powers. Alternatively, there could be some difference in the exposure conditions for each grating despite them being fabricated consecutively. The question of which of these three possibilities is the most likely will be returned to at the end of this section.

As the grating grows there is also a shift in the Bragg wavelength of the grating. This is due to an increase in the effective refractive index of the fibre core during the exposure. This effect is illustrated in Figure 3-13 where the Bragg wavelength for the same gratings described above are measured over the exposure period. The Bragg wavelength decreases rapidly initially and then slows down as the photosensitivity saturates.

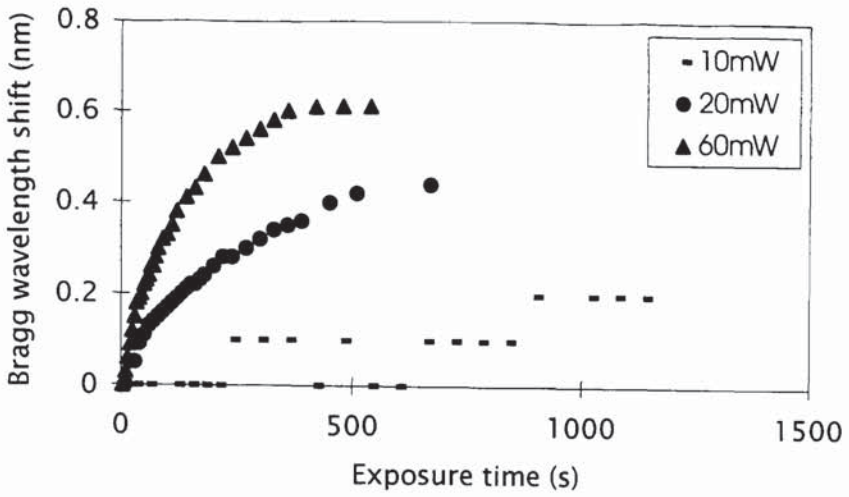

Figure 3-13 Increase in Bragg wavelength during exposure for write powers of 10, 20 and 60mW.

The shifts in the Bragg wavelength are due to a corresponding increase in the effective refractive index of the core of 1.89×10^{-4}, 4.16×10^{-4} and 5.78×10^{-4} for write powers of 10, 20 and 60mW respectively. The index change is proportional to the shift in wavelength and follows the same trend here as that observed by Hand *et al* [58]. The Δn values can also be calculated from the maximum reflectivities, shown earlier in this section, and are 8.3×10^{-5}, 1.67×10^{-4} and 2.4×10^{-4} respectively. There is a discrepancy between the change of refractive index and the Δn contributing to the grating strength. In this case the Δn value is on average 0.42 times the value of the total refractive index change. Dong *et al* [86] have stated that for a linear process this factor would be 0.5 which would decrease depending on the fringe visibility. It would seem that this data broadly supports a linear relationship between exposure power and refractive index change with the possibility of the fringe visibility being less than 100%. This is in contrast to Dong's results obtained using a pulsed laser source with high peak powers where the refractive index growth was non-linearly dependent on exposure power and a maximum of ~20% of the available refractive index change could be accessed.

The data gained from the wavelength shift during exposure can be used to shed light on the question of why the maximum reflectivities for the

gratings written at different powers were unequal. The fact that the measured wavelength shifts by unequal amounts for gratings written at different powers indicates that there is some inherent power dependency and that it was not instabilities or different exposure conditions that were causing a depressed maximum reflectivity for low write powers. Both of these factors would have limited the maximum grating reflectivities but the maximum change in the fibre refractive index would have been equal unless there was something else contributing to the refractive index changes.

3.5 The Effect of Laser Write Power on Exposure Time

The power of the write laser beam affects the length of time that it takes to write a grating. Certainly for non-hydrogenated fibre there appears to be a linear inverse power relationship between the power of the ultra violet beam and the exposure time required for a grating to reach a set reflectivity. Figure 3-14 shows the inverse of the exposure time required to fabricate 100% reflecting gratings in hydrogenated and 80% reflecting gratings in non-hydrogenated boron doped fibre (CII) plotted for different laser output powers. The hydrogenated fibre was hydrogen loaded under a pressure of 120 atmospheres at room temperature for five days.

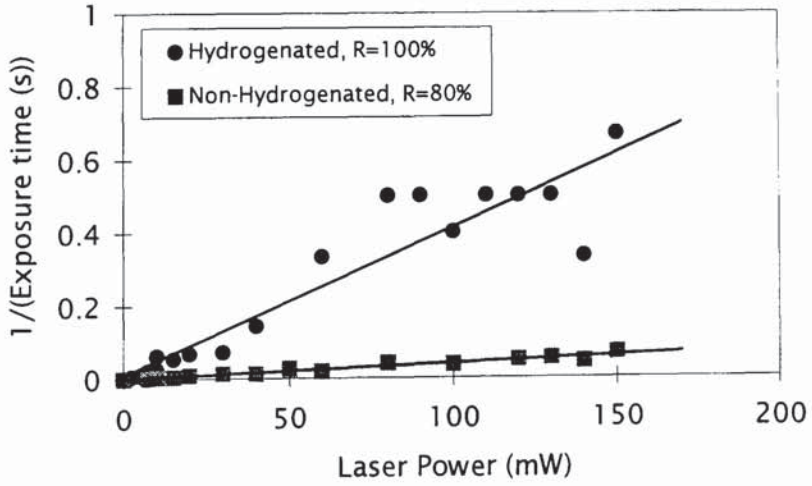

Figure 3-14 Plot of the inverse exposure time in seconds for a grating to reach 100% for the hydrogenated fibre and 80% for the non-hydrogenated fibre against the laser power in mW.

The large amount of scatter seen on Figure 3-14 at high laser powers for the hydrogenated fibre is due to the very small exposure times (~2 seconds) and consequent mensural difficulties. The exact relationship is determined by the photosensitivity of the fibre; ideally the exposure time will be as short as possible to limit environmental instabilities.

By plotting the exposure times directly, for the hydrogenated and non-hydrogenated fibre, an idea of the required exposure powers becomes apparent. Figure 3-15 illustrates typical results. The graph shows that for boron doped fibre (CIII) the difference between using 100 and 150mW of power is very small in terms of the exposure time. However, by dropping below 50mW the exposure times become significantly larger.

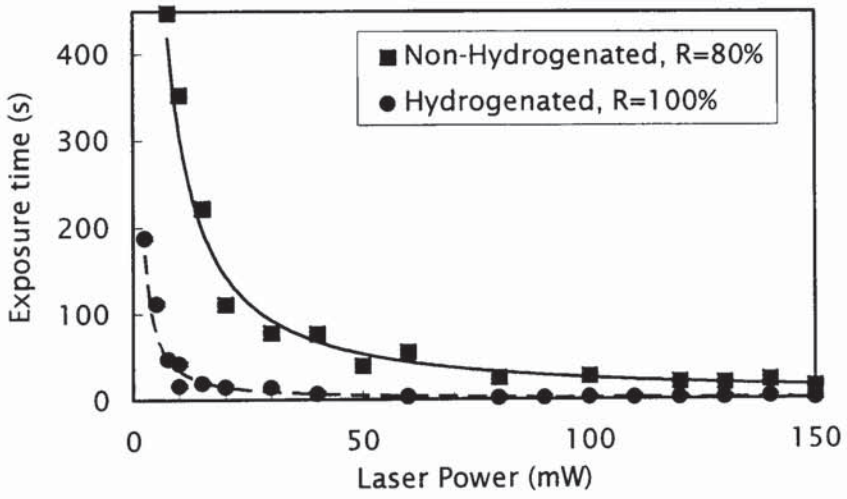

Figure 3-15 Power dependence of grating growth in non-hydrogenated boron-doped fibre (CIII) and in the same fibre hydrogen-loaded.

For the hydrogenated case there is still an inverse relationship between laser power and exposure time but much lower powers can be used to fabricate a grating with the same exposure time. 20mW of laser power was sufficient to fabricate a linear grating in around the same time as an exposure of 150mW with the non-hydrogenated fibre.

3.6 *Effect of Hydrogenation on Post Exposure Stability*

Gratings fabricated in hydrogen-loaded fibre shift in wavelength over time. During UV exposure some of the hydrogen is combined into the glass structure, and a variable amount of uncombined gas remains. The uncombined hydrogen diffuses out through the fibre cladding into the atmosphere. This diffusion causes the refractive index of the fibre to change over time. There are two diffusion processes occurring[87]: after a grating is made there is less uncombined hydrogen in the core than in the cladding so hydrogen diffuses inwards; at the same time hydrogen will also diffuse out of the cladding into the atmosphere. The inward diffusion involves short distances and so occurs over a short time period (a few hours), causing an increase in the refractive index of the core and an up-shift in the Bragg wavelength. The outward diffusion of hydrogen into the atmosphere involves greater distance and so takes longer (a few weeks). The concentration of the hydrogen decreases and so the Bragg response shifts to shorter wavelengths. As a consequence, at room temperature, the grating wavelength shifts upwards initially over the first couple of hours and then downwards for the following few weeks. This process is temperature dependent and so can be accelerated by keeping the fibres at an elevated temperature.

The magnitude of the wavelength shift is dependent on the amount of unreacted hydrogen that remains in the core post exposure. A grating that incorporates a small percentage of the hydrogen into the permanent structure experiences a small up-shift in wavelength as a small amount of hydrogen diffuses in to replace the small amount 'lost'. This is followed by a large down-shift due to the subsequent out-diffusion resulting in the final wavelength being several nm lower than the post-exposure wavelength.

A grating that incorporates a large percentage of the available hydrogen experiences a large upward wavelength shift as a large amount of hydrogen diffuses into the core, the out-diffusion will then lower the wavelength but to only just below the initial post-exposure wavelength. It is the difference in the concentration of gaseous hydrogen between the core and the atmosphere that determines the magnitude of the

absolute wavelength shift. The difference between the core and cladding concentrations is what determines the maximum up-shift in wavelength.

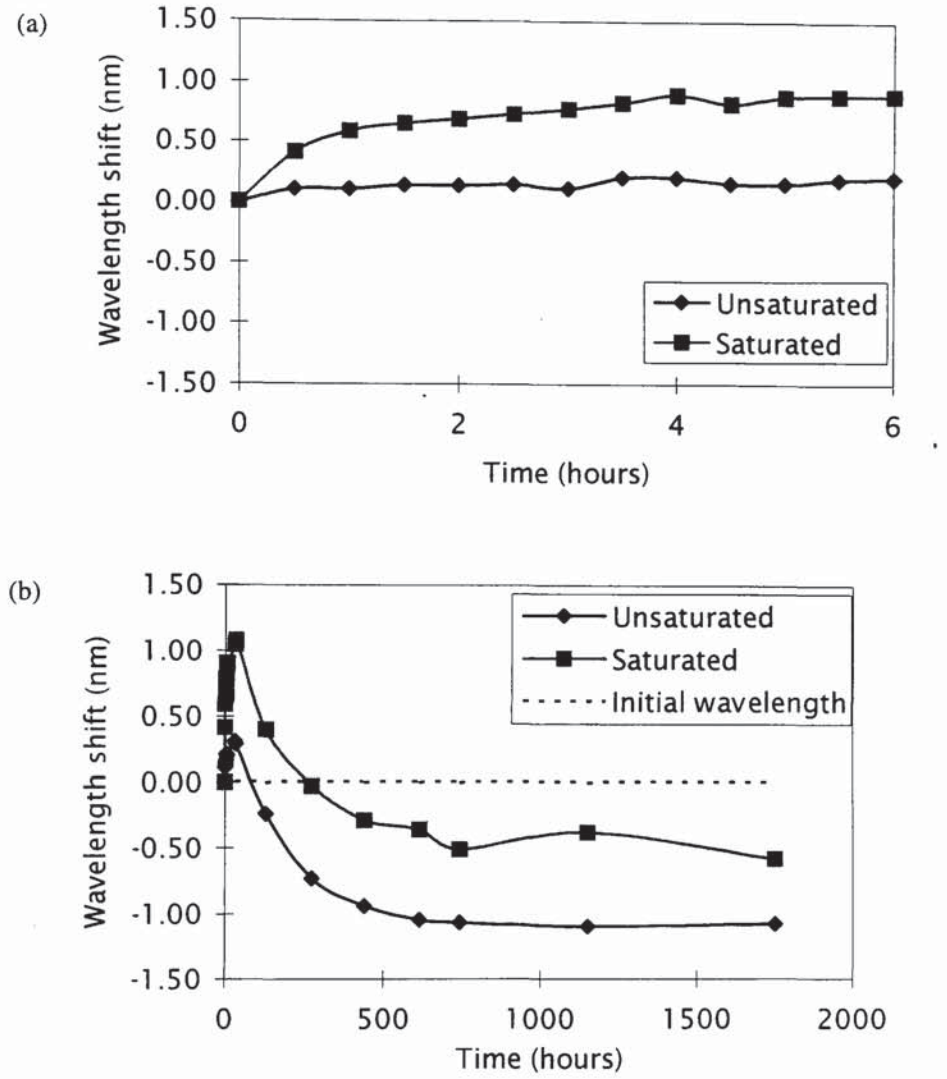

Figure 3-16 Post-exposure wavelength shift of linear gratings written in hydrogenated boron fibre. Graph (a) follows the wavelength shift over the first six hours, graph (b) over 1750 hours.

Figure 3-16 shows the wavelength shift of two linear gratings, written in hydrogen-loaded boron doped fibre. The first grating was fabricated with a long exposure so that it had a strong reflectivity, the other was an unsaturated grating with weak reflectivity. The initial Bragg wavelengths were measured on a spectrum analyser. The gratings were left at room temperature and the subsequent peak wavelengths were monitored at regular intervals. The Bragg wavelengths of both the gratings increases

after the exposure for the first few hours and then the shift is reversed and the peak wavelength starts to shift to shorter wavelengths over the following two weeks. The peak wavelength of the unsaturated grating is seen to shift by only small amounts initially but then drops to a wavelength over 1nm below the initial value. The peak wavelength of the saturated grating up-shifts by over 1nm but then decreases in wavelength to approximately 0.5nm below the initial wavelength.

The wavelength shifts for saturated and unsaturated gratings fabricated in hydrogen loaded BT standard fibre and germania doped fibre (CA2114) were also monitored. Similar trends in the wavelength shifts were observed.

Table 3-2 summarises the data for the three fibres and gives the maximum difference between measured wavelengths and the initial starting wavelength.

Fibre	Grating type	Maximum upward wavelength shift (nm) from t=0	Maximum downward wavelength shift (nm) from t=0
Boron doped	Unsaturated	0.31	1.08
	Saturated	1.08	0.58
Germania doped CA2114	Unsaturated	0.22	0.94
	Saturated	0.64	0.57
BT standard	Unsaturated	0.15	1.21
	Saturated	0.34	1.36

Table 3-2 Summary of wavelength shifts observed with saturated and unsaturated gratings in different hydrogenated fibres.

This wavelength shift causes problems when trying to meet tight wavelength specifications. In order that the grating experiences the least eventual shift in wavelength, the fibre and amount of hydrogen-loading should be selected so that as much of the hydrogen as possible is used in the reaction.

3.7 Conclusions

Many uniform gratings have been successfully fabricated at wavelengths between 850nm and 1600nm. For short gratings where an aperture has been used to select the central part of the laser beam during fabrication the response agrees well with the predictions of grating response given by simple coupled mode theory in Chapter 2. The reflectivity has been shown to decrease as the grating length decreases and the bandwidth to correspondingly increase as predicted. Where a Gaussian profile laser beam is used to fabricate the grating the side bands are significantly suppressed by the resulting profile shading.

Photosensitivity is strongly fibre dependent. Germania increases the photosensitivity and the addition of boron enhances it still further. This photosensitivity determines the maximum reflectivity that can be achieved for a grating of given length. Hydrogen loading increases the photosensitivity by a factor of 10. The change in the refractive index achieved during exposure to UV radiation appears to be power dependent. Increasing the exposure power increases the maximum reflectivity of resultant gratings.

Diffusion of the uncombined hydrogen occurs after grating fabrication. Initially the Bragg wavelength increases as hydrogen diffuses from the cladding to the core. Eventually the out-diffusion of the hydrogen from the fibre becomes the dominant process and the wavelength decreases.

4. Chirped Fibre Gratings

In this chapter three different techniques for holographically fabricating chirped gratings are presented. The techniques are not discussed in a chronological order but more in order of their usefulness to the applications described in Chapters 5 and 6.

The first technique discussed is based on the use of dissimilar interfering wavefronts to produce non-uniform fringe patterns[33,35], Section 4.1; the wavefronts are dissimilar in that they have unequal radii of curvature. This technique has been extensively studied and found to provide a powerful and flexible tool for fabricating chirped gratings with a wide range of parameters. Three different variations on the generalised optical arrangement of this technique are discussed in the context of three types of chirped gratings: superbroad gratings[35] (>100nm); narrow bandwidth linear chirped gratings[88] (0.2-30nm); and quadratic chirped gratings[88] (5-100nm). The first ever reported technique for holographically writing chirped gratings directly into the fibre core[38] is discussed in Section 4.2. A uniform grating is written into a piece of tapered fibre. The decrease in the fibre radius along the taper causes a reduction in the corresponding refractive index which in turn induces the chirp. An alternative method for fabricating chirped gratings is that discussed in Section 4.3. Again a set up used for producing uniform gratings is used but the fibre is deformed in some way to produce a curvature with respect to the interference fringes[36]. Section 4.4 concludes the chapter with a summary of all the techniques and their areas of application.

4.1 Two Beam Interference Using Dissimilar Wavefront Curvatures

Chapter 3 describes how a standard kite interferometer produces linear gratings where the angle of incidence between the two interfering laser beams remains constant across the width of the overlapping region. By introducing vertically mounted cylindrical lenses into the interferometer

arms, in the area indicated in Figure 4-1 the beams can either be made to diverge or converge and so create a dissimilarity in the wavefront curvatures. The angle of incidence between the two beams then varies along the width of the intersecting volume leading to a positional variation in the reflected wavelength along the length of the grating formed.

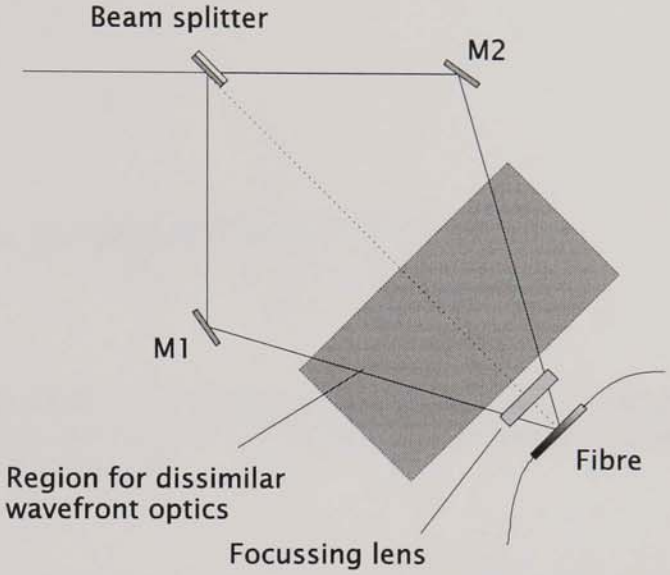

Figure 4-1 Arrangement for producing wavefronts with a dissimilarity in curvature for the fabrication of chirped fibre gratings. The shaded box indicates the general area in which lenses are placed to distort the plane wavefronts.

Figure 4-2 shows the geometry of a generalised dissimilar wavefront holographic set-up used to fabricate chirped gratings. The two UV beams are focused and intersect on the fibre plane centred at the origin. Defining z as the distance along the fibre from the origin, $D_{1,2}$ as the distances from the focal points to the origin, and $\phi_{1,2}$ as the angles between the beams and the grating plane, then the path difference ($\Delta L=L_1-L_2$) between the two beams at point z along the fibre can be expressed as

$$\Delta L = L_1 - L_2 = \sqrt{D_1^2 + 2 \cdot D_1 \cdot \cos(\phi_1) \cdot z + z^2} - \sqrt{D_2^2 - 2 \cdot D_2 \cdot \cos(\phi_2) \cdot z + z^2}$$

Equation 8

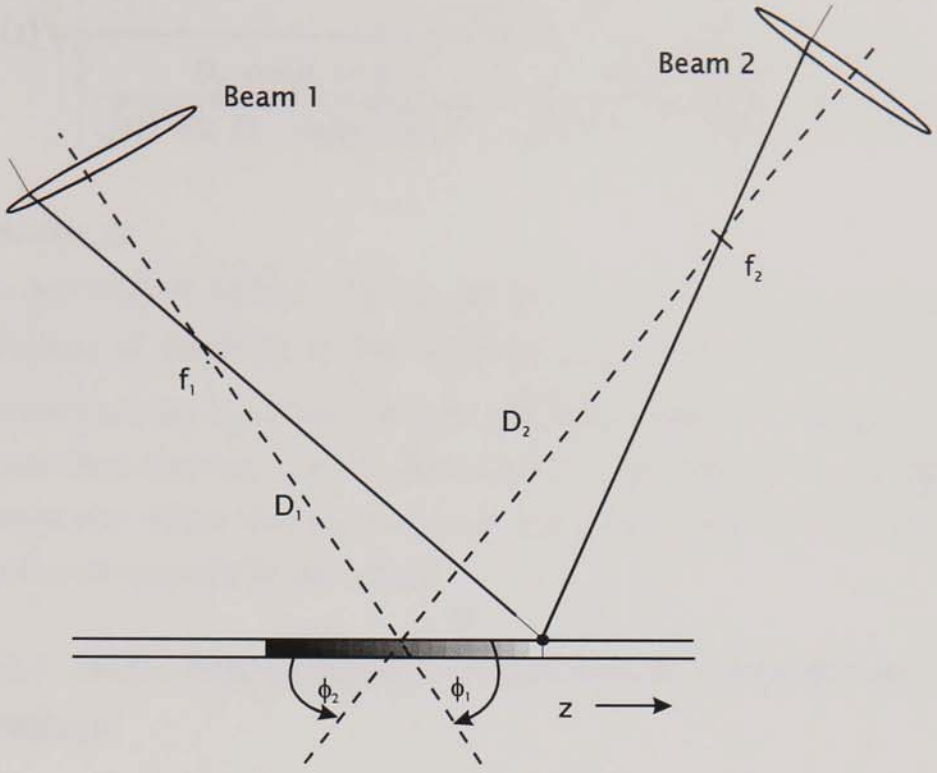

Figure 4-2 Generalised arrangement for the fabrication of chirped fibre gratings. The radius of curvature of the wavefronts of the beams is unequal causing a uneven interference pattern.

This expression uses geometrical optics and ignores diffraction effects. For light incident with wavevector, k, the phase difference will be $\Delta\phi = k \cdot \Delta L$, where $k = 2\pi\lambda_{UV}$. Substituting Equation 8 into the expression for the phase difference and differentiating with respect to z gives an expression for the fringe pattern in terms of the grating wavevector K(z) such that

$$K(z) = k \cdot \left[\frac{D_1 \cdot \cos(\phi_1) + z}{\sqrt{D_1^2 + 2 \cdot D_1 \cdot \cos(\phi_1) \cdot z + z^2}} + \frac{D_2 \cdot \cos(\phi_2) - z}{\sqrt{D_2^2 - 2 \cdot D_2 \cdot \cos(\phi_2) \cdot z + z^2}} \right]$$

Equation 9

where K(z) is connected to the grating fringe separation by the expression $K(z) = \frac{2\pi}{\Lambda(z)}$. Equation 9 can then be written in terms of grating fringe separation in terms of position z such that

$$\Lambda(z) = \frac{\lambda_{UV}}{\left[\frac{D_1 \cdot \cos(\phi_1) + z}{\sqrt{D_1^2 + 2 \cdot D_1 \cdot \cos(\phi_1) \cdot z + z^2}} + \frac{D_2 \cdot \cos(\phi_2) - z}{\sqrt{D_2^2 - 2 \cdot D_2 \cdot \cos(\phi_2) \cdot z + z^2}}\right]}$$

Equation 10

As mentioned before this is related to the Bragg wavelength as a function of position by the equation $\lambda_B(z) = 2n_{eff}\Lambda(z)$. D_1 and D_2 are determined by the divergence of the beams and so systems containing more than one lens can be described by Equation 10 by looking at the composite effect that lenses in any one arm of the interferometer have on the divergence of the beam.

4.1.1 Single lens approach for fabricating of superbroad gratings

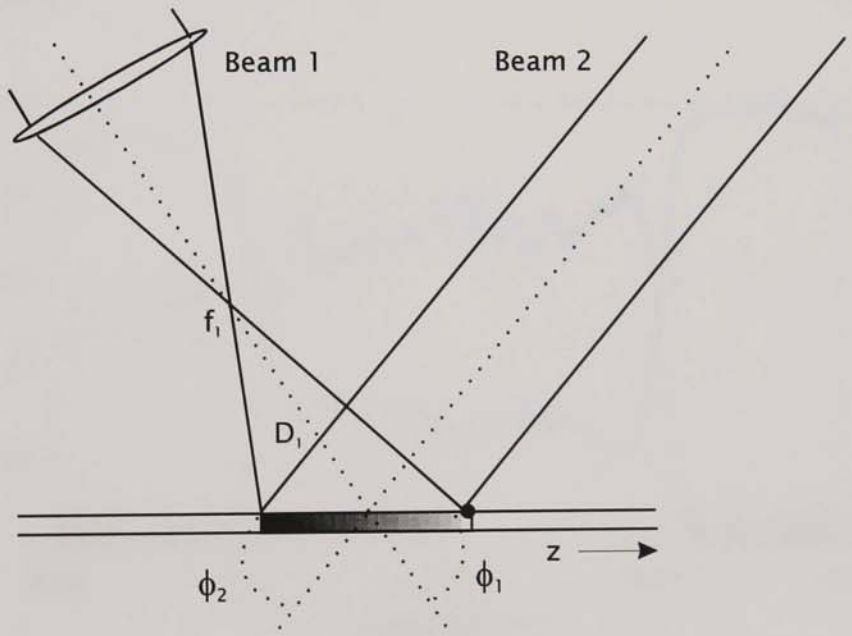

Figure 4-3 Optical arrangement for fabricating superbroad chirped gratings.

The simplest lens arrangement, Figure 4-3, gives the largest bandwidth gratings. A single lens positioned at twice its focal length away from the fibre in one of the interferometer arms produces one diverging wavefront. In this case, $D_2 \to \infty$, and Equation 10 simplifies to

$$\Lambda(z) = \frac{\lambda_{UV}}{\left[\frac{D_1 \cdot \cos(\phi_1) + z}{\sqrt{D_1^2 + 2 \cdot D_1 \cdot \cos(\phi_1) \cdot z + z^2}} - \cos(\phi_2)\right]}$$

Equation 11

Figure 4-4 shows the transmission and reflection profile of a superbroad chirped grating. The grating was fabricated in a germania doped fibre (CA2114) that had been hydrogen loaded for eight days at 110 atmospheres pressure and room temperature. The ~4mm long grating, centred at 1550nm, has a bandwidth of 104nm and is between 60-80% reflecting. It was fabricated using a lens with a focal length of 9cm that was positioned ~21cm from the fibre. The profiles show good reciprocity indicating that there is little loss due to modal outcoupling although there is a small amount of loss apparent on the short wavelength side of the transmission spectrum outside of the grating bandwidth.

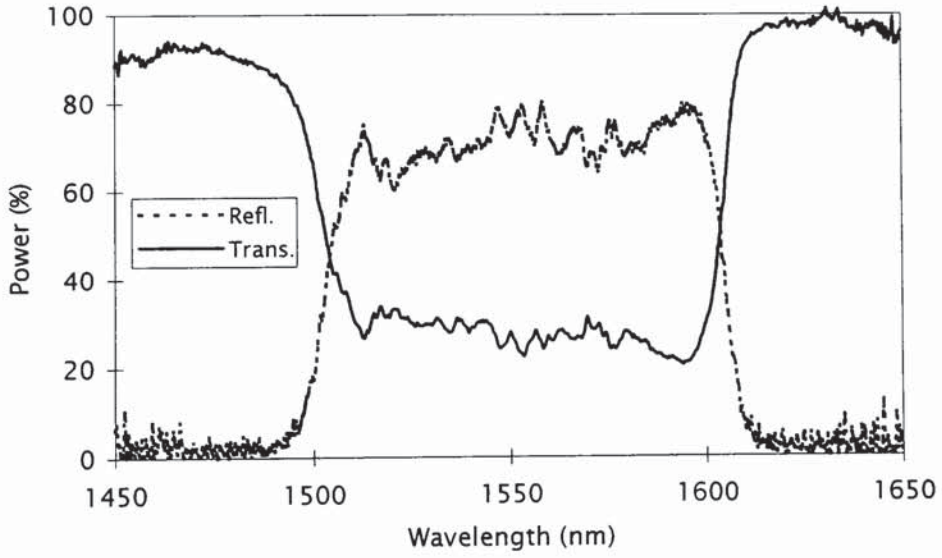

Figure 4-4 Transmission and reflection profile of a 4mm long superbroad chirped grating. The grating was fabricated using one cylindrical lens of focal length 9cm that was positioned approximately 21cm from the fibre.

Figure 4-5 illustrates the calculated relationship between wavelength and distance for the grating shown above. There is good agreement between the predicted and experimentally measured reflected

wavelengths. The calculations predict that reflected wavelength changes in a linear manner along the length of the grating.

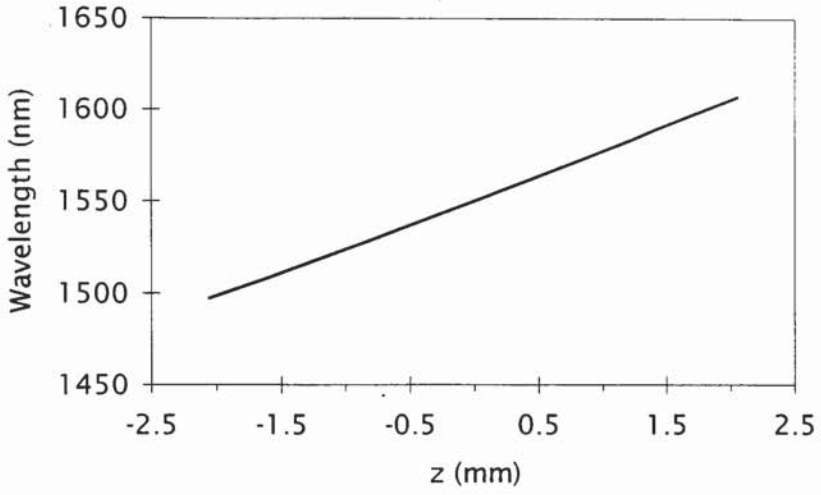

Figure 4-5 Calculated wavelength profile of a ~4mm superbroad grating with focal length f=0.09m. The lens is a distance x=0.21m away from the fibre.

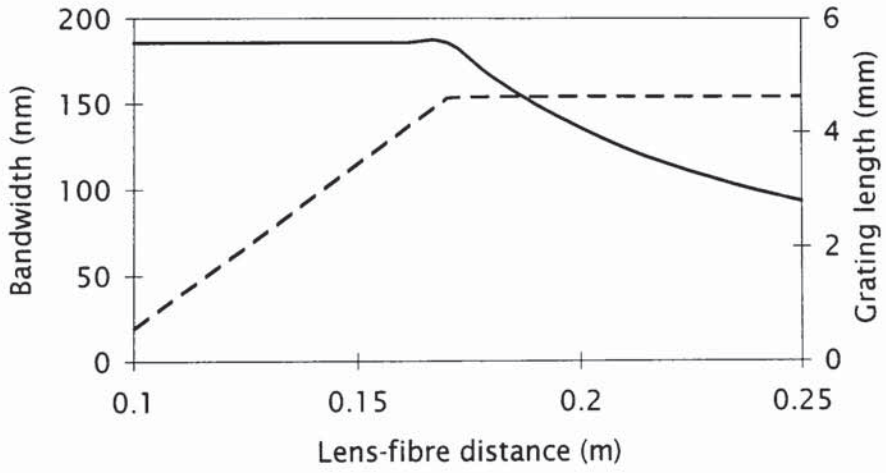

Figure 4-6 Calculated bandwidth variation produced as a 0.09m focal length lens is moved away from the fibre (solid line). The corresponding grating length determined by the size of overlap of the two beams (dotted line).

The optimum position to give the widest bandwidth gratings is for the lens to be just short of twice its focal length from the fibre. With a 9cm focal length lens experimental bandwidths of up to 185nm have been

achieved in this way with ~4.6mm long gratings. The relationship between grating bandwidth, grating length and lens positioning is illustrated in Figure 4-6. The lens is assumed to have a 9cm focal length and the beam width is 4.5mm.

The ideal situation is where both beams are the same size and overlap completely at the point of intersection; this occurs when the lens is at a distance between 0.17 and 0.18m from the fibre. Moving the lens further back from the fibre increases the beam size at the fibre and so decreases the angle variation across the overlapping region. This has the effect of decreasing the chirp and this is coupled with an increasing disparity in beam intensities as the diverging beam increases in width. Conversely, moving the lens forward decreases the beam size. The same chirp results but the grating length decreases along with an increasing mismatch in the intensities of the two beams. With two beams of different dimensions the fringe visibility decreases and so less efficient gratings with lower reflectivities can be fabricated.

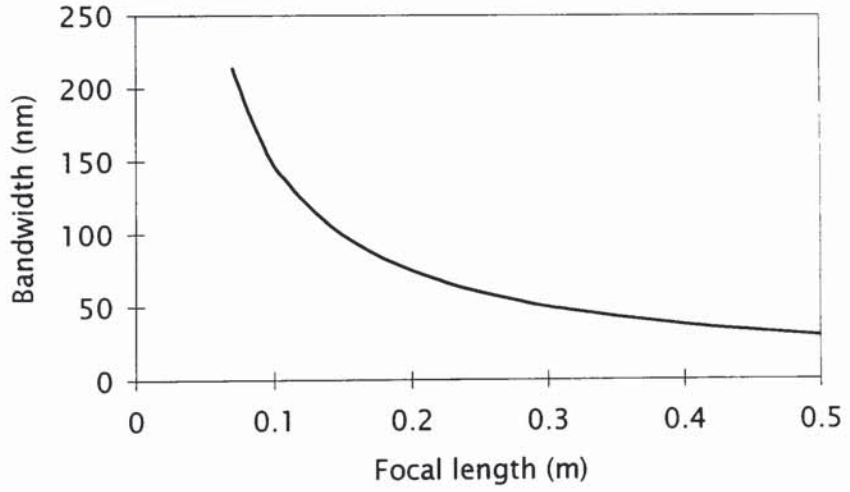

Figure 4-7 Calculated variation of the grating bandwidth fabricated with lenses of different focal length. The lenses are placed at twice their focal length (2f) from the fibre.

The scope over which this arrangement is applicable depends on two factors: that a range of different focal length lenses is available to give a range of bandwidths and that twice the focal length of the lenses is a smaller distance than the length of the interferometer arm. The calculated bandwidths that could be achieved with different focal length

lenses for gratings centred at 1550nm are shown in Figure 4-7. For small bandwidth gratings very long focal length lenses are required precipitating the need for a very large interferometer. For example, to produce a 30nm bandwidth grating at 1550nm a 50cm focal length lens placed 1m away from the fibre would be required. When it is considered that for many dispersion-type applications gratings of only a few nanometres bandwidth are required the size of the interferometer needed to accommodate the appropriate lenses becomes at best inconvenient and at worst unstable.

It was found that this set-up is only useful for fabricating superbroad gratings, such as those that reflect across the entire erbium fluorescence region. The technique relies heavily on the availability of a large number of different focal length lenses to give bandwidth flexibility. Moving the lens from the $2f$ position does alter the bandwidth of the grating but at the expense of markedly changing the beam width.

4.1.2 Telescope approach for the fabrication of linear chirped, small to medium bandwidth, gratings

As an alternative to the arrangement described in Section 4.11 two lenses can be used in one arm of the interferometer to produce a telescope, Figure 4-8. The telescope can be slightly detuned to give either a slowly diverging or slowly converging beam and so mimics the effect of introducing very long focal length lenses into the interferometer but requires very much less space.

Two lenses of equal focal length, mounted vertically, are required for the telescope. They are aligned in one arm of the interferometer at a distance of twice their focal length apart to give a unity magnification telescope configuration. The front lens should be introduced into the interferometer first and placed at a distance equal to its focal length away from the fibre. This keeps to a minimum the variation on the beam width incident on the fibre as the telescope is detuned. On introducing the second lens into the system it is moved back and forth until the focal positions of the incoming beam through the back lens and that of the reflected beam of the other interferometer arm through the front lens are coincident. This ensures the correct distance between the two

lenses. At this point the output beam of the telescope is collimated and the resulting interference pattern between the two beams is linear. The back lens mounting incorporates a translational stage so that the lens can be moved with precision along the path of the interferometer arm. To introduce a chirp the back lens is moved a small distance δx towards or away from the other lens.

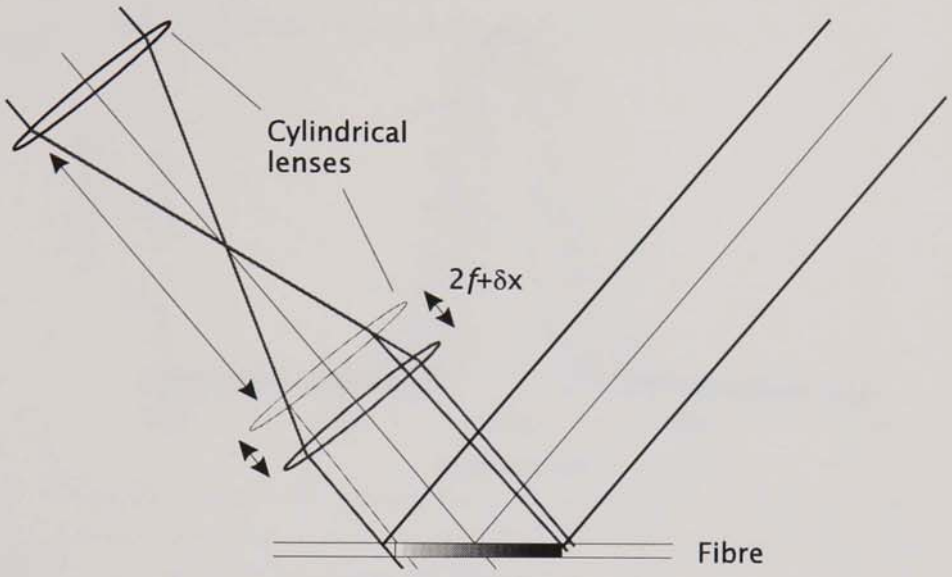

Figure 4-8 Telescopic arrangement to produce dissimilar wavefront curvatures.

The effective focal point of the lens system can be calculated using the paraxial lens formula. This value can then be subtracted from the distance that the front lens is from the origin to give a value for D_1 that can then be substituted into Equation 11. Where both lenses have equal focal lengths then $D_1 = d - \frac{f(a-f)}{(a-2f)}$. For a>2f the second term is positive and the beam is therefore converging, for a<2f the second term is negative and the beam is diverging.

With this telescopic technique it becomes simple to produce a succession of gratings that progressively show a small controlled increase in bandwidth. Figure 4-9 shows the reflection profiles of eleven gratings that were made consecutively with bandwidths over the range

0.5-22.9nm. The ~4.5mm gratings were fabricated in boron doped fibre (CIII) that was hydrogen-loaded for six days at 130 atmospheres pressure and room temperature. The back lens was moved a total distance of 12mm between fabricating the narrowest and broadest gratings.

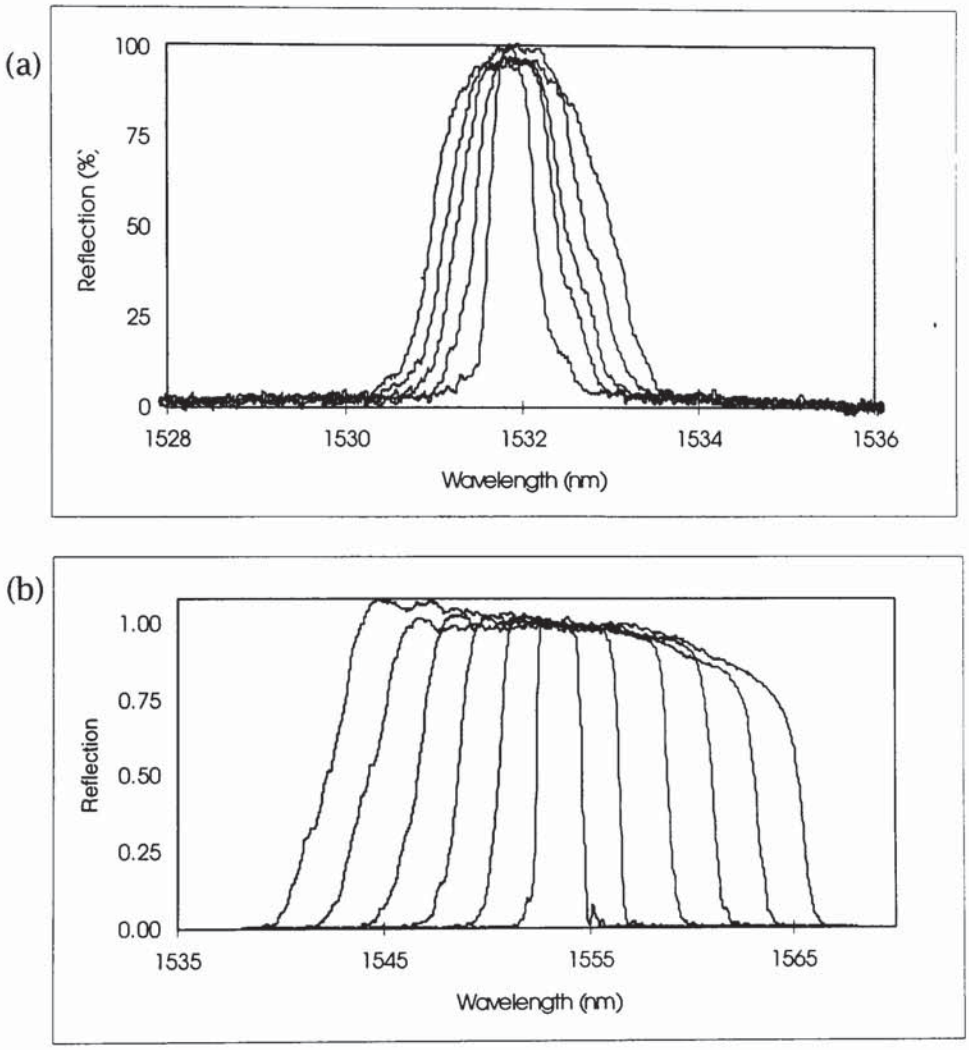

Figure 4-9 Reflection profiles of gratings successively fabricated using the telescopic approach with bandwidths in the ranges (a) 0.5-2.1nm, (b) 2.2-22.9nm.

The bandwidth of gratings therefore no longer relies on the focal length of the lenses but on their separation. Figure 4-10 shows an example of the bandwidth control that this method gives. The back lens was moved in steps away from the 2f position and a series of gratings were fabricated. The experimental bandwidths for each step are shown on the graph as plotted points, the solid line shows the corresponding

calculated values. There is good agreement between the experimental data and the calculated values.

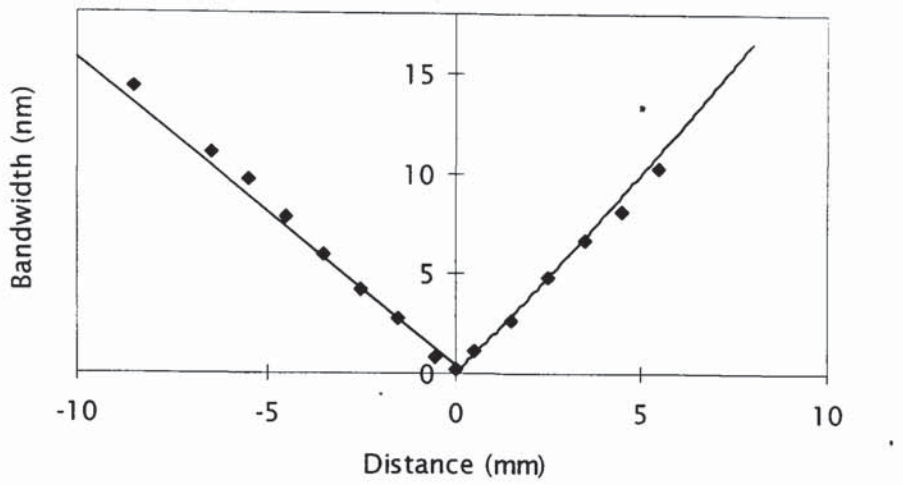

Figure 4-10 Calculated (solid line) and experimental (plotted points) data for the grating bandwidth as the back lens is moved away from the 2f point. On the x-axis negative values for distance denote a>2f (converging beam), positive distances denote a<2f (diverging beam).

Apart from the control and flexibility that this arrangement offers, the importance of this set-up is that it can produce linear chirped gratings that are narrow in bandwidth. The calculated wavelength profiles for various gratings are shown in Figure 4-11. The lenses are assumed to have focal lengths of 0.09m with the front lens positioned 0.09m from the fibre. The beam width is taken to be 4.5mm. The plotted lines show the calculated wavelength profile for gratings separated by 0.36, 0.359, 0.357, 0.353 and 0.35m. As the separation between the lenses decreases the bandwidths of the gratings increases. The relationship between the wavelength reflected and the position on the grating is linear for all the profiles shown.

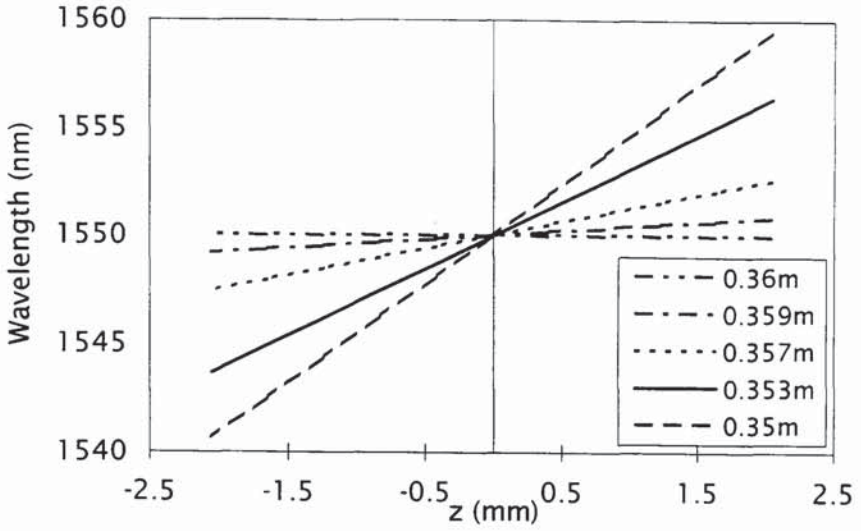

Figure 4-11 Calculated wavelength profiles of a selection of gratings produced by the telescopic approach. The legend gives the distance between the two cylindrical lenses for each case.

All these calculations assume a uniform beam profile. Any shading of the beam will have an effect on the grating profile but it is assumed that for the central section of the grating this effect is not large. The smoothness of the grating profiles depends on several factors: that the centres of both beams overlap; that the beam is of high quality; and that the fibre is clean. If one or more of these conditions is not met then the resulting variation in beam intensity causes the gradient of the chirp to be non-uniform and may even result in it changing sign. Resonances and dips in the reflection and dispersion profile then occur.

To confirm that the dispersion was linear gratings were measured by the technique described in Chapter 2.4.2. Figure 4-12 shows the (a) refection and (b) measured phase delay of one such grating. The grating was fabricated in boron doped fibre (CIII) that had been hydrogen loaded for five days at 120 atmospheres pressure and room temperature. The grating is centred at 1552.5nm and has a reflection bandwidth of ~8.2nm.

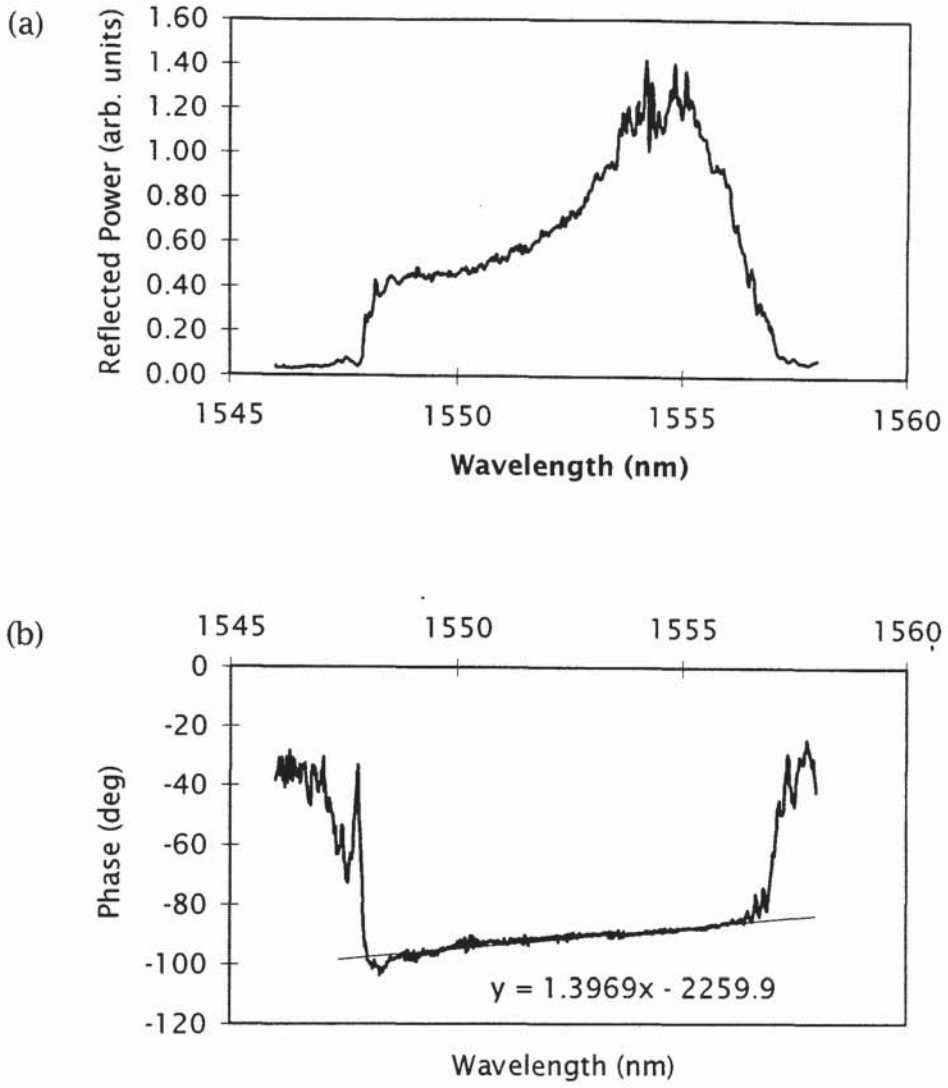

Figure 4-12 (a) Reflection and (b) measured phase delay of an 8.2nm bandwidth grating made with a telescopic arrangement of dissimilar wavefronts.

In conclusion, this optical arrangement gives a highly flexible system for fabricating medium to small bandwidth linearly chirped gratings. Chirped grating with bandwidths from 0.2nm to 30nm have been produced with a good degree of linearity in the chirp. Advantages of compactness and high control are evident over the previously described technique.

4.1.3 Quadratic chirped gratings

In some situations, a linear wavelength change along the length of the grating may not be necessary. Indeed a linear response may not be desirable[89,90,91], for example, in the case of second order dispersion compensation. The lens arrangement described in this section produces gratings where the chirp is nonlinear along the length of the grating. Contrary to phase mask imprinted gratings where the gratings are divided into a number of linear sections, the chirped gratings from this arrangement can be made to vary in a continuously quadratic nature rather than in a stepped form.

This arrangement follows the generalised form, with a single cylindrical lens in each arm, that was illustrated in Figure 4-2. If the lenses are positioned at twice their focal length from the fibre, then a narrow bandwidth grating ~1nm wide will be formed. In this instance, the centre of the grating will reflect the lowest wavelength and moving out from the centre the reflected wavelengths will increase symmetrically. This produces a resonating structure since wavelengths within the grating bandwidth are reflected from two separate locations in the grating.

Moving one of the lenses away from the $2f$ position increases the bandwidth of the grating formed. As the bandwidth increases, an asymmetry in the profile of the chirp occurs. Eventually, the chirp gradient acquires the same sign across the length of the grating and this is indicated by the disappearance of resonances on the reflection spectrum. This occurs, for a beam width of 4.5mm and lenses of 0.09m focal length, at a point where the grating bandwidth reaches 2-3nm. As the bandwidth broadens the chirp gradient remains quadratic although the effect of the quadratic term diminishes. As the gratings start to exceed bandwidths of 10nm the wavelength profiles tend not to be that different to the linear case. Figure 4-13 illustrates the calculated wavelength profiles for gratings from this arrangement. Assuming the lenses have focal lengths of 0.09m and one lens is positioned 0.18m from the fibre then the profiles shown correspond to the second lens being 0.18, 0.181, 0.186 and 0.19m from the fibre. These results are calculated for a beam width of 4.5mm.

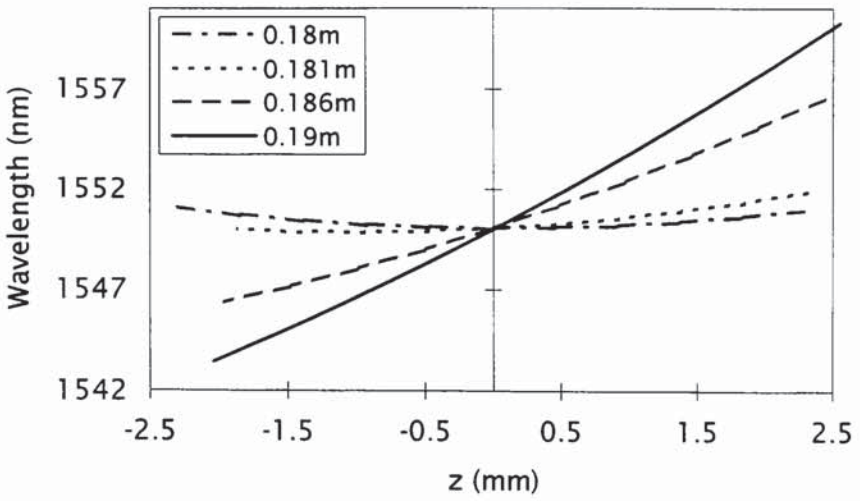

Figure 4-13 Effect of broadening the grating bandwidth on the chirp profile. Calculated results for 9cm focal length lenses where one lens is 0.18m from the fibre and the second lens is 0.18, 0.181, 0.186 and 0.19m from the fibre.

Gratings of this type have been fabricated and their dispersion measured. The optical time delay of one such grating is shown in Figure 4-14. The grating was fabricated in germania doped fibre that was hydrogen loaded for five days at 130 atmospheres and room temperature. The central reflection wavelength of the 4.5mm grating is 1552nm and the bandwidth is 9.5nm.

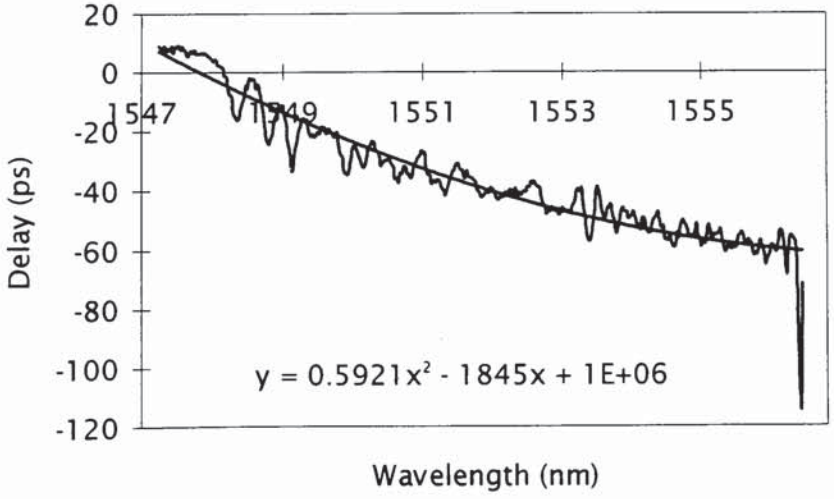

Figure 4-14 Time delay profile of a quadratic chirped grating with a theoretical fit (smooth curve) included for comparison.

This arrangement has also be used to fabricate broadband gratings but as previously mentioned these exhibit low levels of nonlinearity. Figure 4-15 shows a 4.6mm grating fabricated in boron doped fibre (CII) that was hydrogenated for seven days at a pressure of 110 atmospheres and room temperature. The reflectivity approaches 100% over most of the 44nm bandwidth. There are two reflection profiles shown. One taken from the short wavelength side of the grating and one from the high wavelength side. The profile from the high wavelength side exhibits substantial short wavelength loss due to modal outcoupling.

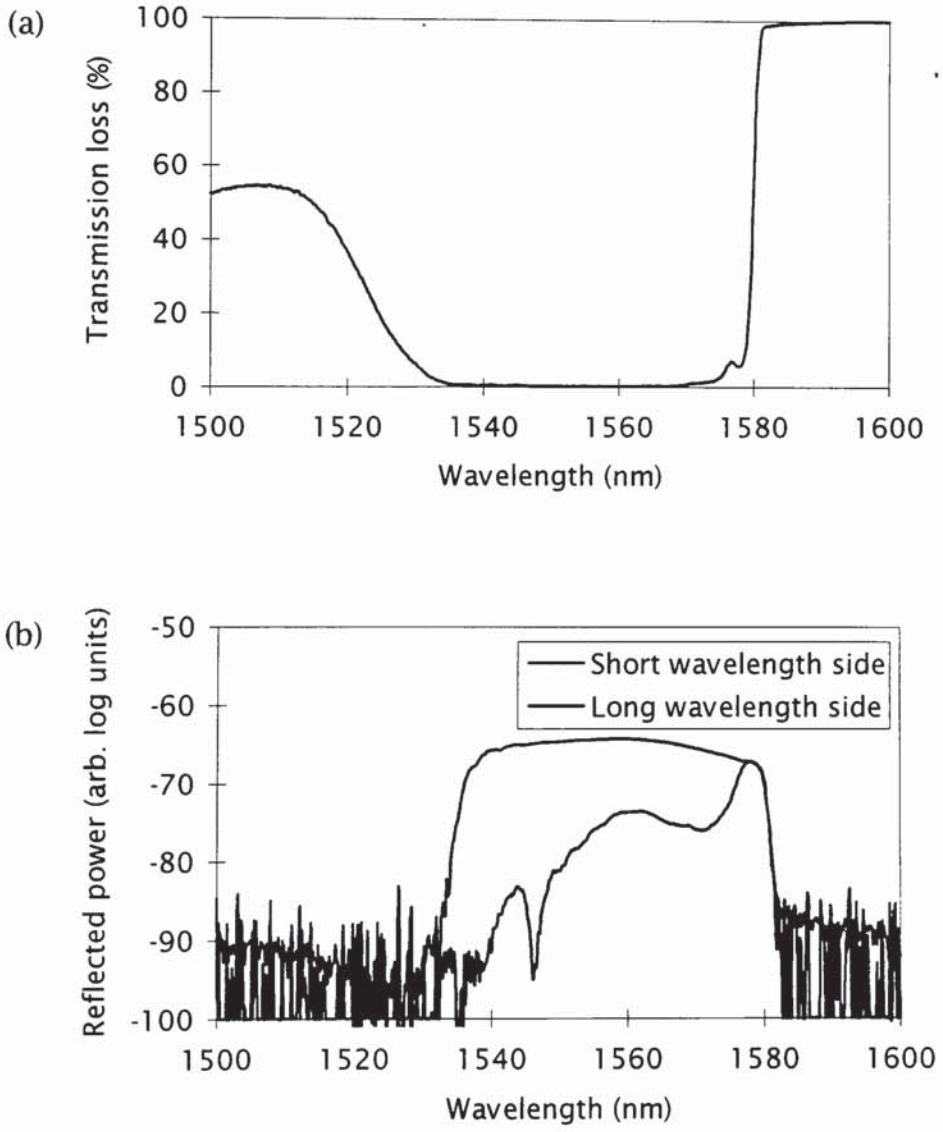

Figure 4-15 Broad bandwidth grating fabricated using a cylindrical lens in each arm of the interferometer. (a) shows the transmission spectrum, (b) shows the reflection spectrum taken from the short and long wavelength side of the grating.

In conclusion, this particular variation of the dissimilar wavefront curvatures technique has been used to fabricate gratings with bandwidths ranging from 5nm to 80nm. For the narrow bandwidth gratings the chirp profile is quadratic. The quadratic nature of the chirp decreases as the grating bandwidth increases.

4.2 Tapered Fibres

The method described in this section uses a variation in the effective refractive index of the fibre to produce a chirp. This work was done in collaboration with K Byron and T Bricheno at BNR Europe Ltd. A fibre taper is used to exploit the dependence of the fibre effective refractive index on the fibre radius. The technique combines the well established techniques for writing linear gratings with the high precision taper capabilities that exist at BNR Europe Ltd. It lends itself to situations where highly controlled but relatively small chirps are required.

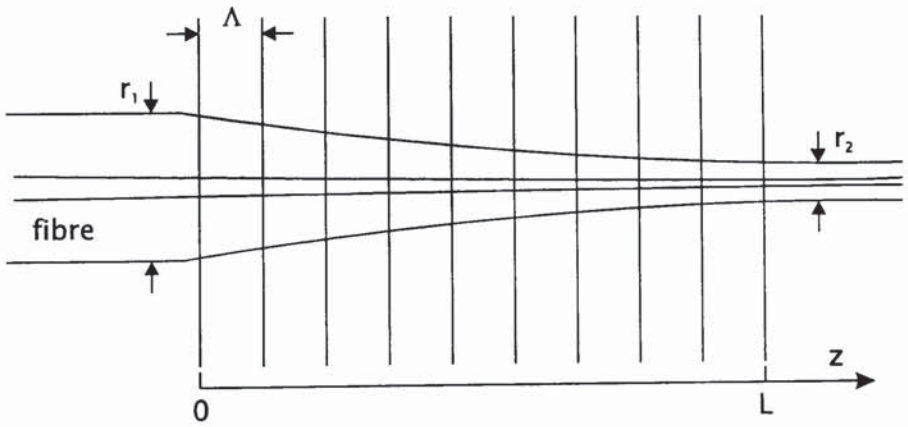

Figure 4-16 Fabrication of chirped Bragg gratings in tapered fibre.

If a linear grating is written on a fibre taper, Figure 4-16, then the reflected wavelength changes along the length of the grating because the effective refractive index decreases with the reduction in fibre radius. Tapers were designed such that the fibre diameter decreased smoothly from 125μm to 50μm over a distance of 10mm. The taper technology is such the fibre could have been tapered to any radius between 125 and 50μm. Figure 4-17 shows the effective refractive index

variation along the length of the taper modelled using in-house numerical computation of the propagation constant of the fundamental mode along the taper. For most of the length the chirp rate is approximately linear. Assuming no changes in the stress-induced refractive index this produces a roughly linear chirp in the Bragg grating. Thus, for a uniform intensity and spatial coherence across the beam, a grating formed along the entire length of a 50μm taper could be expected to have a bandwidth of ~4.4nm when fully exposed.

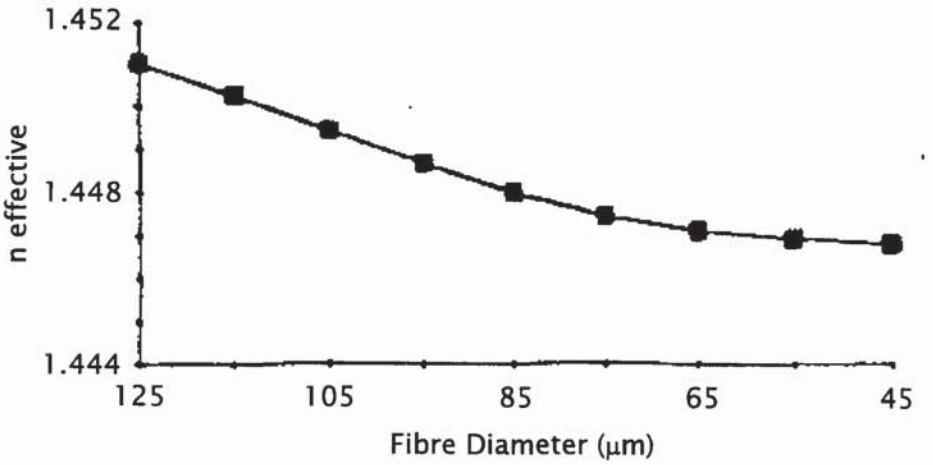

Figure 4-17 Variation of the effective refractive index along the length of a taper[38].

Gratings were written in untapered and 125-50μm tapered fibre respectively. The gratings were written using the holographic two beam interference method described for linear gratings in Chapter 3. The grating length was ~8mm. The fibre used was boron doped (CIII) and the UV exposure power was 55mW. The fibre had an index difference of $13x10^{-3}$ and a core diameter of 4.8μm.

The grating written in untapered fibre, Figure 4-18, was ~8mm in length. The grating reflection bandwidth (FWHM) was 0.25nm and the reflection was centred around 1.5334μm. Figure 4-19 shows the chirped reflection response of the grating formed on the 50μm taper. The grating exhibits a peak reflectivity of 20% at 1.5312μm. The reflection bandwidth is 2.7nm i.e. a ten-fold increase on the equivalent unchirped bandwidth. The bandwidth is less than the maximum predicted because the grating

was not written over the entire length of the taper. Although the reflectivity is lower than the linear grating case this could be compensated for by using hydrogen-loaded fibres which have higher photosensitivity but were not available at the time.

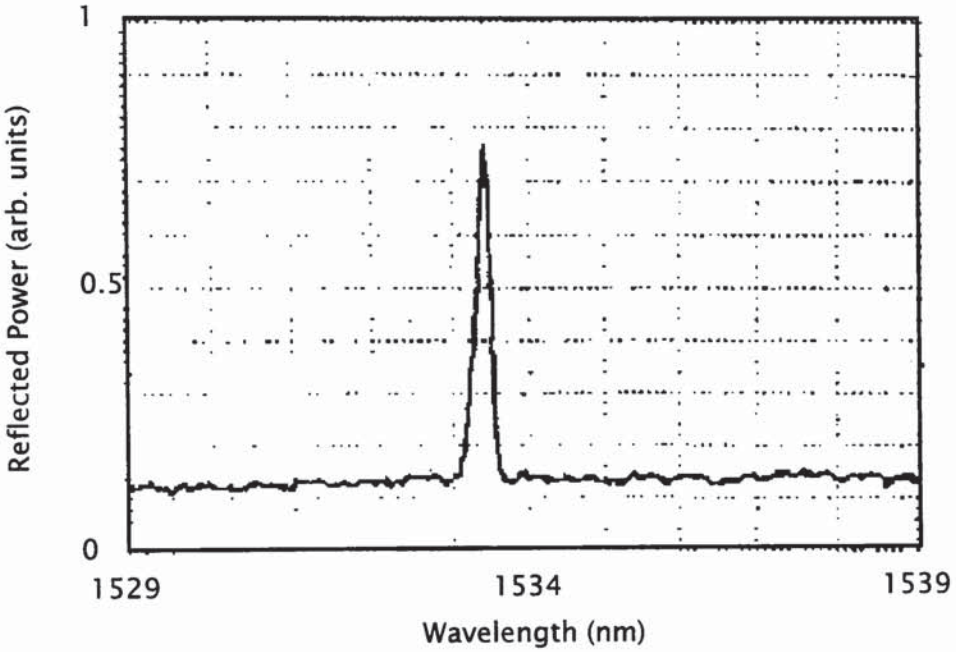

Figure 4-18 Reflection profile of a grating written in untapered fibre.

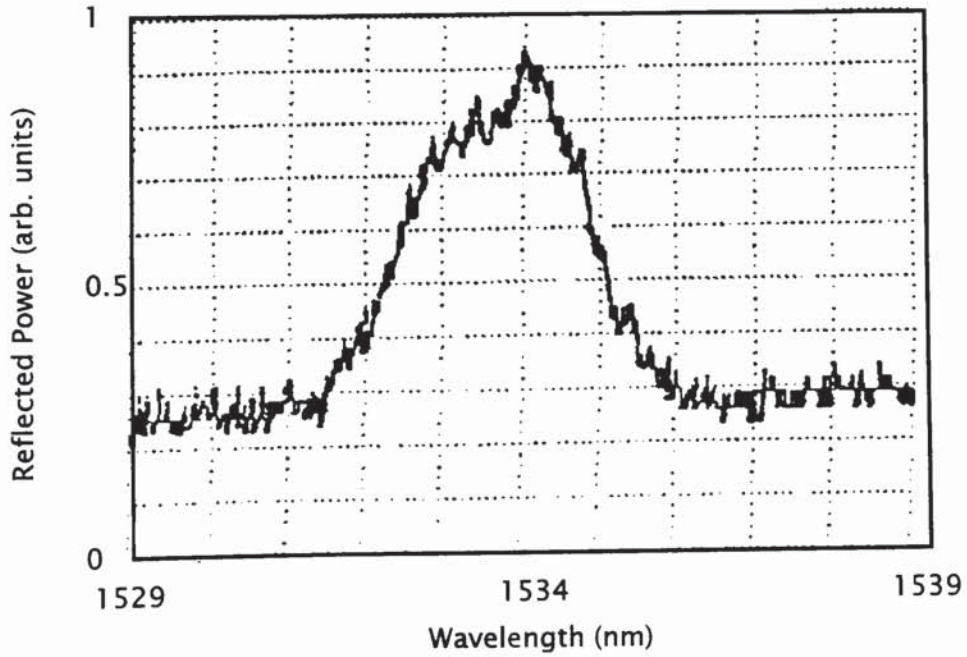

Figure 4-19 Reflection profile of a grating written in fibre tapered to a waist of 50μm over a distance of 10mm.

The main limitation to this technique, aside from the inconvenience of relying on taper fabrication, is the amount by which the fibre radius can be decreased before weakening the fibre or diminishing its guiding properties. This means that only gratings with a relatively small bandwidth (<5nm) can be produced. However, since the fibre radius is dependent on the pulling speed when the fibre is being drawn from the preform, it is possible to imagine a situation where a momentary, graduated change in pulling speed is combined with in-line grating fabrication techniques as now demonstrated, for example by NRL and Southampton University, to give a series of chirped gratings along a fibre. Although this technique has been largely superseded by other methods of fabricating chirped gratings it was the first published technique for directly writing chirped gratings into optical fibre.

4.3 Fibre Deformation

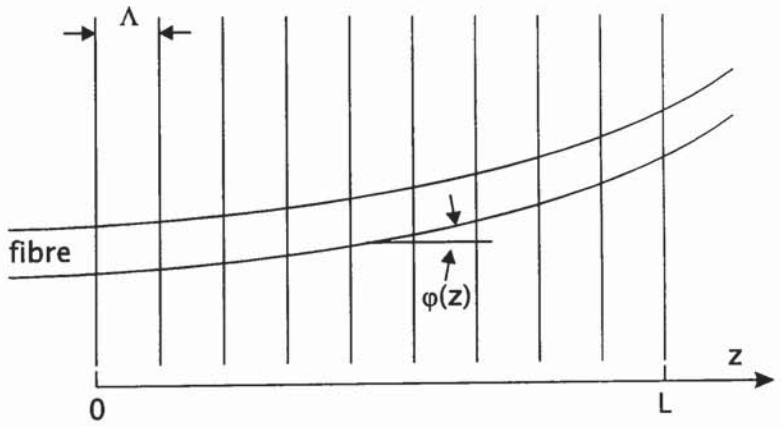

Figure 4-20 Fabrication of chirped gratings by fibre deformation.

In this third technique for fabricating chirped fibre gratings, the chirp originates from a physical deformation of the fibre during exposure to uniform interference fringes, Figure 4-20. In the historical context this was the first published method of fabricating chirped gratings that did not involve several fabrication stages, the previous methods involving side etching or tapering of the fibres. This technique was proposed as a simple and inexpensive method of writing chirped fibre gratings with

the minimum of both required optics and time consuming alignment procedures.

The fibres are fixed in a circular arc by two posts and positioned in a uniform fringe pattern of period Λ produced by two beam interference. The period $\Lambda(z)$ of the grating written into the fibre varies as $\Lambda/\cos\varphi(x)$, where $\varphi(x)$ is the angle between the fibre and the normal to the exposure fringe pattern at position z. This results in the fringe pattern spacing $\Lambda(z)$ varying along the fibre axis from Λ to a maximum of $\Lambda/\cos\varphi(L)$. Figure 4-21 shows the wavelength variation induced when the fibre is curved through an angle of 10°, which corresponds to a grating bandwidth of ~24nm.

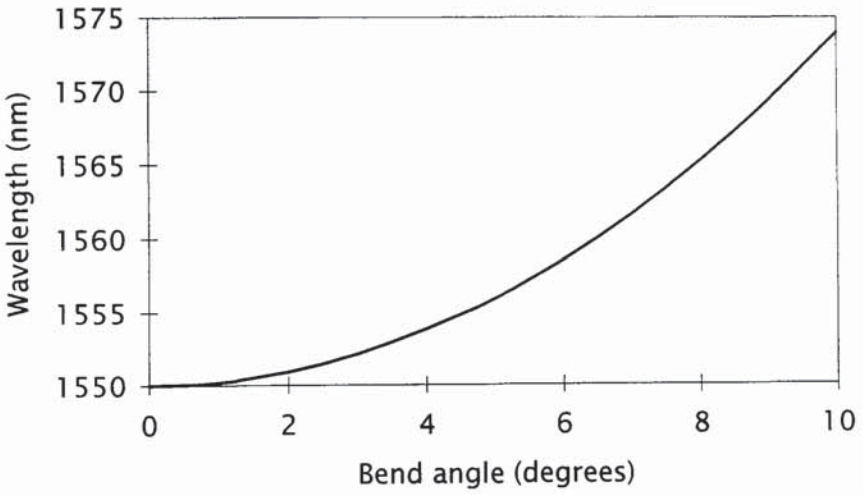

Figure 4-21 Reflected wavelength from fibre position corresponding to bend angles of 0-10°.

The gratings shown in Figure 4-22 were written in boron doped fibre (CIII). The exposure length was ~5mm and each grating was written with a successive increase in the curvature. Figure 4-22(a) shows a grating resulting from no curvature of the fibre i.e. it is unchirped. The peak reflectivity is 88% and the corresponding bandwidth is 0.4nm. A small amount (~3.5°) of curvature was then introduced before fabricating the following grating, Figure 4-22(b). The grating bandwidth increased to 2.9nm and the peak reflectivity decreased to 40%. The reflectivity

continued to decrease as each subsequent grating showed an increase in bandwidth; 13% for a bandwidth of 4.4nm, Figure 4-22(c), and ≥4% for a bandwidth of 17.3nm, Figure 4-22(d). The angles φ(L) for these two gratings were estimated to be ~4.3° and 8.5° respectively. Although this method introduces a tilt on the fringes with respect to the fibre axis no induced short wavelength loss was observed.

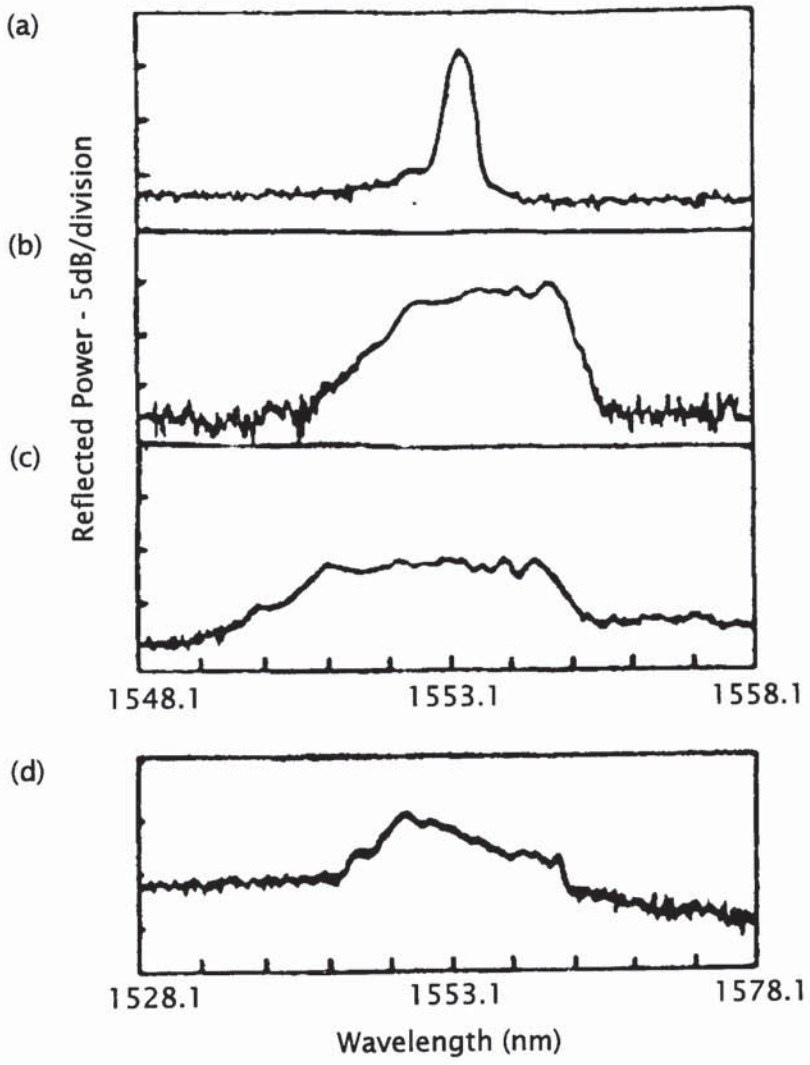

Figure 4-22 Reflection profiles of gratings formed in (a) non-deformed fibre, (b)-(d) progressively more deformed fibre.

To counteract the decreasing reflectivity with increasing bandwidth hydrogen-loaded fibre is used to increase the fibre photosensitivity. Figure 4-23 shows the reflection profile of a grating fabricated in the same fibre but which had been hydrogen-loaded for seven days at 100

atmospheres pressure and room temperature. The reflectivity of this grating is >99.9% over a bandwidth of 7.5nm.

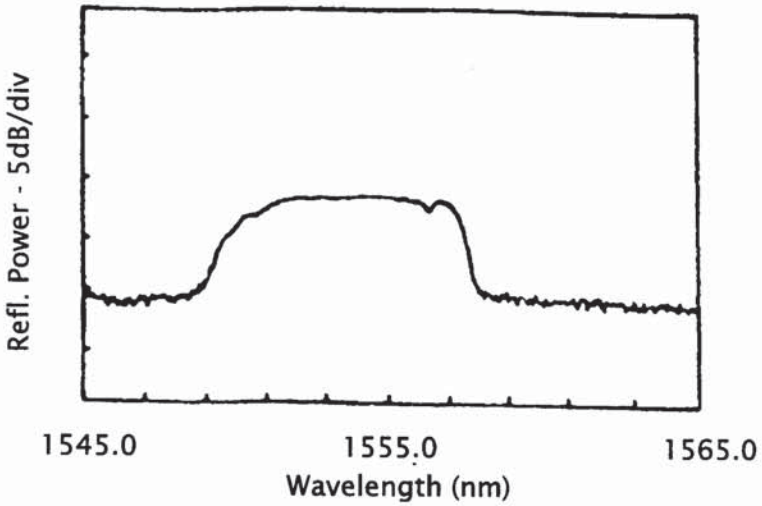

Figure 4-23 Reflection response of a chirped grating written in hydrogenated germania doped fibre (CA2114) by fibre deformation technique.

4.4 Summary of Fabrication Techniques

Table 4-1 summarises the techniques presented in the chapter for the fabrication of chirped gratings.

Technique	Variation	Bandwidth range	Chirp profile	Applications
Dissimilar wavefront curvatures	"Superbroad"	100-200nm	Linear	Filters, broadband mirrors
	Telescopic	0.2-30nm	Linear	Dispersion compensation, pulse compression
	Quadratic	4-100nm	Quadratic	Higher order dispersion compensation
Tapered fibre		0.2-4.5nm	Near-linear	Dispersion compensation
Fibre deformation		0.2-30nm		Sensors

Table 3 Summary of techniques for the fabrication of chirped gratings.

5. Resonators

5.1 Introduction

Filters are important components for many optical systems. Noise reduction and wavelength demultiplexing are crucial to the success of optical telecommunication systems especially where erbium fibre amplifiers are used. This chapter details how chirped fibre Bragg gratings were used for the first time in the fabrication of distributed wideband fibre integrated Fabry-Perot and Moiré filters. Previous to this work only linear grating resonators had been demonstrated. The extension to broadband devices was made practical by the use of hydrogenation since that precipitated the ability to fabricate wideband, highly reflecting gratings.

5.2 Fabry-Perot Resonators

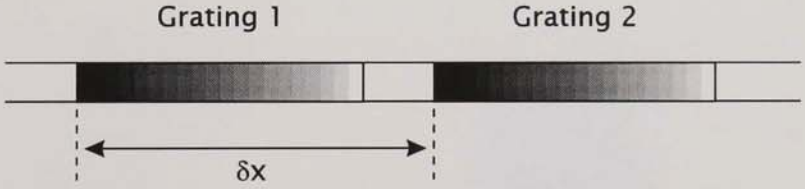

Figure 5-1 Schematic of the wideband Fabry-Perot structure.

To date, it has been difficult to produce the Fabry-Perot filter, which is a fundamentally important component in optical systems, in a format compatible with optical fibre systems. The Fabry-Perot filter has been demonstrated for noise rejection and wavelength division multiplexing in soliton transmission systems[92] and also for the harmonic modelocking of short pulsed fibre lasers[93,94]. However, the devices being used for these applications were typically bulk devices that were less than ideal for incorporating into fibre based systems. Narrowband fibre grating resonators made with linear gratings[95] had previously been reported however, for the applications in short pulsed lasers and high

speed communication systems responses over several nanometres are required. Consequently, there was a motivation to fabricate Fabry-Perot resonators that were all-fibre in nature, that could be made with a broad range of free spectral range and finesse values and that could be made to work over large bandwidths if required. Devices to this effect will be described here in this chapter.

A chirped Fabry-Perot grating resonator consists of two chirped fibre gratings that are displaced along the fibre axis by a distance δx, Figure 5-1. Ideally the gratings are linearly chirped and of uniform strength in order to give a predictable response profile. The reflectivity and bandwidth of the gratings are therefore determined by the amplitude of the refractive index modulation, the grating length and the rate of chirp. As for a standard Fabry-Perot resonator the free spectral range is dependent on the displacement between the two gratings and, if there are no internal losses, the finesse can consequently be determined from the reflectivity of the mirrors.

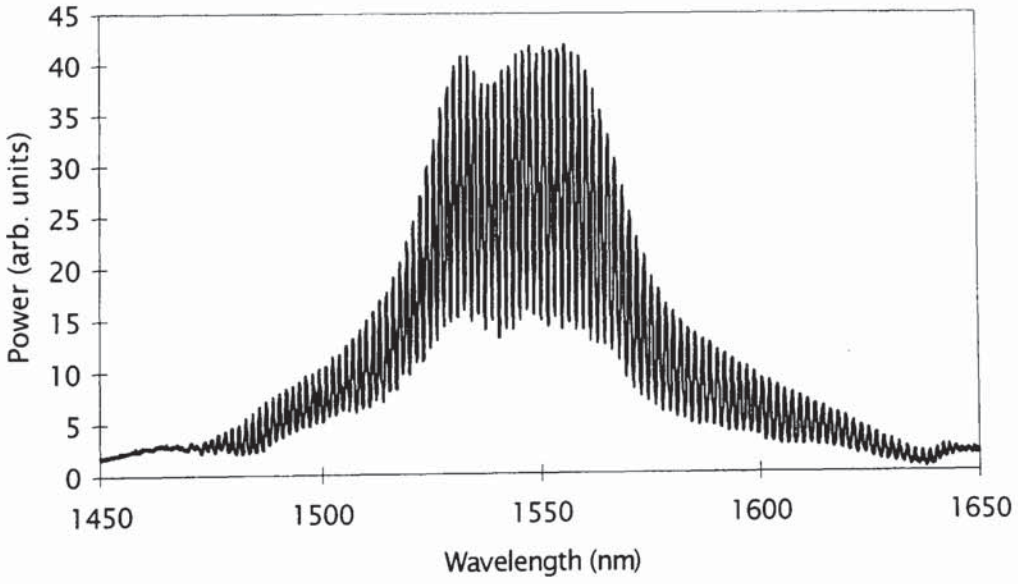

Figure 5-2 Transmission profile of a Fabry-Perot resonator that operates over a 200nm bandwidth. The transmission profile is superimposed onto an erbium fluorescence spectrum. The resonator free spectral range is 1.5nm and the finesse ~1. The resonator was fabricated in hydrogen loaded boron doped fibre (CIII) and the grating displacement is 0.55mm.

Chirped fibre gratings have been used to produce a large number of Fabry-Perot resonators that can operate over a wavelength span up to 200nm (for example Figure 5-2) and that have been fabricated with peak separations of between 0.09 and 11.27nm. These broadband resonators have subsequently been used to demonstrate the CW multiwavelength operation of an erbium-doped fibre laser with eleven simultaneous operating wavelengths. The resonator devices are also being incorporated into sensor addressing systems and into a transmission systems as a multiwavelength filter.

5.2.1 Experimental results

The gratings are written sequentially on a highly photosensitive fibre. The chirp is achieved using interfering wavefronts of dissimilar curvature by one of the arrangements described in Chapter 4.2. The exact optical arrangement that is used depends on the required bandwidth of the resonator. Between exposures the fibre mount is translated parallel to the fibre axis by a distance δx. Each exposure is monitored using an optical spectrum analyser in the standard way described in Chapter 2. The second exposure is halted when the fringe depth stops growing. In cases where the fringe width or the free spectral range are narrower than the resolution of the optical spectrum analyser this may lead to a mismatch in the grating reflectivities. These gratings are measured more accurately after the exposure by using a narrow linewidth tuneable laser. All the gratings are fabricated in highly photosensitive fibre that is also hydrogen loaded. Will short gratings this is the only way of producing broad bandwidth gratings that exhibit sufficient reflectivity.

Figure 5-3 shows the spectral response of a resonator measured in transmission and reflection using a tuneable diode laser (linewidth <0.001nm) and an optical power meter. Each grating mirror is 4mm long and has a reflectivity of approximately 80% over a bandwidth of 150nm. The gratings are separated by about the length of one grating, so they do not overlap. The peak separation is 0.09nm, the half width of the peaks is of the order of 0.02nm. With these parameters the Fabry-Perot resonator would be expected to have finesse of 14, a free spectral

range of 0.083nm and a width (FWHM) of 0.013nm. The amplitude and phase response of the resonator as a function of wavelength was computed numerically for transmission and agreed well with the experimental results except that the predicted finesse is higher than is actually observed. The slight discrepancy between the measured finesse and the theoretical one can be accounted for by a loss to the system due to outcoupling or absorption.

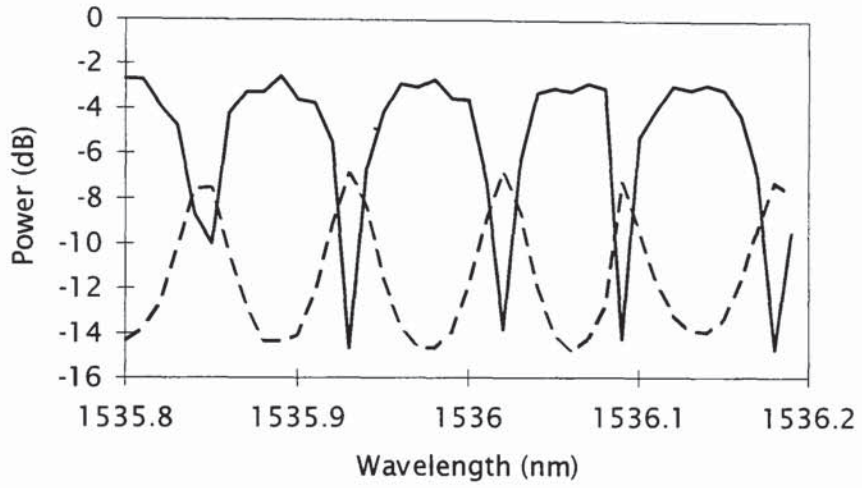

Figure 5-3 Transmission (solid line) and reflection (dashed line) response of a Fabry-Perot resonator comprising of two 4mm gratings displaced by ~9.5mm.

A transmission plot of another resonator, that has a low finesse and large free spectral range, is shown in Figure 5-4. The gratings were written in boron doped fibre (CII) that had been hydrogen loaded for six days at 120 atmospheres pressure and room temperature. The ~3mm gratings exhibited a reflection bandwidth of 38.5nm. To obtain the large free spectral range it was necessary to overlap the two gratings in the fibre. The displacement between the two gratings is 0.15mm. The spectral response of the resonator was measured in transmission (a) and reflection (b). The resonator has a finesse of 4.3, and a free spectral range of 5.6nm.

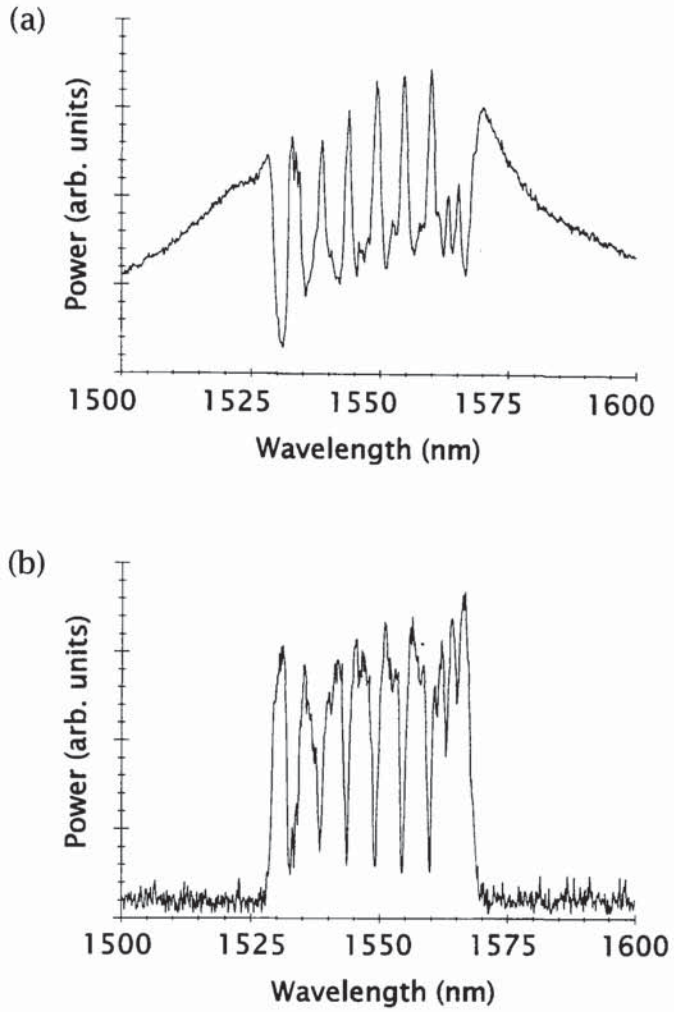

Figure 5-4 (a) Transmission and (b) reflection profiles of a fibre resonator fabricated in hydrogen-loaded boron doped (CII) fibre. The ~3mm grating displaced by 0.15mm.

There is a trade-off between bandwidth and finesse because of the limit on the grating reflectivity from the available photosensivity and due to the losses that are introduced by modal outcoupling and the effect of combining hydrogen into the structure of the glass. Figure 5-5 shows a 11.5nm broad resonator, fabricated in hydrogen-loaded germania doped fibre (CA2114). This fibre had a high numerical aperture value and so was strongly guiding, this decreased the modal outcoupling losses. The 4mm gratings were displaced by 0.5mm resulting in a resonator with a free spectral range of 1.43nm and a finesse of ~7.7.

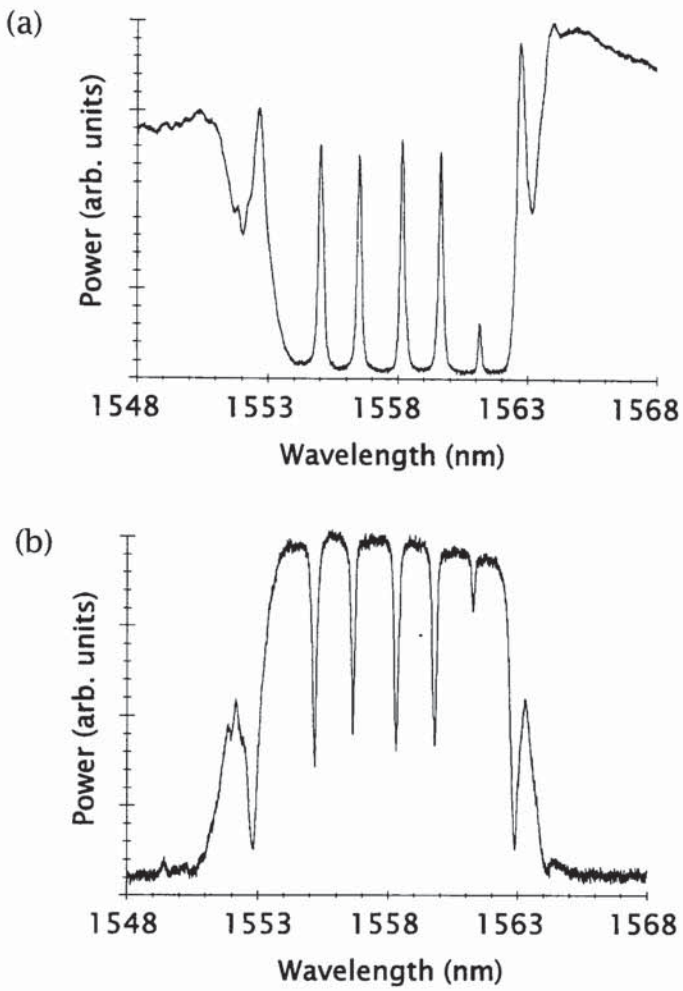

Figure 5-5 (a) Transmission and (b) reflection profiles of a resonator fabricated in hydrogen-loaded germania doped fibre (CA2114). The gratings are displaced by 0.5mm, the resonator has a free spectral range of 1.43nm and a finesse ~7.7.

Resonators were fabricated with an extensive selection of grating displacement distances. The corresponding free spectral range versus distance data is shown in Figure 5-6. This illustrates the large variety of resonators that can be fabricated in fibre by this technique and also how closely this type of resonator mimics the traditional Fabry-Perot resonator in so far as the free spectral range relation to the displacement.

It should be noted that since strong gratings incur low wavelength losses and these fall within the bandwidth of a chirped resonator that fabricating very high finesse resonators is difficult. Again, the short wavelength loss can be reduced by using a high NA fibre. There is a trade off between bandwidth and loss since for a larger bandwidth

grating it requires a larger amplitude of refractive index modulation to achieve the same reflectivity than for a narrower grating of the same length. To reduce loss for any given set of parameters one possibility is to increase the length of the grating. Absorbed hydrogen in the fibre causes a fibre loss due to an absorption resonance of the -OH bond, see Chapter 2.5. This can be shifted out of the operational wavelength region by substituting deuterium in the loading process. One disadvantage of this substitution is that deuterium costs approximately 100 times as much as hydrogen.

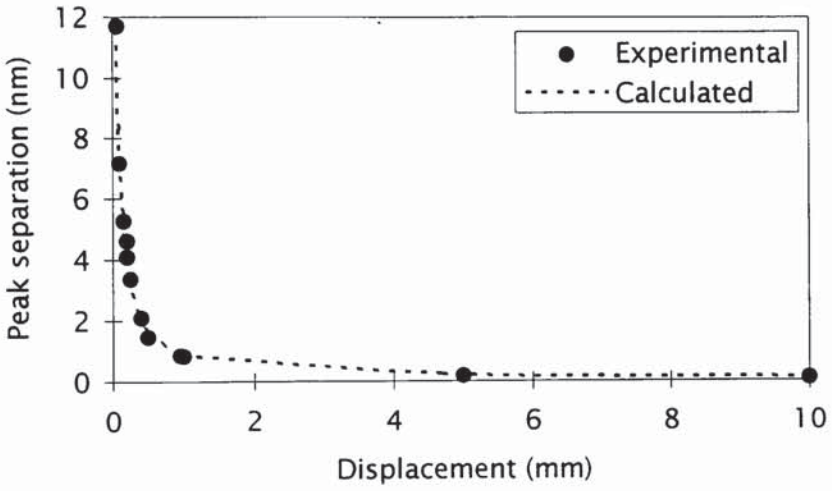

Figure 5-6 Variation in the resonator peak separation as the displacement between the two gratings of the Fabry-Perot resonator is increased.

5.2.2 Conclusion

Wideband Fabry-Perot filters may be fabricated in photosensitive optical fibres using distributed mirrors formed by chirped Bragg gratings. The spectral response has been shown both numerically and experimentally to be similar to Fabry-Perot resonators made with plane mirrors, except for some added dispersion. The maximum finesse of the resonator is limited by the loss. This can be decreased by using strongly guiding fibres and substituting deuterium for hydrogen in the loading process. The resonators have many applications including in fibre lasers and a frequency-guiding filter for soliton systems.

5.3 Moiré Grating Resonators

5.3.1 Introduction

Moiré resonators are produced by the sequential exposure of the same length of fibre to two fringe patterns of slightly different frequency. The following sections will describe how chirped gratings can be used to form Moiré resonators to produce single passband filters that exhibit wide stopbands and narrow passbands[96,97].

For many application, such as the suppression of noise from amplified spontaneous emission (ASE) in single wavelength transmission systems, the multi-passband Fabry-Perot approach is unsuitable, despite the high finesse achieved. Instead, single passband structures are required. Previous to the work described here, single passband filters had been limited to either wide passband / wide stopband or narrow passband / narrow stopband scenarios. Fabrication concepts for filters that combined narrow passbands with wide stopbands within grating devices had proved elusive.

Work on producing single passband filters can be split into the areas of resonating and non-resonating systems. A variety of non-resonating systems have been proposed. Chirped gratings had been used to fabricate filter by using amplitude masks[35] during the exposure wavelength to leave a central non-reflecting region. Two very strong linear gratings, separated spatially and in wavelength have also been used[98]. Both methods are limited to producing fairly wide transmission bands to avoid interference effects from the reflection tails of the blocking sections across the central passband region. The latter method also required very high NA fibres to push the outcoupled modes towards lower wavelengths to avoid the passband. Chirped gratings have also been post-exposed to UV radiation to erase selected sections to produce passbands across a grating[99].

A number of other resonating systems have also been proposed. However, other than the Fabry-Perot work described in the previous section, they concentrated on using linear gratings. The Moiré approach to fibre grating resonators was first described for etched, surface relief

structures based on uniform-period gratings by Reid *et al*[100]. The first results for uniform-period Moiré gratings, written holographically into the fibre core, were published by Legoubin *et al*[101]. However, filters from both these techniques have not exceeded ~1.2nm total bandwidth.

A similar structure to that described by Legoubin is shown in Figure 5-7. The resonator comprises of two, slightly wavelength shifted, 4mm gratings written sequentially in boron doped fibre (CIII) that had been hydrogen loaded at 150 atmospheres pressure and room temperature for 120 hours prior to exposure. A tuneable wavelength source with a 0.001nm linewidth in the arrangement described in Section 2.4.2 was used to characterise resonators of this type because of the very high resolution requirements.

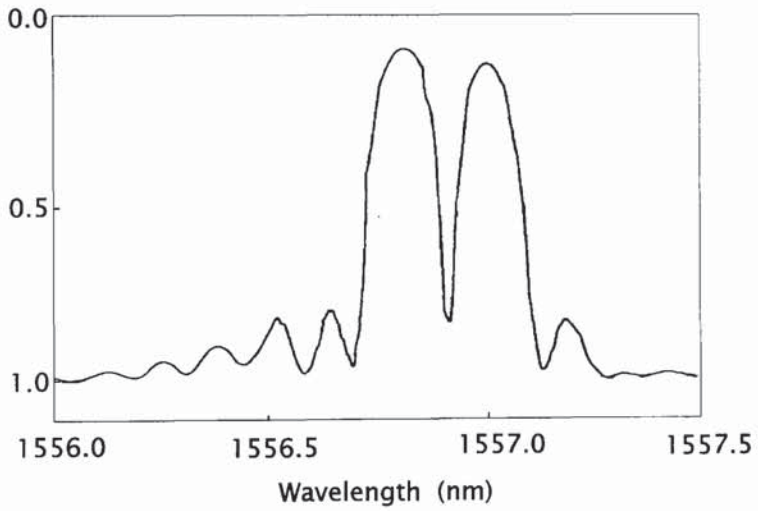

Figure 5-7 Normalised transmission spectrum of a uniform-period grating Moiré resonator. The FWHM passband width is 0.036nm, and the stopband width is ~0.3nm.

This chapter describes the first published work on chirped Moiré structures and illustrates how the concepts behind linear Moiré resonators can be extended to broadband structures. This allows filters to be fabricated with substantially broadened stopbands. The filters can then be concatenated to produce very wide stopband / narrow passband filters.

5.3.2 Concept of Moiré resonators

For uniform-period gratings of equal refractive index amplitude δn with periods Λ_1 and Λ_2, the resulting fringe pattern can be described by

$$\Delta n(z) = 2\delta n\left(1+\cos\left(\frac{2\pi z}{\Lambda_S}\right)\cos\left(\frac{2\pi z}{\Lambda_C}\right)\right)$$

Equation 12

where Δn(z) is the refractive index modulation at distance z along the fibre axis, $\Lambda_S = 2\Lambda_1\Lambda_2/(\Lambda_1+\Lambda_2)$ and $\Lambda_C = 2\Lambda_1\Lambda_2/(\Lambda_1-\Lambda_2)$.

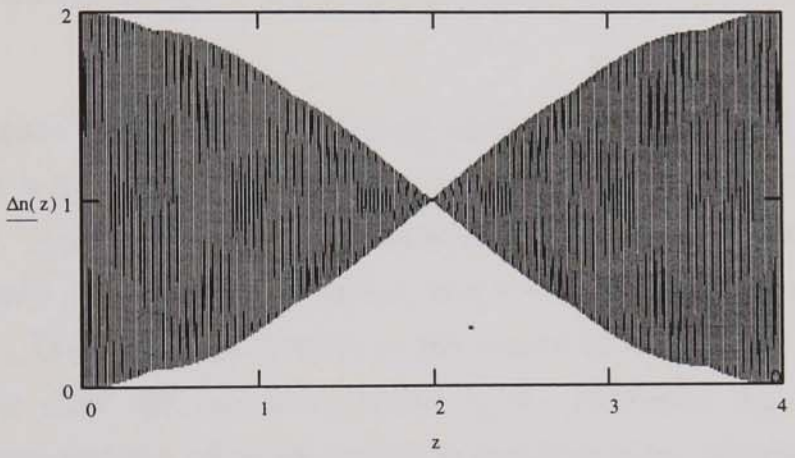

Figure 5-8 Calculated refractive index profile of a linear Moiré grating comprising two 4mm gratings shifted in wavelength by 0.184nm.

The physical significance of Equation 12 is illustrated by Figure 5-8, which shows the calculated refractive index modulation envelope of a Moiré resonator. The 4mm long gratings that form the resonator have Bragg wavelengths of 1460 and 1460.184nm. As can be seen the refractive index modulation decreases in amplitude moving towards the centre of the grating. At the centre there is a crossover point where the phase of the grating changes intrinsically by π, producing an optical phase change of π/2, and so the Moiré grating is equivalent to a λ/2 phase-shifted grating. This is easier to see in diagrammatic form if non-optical frequencies are used in the calculation.

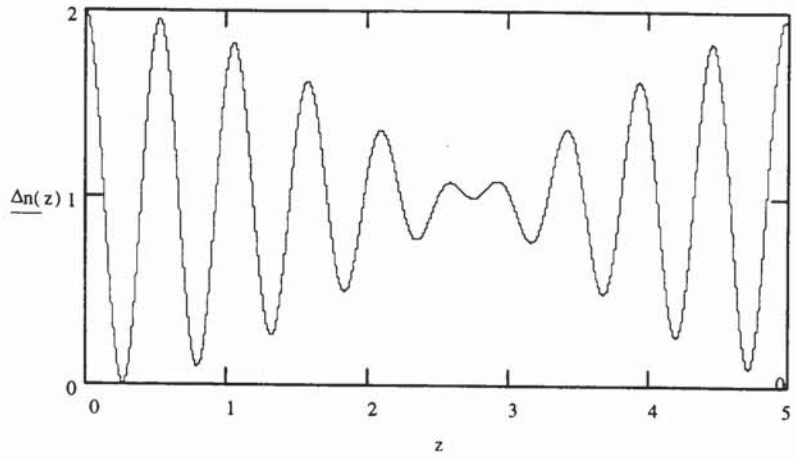

Figure 5-9 Calculated refractive index profile of a linear Moiré grating. The gratings are 5mm in length and have periodicities of 0.5 and 0.5502mm.

Figure 5-9 shows the response where periodicities of 0.5 and 0.5502mm have been used for convenience. It now becomes clearer that Equation 12 represents a spatially amplitude-modulated waveform that has a rapid variation with period Λ_s and a slowly varying envelope with period Λ_c. The $\pi/2$ phase change in the centre of the grating is also visible. In this case the envelope period Λ_s is ~10.96mm. To achieve a central passband the envelope period is requires to be approximately twice the grating length. If the envelope period is more than twice the grating length then more passbands will occur within the resonator bandwidth, Figure 5-10.

This concept can be extended to chirped gratings where Λ_1 and Λ_2 vary along the length of the grating. Equation 12 can be alter to include this variation, Figure 5-11 shows the calculated amplitude of the refractive index modulation for two 1mm gratings of bandwidth 14.6nm where the central Bragg wavelengths were separated by 0.73nm. The dashed straight line on the graph shows the change in nm/10 of the Bragg wavelength reflected from along the resonator length.

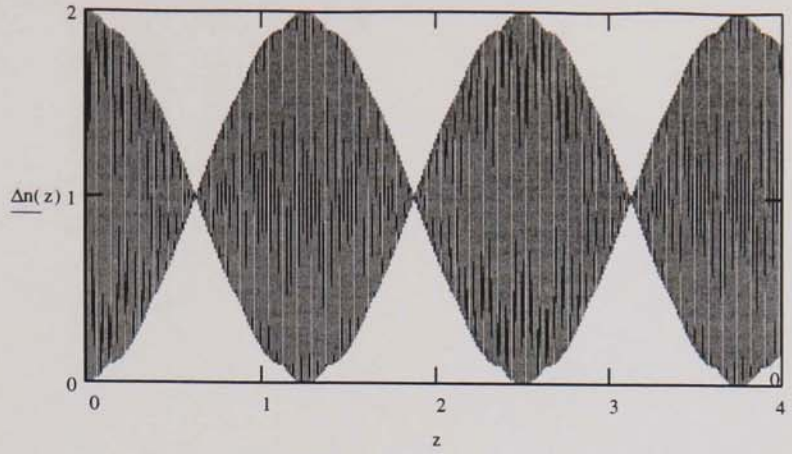

Figure 5-10 Calculated refractive index profile of a linear Moiré grating comprising of two 4mm gratings with a wavelength shift of 0.584nm.

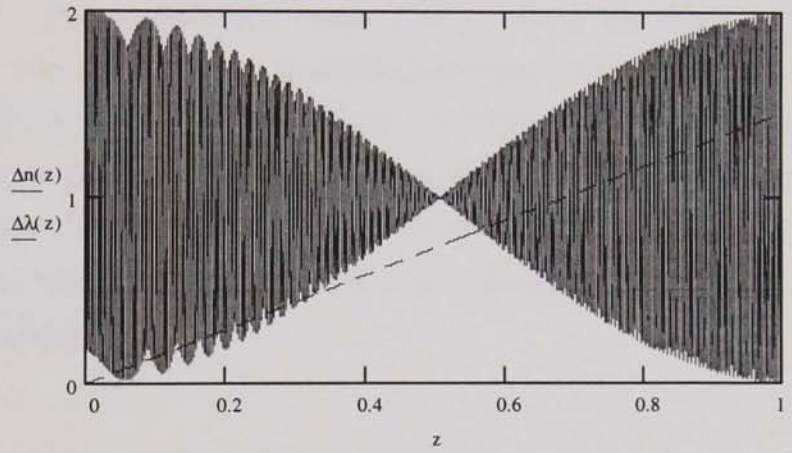

Figure 5-11 Amplitude and (wavelength shift)/10 variations along the length of a 1mm Moiré resonator filter. The gratings were 14.6nm bandwidth and the central frequencies were shifted by 0.73nm.

Again, it is easier to visualise this situation when non-optical frequencies are used in the modelled results. Figure 5-12 shows the calculated response of a 1mm resonator, using grating periodicities of 0.05 and 0.0541mm. The grating bandwidth is 0.025nm. The $\pi/2$ phase shift is again visible in the centre of the grating as is the slowly varying envelope imposed upon the increasing period refractive index modulation.

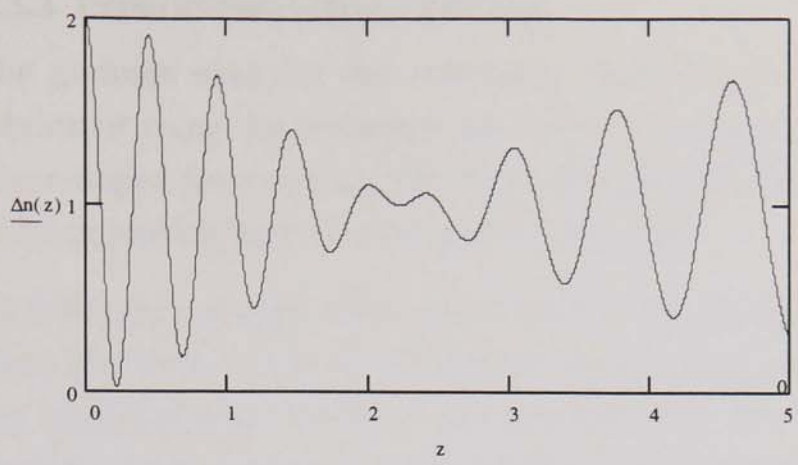

Figure 5-12 Amplitude variations along the length of a 1mm long chirped Moiré resonator.

In common with the linear case, shifting the central Bragg wavelengths by too much causes multiple passbands within the resonator bandwidth, Figure 5-13. This calculated response assumes a resonator with all the same grating characteristics as for Figure 5-11 with the exception of the central wavelength shift between the gratings which is in this case 2.92nm. This has caused four passbands to appear in the modelled response.

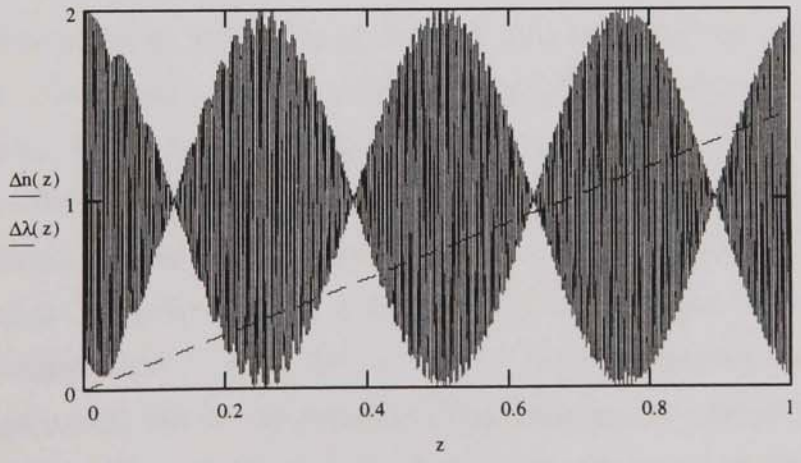

Figure 5-13 Amplitude and (wavelength shift/10) variations along the length of a 1mm Moiré resonator filter. The gratings were 14.6nm bandwidth and the central frequencies were shifted by 2.92nm.

5.3.3 Experimental Moiré gratings

The gratings used for the resonators described in this section were fabricated using the technique described in Chapter 4.1. Hydrogenated boron doped fibre was used because high photosensitivity was required to fabricated strongly reflecting chirped grating.

To fabricate a chirped Moiré resonator the first grating is written on the fibre. The fibre is then moved forward fractionally along the bisector of the interferometer. With the set-up being used this has the effect of changing very slightly the angle between the incoming wavefronts. The consequent exposure therefore fabricates a second grating, with a shifted central Bragg wavelength, on top of the first grating, thus forming the Moiré resonator. For narrow bandwidth structure measurement of the passband formation during the fabrication is difficult. When the passband exceeds ~0.05nm structure the passband formation, although not fully resolved, can be observed on an optical spectrum analyser and the second exposure is halted when the passband appears to stop increasing in transmissivity. The resonator is then characterised more fully using a narrow linewidth tuneable wavelength source.

Figure 5-14 shows the transmission spectra of two wide-stopband chirped Moiré resonators produced by this technique. The first structure (a) was fabricated in a germania doped fibre (CA2114): it has a transmission linewidth of 0.17nm in a stopband of width 4.3nm centred at 1545.2nm, corresponding to an effective finesse of ~25. For this filter, the passband transmission is >90%, and the stopband reflectivity is ~98%. The second structure, illustrated on the right, was fabricated in boron doped fibre (CIII): it has a 0.4nm transmission linewidth at a centre wavelength of 1559.5nm in a stopband of width 8.4nm, and transmittance >80%. Filters with a 12nm stopband width has also been fabricated but at the expense of increasing the transmission linewidth to 0.7nm. This trend towards increasing transmission linewidth and lower reflectivity with increasing stopband width is a consequence of holding the grating length constant in these devices, thereby effectively increasing the chirp rate.

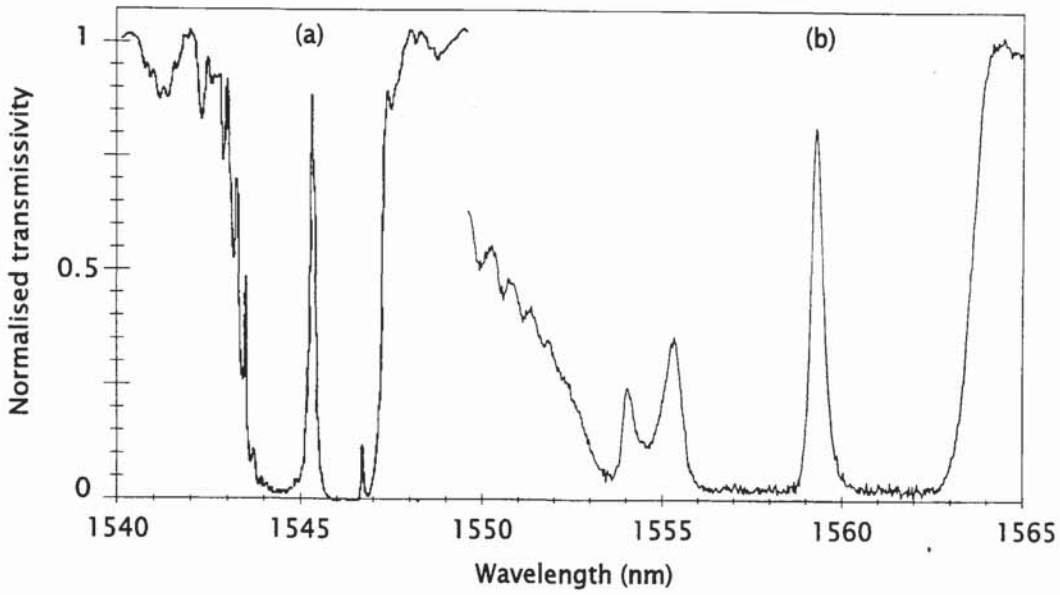

Figure 5-14 Transmission spectra for two wide-stopband chirped Moiré gratings. Passband widths (a) 0.17nm, (b) 0.4nm. Stopband widths (a) 4.2nm, (b) 8.4nm.

Increasing chirp rate dramatically has a tendency to increase the loss caused by the grating due to modal outcoupling. Although the existence of optical loss does not affect the finesse significantly for low reflectivity resonators, its effect on the finesse is considerable when the reflectivities involved are high. For resonators of constant finesse a broadening of the stopband causes the width of the passband to increase; Further decreases in the finesse of the system will increase the passband still further. The loss due to outcoupling can be minimised by using high NA fibre which exhibits stronger mode guiding. A viable alternative, now that the low loss stops bands are relative wide, would be to combine the chirped Moiré gratings with broadband chirped gratings fabricated to reflect light from the regions beyond the stopband of the resonator. This minimises the loss caused by the filter whilst maximising the frequency discrimination and noise suppression.

By concatenating a chirped Moiré resonator between two singly exposed chirped gratings, it is possible to retain the narrow transmission linewidth and greatly increase the effective stopband width. Figure 5-15 illustrates one such combination incorporating the first Moiré structure

described above and two additional chirped gratings each of ~8nm linewidth centred at 1552nm and 1568nm, respectively. The stopband width of the combination is >22nm corresponding to an effective finesse of ~48. The multi-grating approach leads to a compact all-fibre device and fabrication tolerances on the constituent structures are not stringent. The key to this is the use of the chirped resonator which separates the transmission band sufficiently from the edges of its stopband to relax the precision with which the additional grating reflection characteristics must be produced.

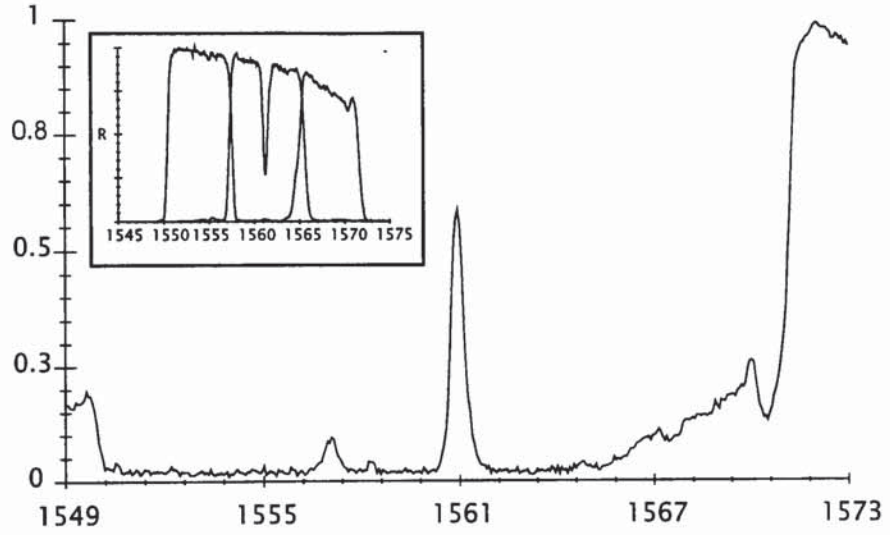

Figure 5-15 Transmission spectrum of a fibre resonator fabricated by the grating-concatenation method. Inset: reflection profiles of the three concatenated gratings.

5.3.4 Conclusions

In conclusion, wide-stop-band fibre transmission filters with a single passband channel has been fabricated by superimposing two phased-shifted, chirped gratings. This approach should be capable of producing a wide range of desired stop-band widths for fibre-optic communication and signal processing systems. In order to achieve a high finesse transmission filter it is important to minimise the optical loss of its superimposed gratings; this can be done using high NA fibres. The concatenation of resonators with chirped gratings remains the only

method of overcoming the problem of an increasing passband as the stopband increases and so is crucial to the fabrication of narrow passband filters that exhibit wide stopbands.

6. Applications of Gratings

6.1 Introduction

The motivation for much of the grating fabrication has been applications driven. This is especially true for the work on chirped fibre gratings. In 1985 Ouellette published a paper proposing the use of chirped gratings as dispersion compensators. However, it was only after the major developments of the side-writing of gratings in 1989 and the hydrogen-loading of fibres in 1993 that there was enough flexibility in the fabrication process to meet the required specifications in terms of bandwidth and reflectivity for in-fibre gratings. The technique described in Chapter 4.1, that uses interfering beams with dissimilar wavefront curvatures, enabled great flexibility in grating fabrication and led to several world-first demonstrations of possible applications. Much of the work in this chapter has benefitted from collaborations with other researchers.

Section 6.2 details the first published demonstration of dispersion compensation using chirped fibre gratings, focusing on the grating requirements for the experiment. This leads on to Section 6.3 where two identical gratings were required for an amplification system of ultrashort pulses that for the first time used in-fibre Bragg gratings instead of bulk optic components. Section 6.4 discusses various applications of chirped gratings to fibre laser systems. Sections 6.4.1 and 6.4.2 demonstrate the use of chirped gratings as modelocking elements in fibre laser cavities. Section 6.4.3 details the use of chirped fibre Fabry-Perot resonators as transmission filters in a CW multi-wavelength laser.

Certain applications of uniform-period gratings are discussed in Section 6.5. Various combinations of fibre couplers and gratings used to produce Michelson mirrors and Mach-Zehnder interferometers have been investigated. The applications include low noise laser output couplers in Section 6.5.1, variable reflectors for laser cavities in Section

6.5.2, and reflectors for gain clamping erbium fibre amplifiers in Section 6.5.3.

6.2 Experimental Demonstration of Dispersion Compensation

This work was in collaboration with J A R Williams at Aston University. Chapter 2.8 introduced the concept of dispersion. Chirped gratings had been proposed as a method of countering this effect but fibres were not photosensitive enough to provide high reflectivity over a wide bandwidth. With increasing fibre photosensitivity the technique of interfering beams with dissimilar wavefront curvatures (Chapter 4.1) was proposed as a method of fabricating chirped fibre gratings. Using this technique it was possible to fabricate the chirped gratings used for the first published demonstration of dispersion compensation[102]. This experiment used pulses that were centred at 908.5nm because of the availability of a laser source at that wavelength, but the results are equally valid for higher wavelengths.

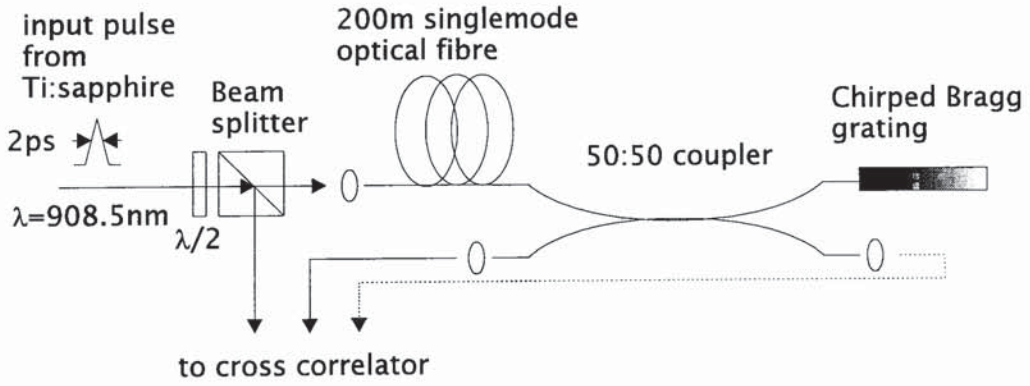

Figure 6-1 Dispersion compensation set-up.

A grating was designed with parameters to provide compensation for ~20ps nm^{-1} of dispersion. The grating was ~5mm long and 2.5nm in bandwidth and had a peak reflectivity of 60%. The central Bragg wavelength was 908.5nm. Using the set-up in Figure 6-1 the group delay dispersion of the grating was measured to be ~20ps nm^{-1} by cross-

correlating pulses reflected from the grating with those transmitted through the coupler. This result agrees with the calculated value considering the given grating parameters (from Chapter 2, $D=2Ln/c\Delta\lambda$). For a fibre that has a refractive index of 1.47 this gives $D\sim19.6ps\ nm^{-1}$.

To demonstrate dispersion compensation experimentally the set-up in Figure 6-1 was used. 1.8ps pulses at 908.5nm from a Kerr-lens modelocked Ti:Sapphire laser were broadened by 200m of single mode optical fibre with a group delay dispersion of $-100ps\ nm^{-1}\ km^{-1}$. Spectral broadening of the pulses arises from self-phase modulation in the fibre. A 50:50 coupler then directed the broadened pulses to the chirped Bragg grating where recompression occurred. The reflected compensated pulses were separated from the forward propagating dispersed pulses by a second pass through the coupler. These pulses were then measured in the temporal regime by cross-correlating them with pulses taken directly from the laser.

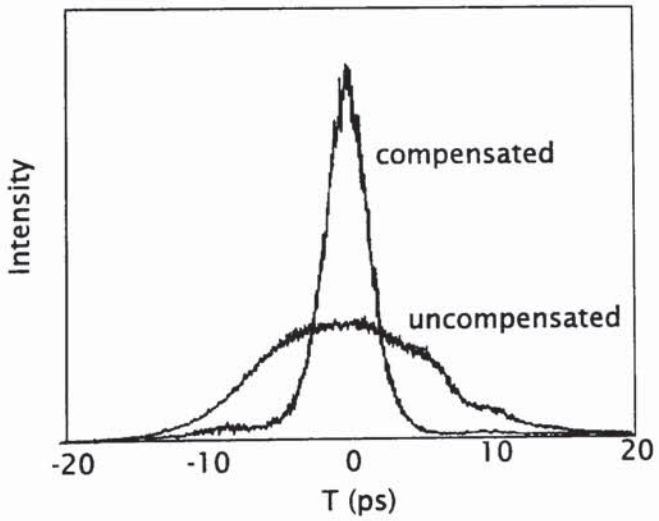

Figure 6-2 Cross-correlation profiles of the dispersed pulse and the dispersion compensated pulse.

Figure 6-2 shows the cross-correlations acquired for the dispersed pulse (wide trace) and the compensated pulse (narrow trace) measured before and after the Bragg grating for an incident peak power of 5W. It shows how the pulse is compressed by the grating to give a narrow undistorted pulse with very little energy remaining in the wings. Figure 6-3 shows

the numerical calculated values. There is strong agreement between the experimental and calculated results leading to the conclusion that both the grating structure and the dispersion compensation have been modelled with some accuracy.

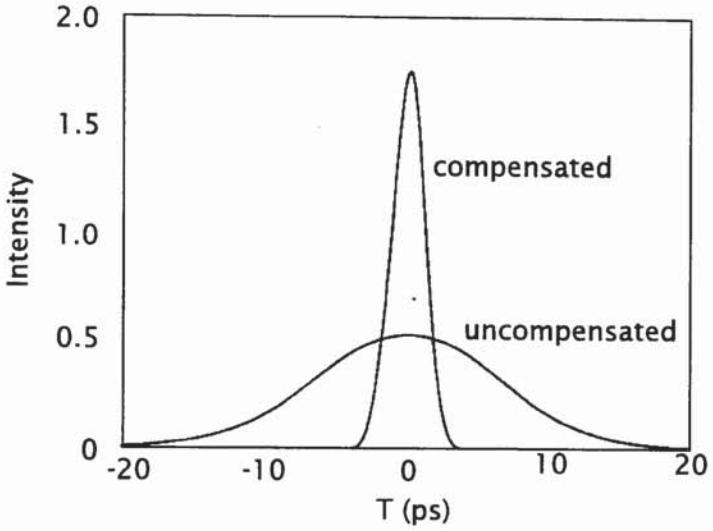

Figure 6-3 Numerical simulation profiles of cross-correlations for dispersed and dispersion compensated pulses.

6.3 All-fibre Femtosecond Chirped Pulse Amplification System

Aspects of the work[103] were collaborative with A Galvanauskas and M E Fermann at IMRA America, Inc. The onset of the non-linearities limits the maximum peak power of ultra-short pulses entering a rare-earth doped fibre amplifier to typically less than 1nJ[104]. This means that the amplifiers must be used at energies considerable lower than the saturation energy (~1mJ). To overcome this problem, chirped pulse amplification systems were developed where the pulse is stretched prior to amplification and then recompressed on the far side of the amplifier[105]. The introduced non-linearities in the amplifier are therefore smaller since the peak powers are substantially lower.

This idea has been demonstrated using pairs of bulk diffraction gratings aligned to introduce a wavelength dependent delay across a pulse[106,107]. The disadvantage of using bulk gratings to do this is that the systems lack compactness, require active alignment and are expensive to produce. Chirped fibre gratings were an attractive alternative for the bulk grating systems. The success relied on the ability to fabricate broadband chirped gratings with near identical dispersion and reflectivity profiles. This reproducibility is possible using the fabrication technique described in Chapter 4.1 where two beams with different wavefront curvatures are interfered to produce a non-uniform pattern of fringes.

Two gratings 5mm in length and 15nm bandwidth, with a centre wavelength of 1561nm were fabricated to demonstrate chirped pulse amplification. The reflectivity of the gratings was higher than 80% and the grating group velocity dispersion was estimated to be ~3.3ps nm^{-1}. The gratings were fabricated in a hydrogen-loaded germania-doped fibre (CA2114). A high NA fibre was chosen so that the short wavelength loss was minimised, as was any asymmetry between the reflection either side of the gratings. Also, by using a fibre that saturates, for broad bandwidth gratings, at a reflectivity less than 100%, the exposure time could be lengthened to allow the grating growth to saturate without inducing too high a refractive index change.

The gratings were integrated into an amplification set-up as shown in Figure 6-4. The input pulses for the system were provided by a passively modelocked fibre laser that generated bandwidth limited $sech^2$ pulses of duration 330fs at a repetition rate of 8MHz. These pulses were split by a 50:50 coupler and reflected from the first chirped grating that was orientated so that it had positive dispersion. This resulted in the input pulses being stretched to ~30ps with a peak power of 20pJ. The reflected pulses then travelled through an erbium doped amplifier, pumped with a 980nm wavelength MOPA (master oscillator power amplifier) laser diode. To minimise dispersion in the amplifier a 4.5m long erbium-doped fibre with low negative dispersion of ~-3ps nm^{-1} km^{-1} was used. The energy of the pulses at the end of the amplifier was 6nJ and the corresponding peak power of the stretched pulses was at the

threshold of nonlinear optical effects. This threshold was the limiting factor for the maximum pulse energy.

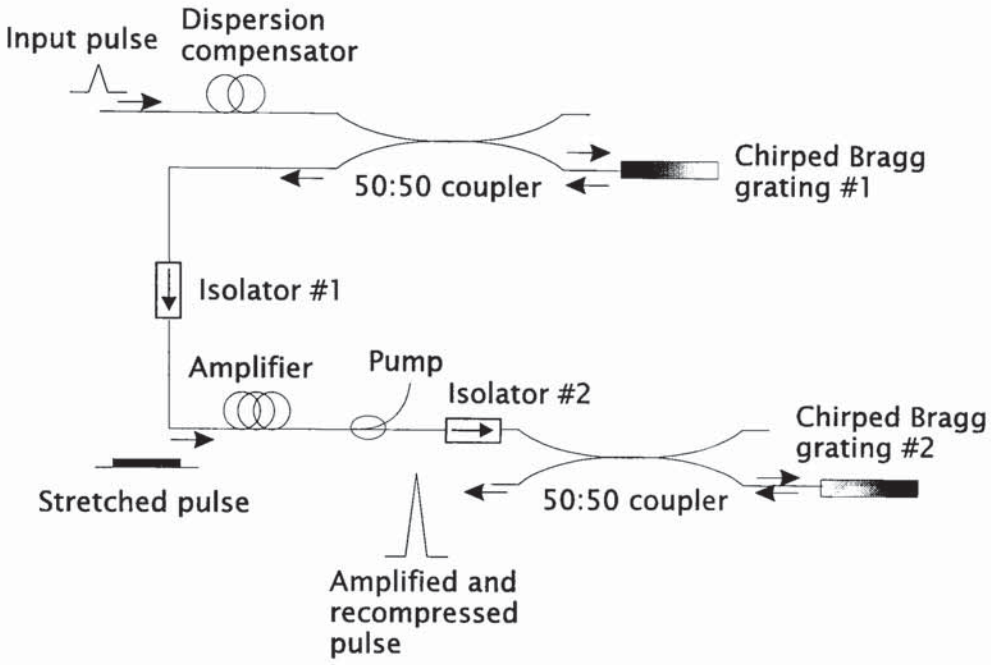

Figure 6-4 Amplification system for ultrashort pulses.

The effect of any net dispersion in the system due to fibre dispersion and any small difference in the fibre gratings was then compensated by using a 70cm length of positive dispersion optical fibre (D~86ps nm^{-1} km^{-1}) at the front of the system.

Autocorrelation traces of the initial and recompressed pulses are shown in Figure 6-5. The recompressed pulse had a duration of 408fs and so the system only increased the pulse width by 20% in total and the pulse shape was maintained. This was a considerably better result than that obtained with the bulk diffraction grating stretchers and compressors.

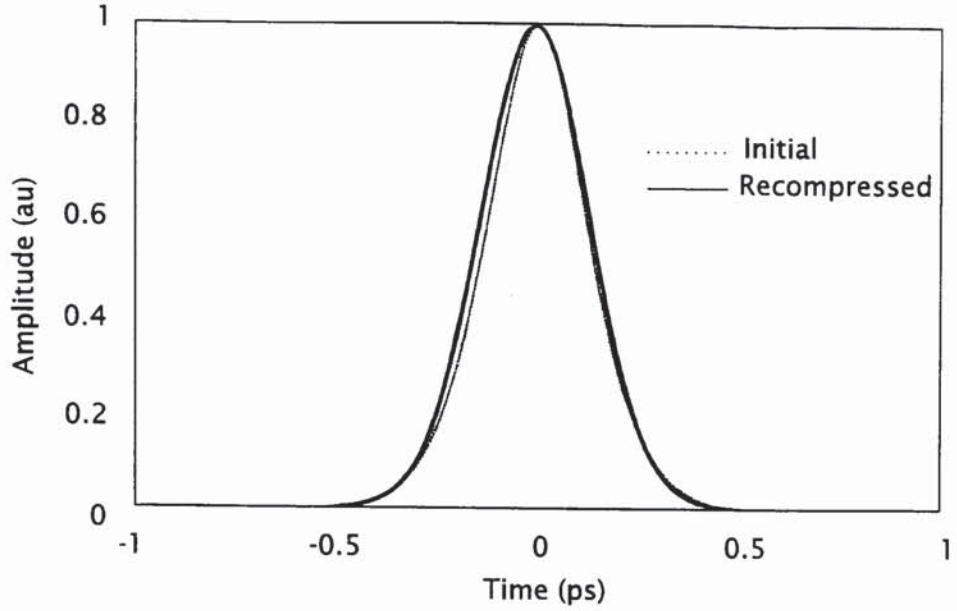

Figure 6-5 Autocorrelation traces of initial and recompressed pulses when two chirped Bragg gratings were used. Initial sech² pulse had 330fs duration and the recompressed pulse duration was 408fs.

For comparison a similar system was set up with a 170m length of standard (Corning SM-28) fibre replacing the stretcher Bragg grating. In this instance, the resulting pulses showed considerable distortion and had a duration of 544fs, the corresponding autocorrelation traces are shown in Figure 6-6. A comparison of the results from the two set-ups highlights the advantage of using a double grating system to preserve the shape, quality, and duration of the pulse due to the reciprocity of the grating dispersion[103]. Using a scheme with non-identical dispersion components introduces pulse distortion because higher dispersion orders are not matched. Figure 6-7 shows the calculated second-harmonic autocorrelation results for a recompressed 300fs pulse for both schemes[103]. There is good agreement between the calculated and experimental results indicating that the chirp profiles of the gratings used were linear to a good degree. The standard SM-28 fibre has an estimated second order dispersion of $1.37 \times 10^5 fs^3\ m^{-1}$. This second order dispersion is unmatched by the grating used as a compressor and so is responsible for the wings on the autocorrelation trace.

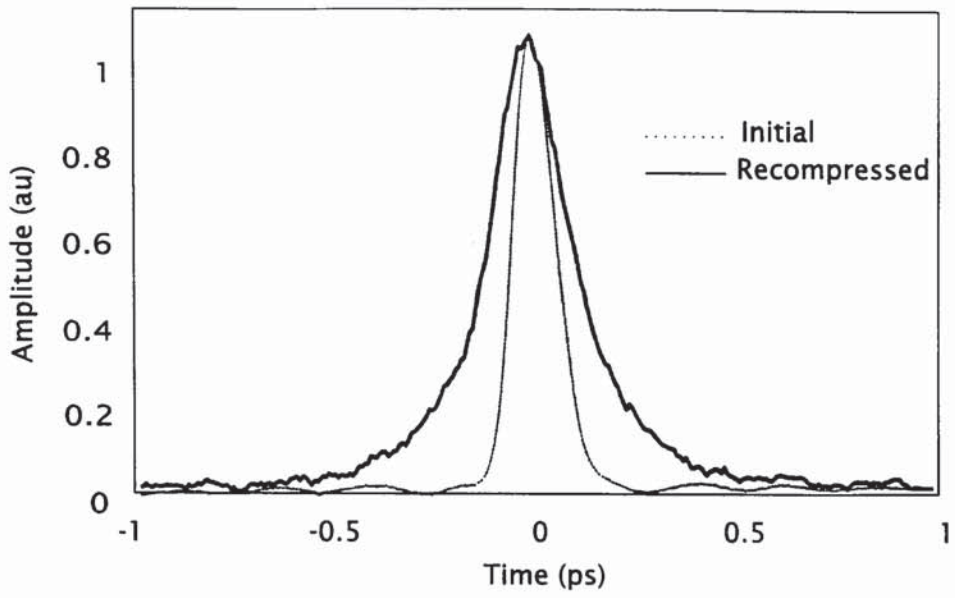

Figure 6-6 Autocorrelation traces of initial and recompressed pulses when a standard fibre as a stretcher and a chirped Bragg grating as a compressor were used. Initial sech² pulse had 330fs duration and the recompressed pulse duration was 544fs.

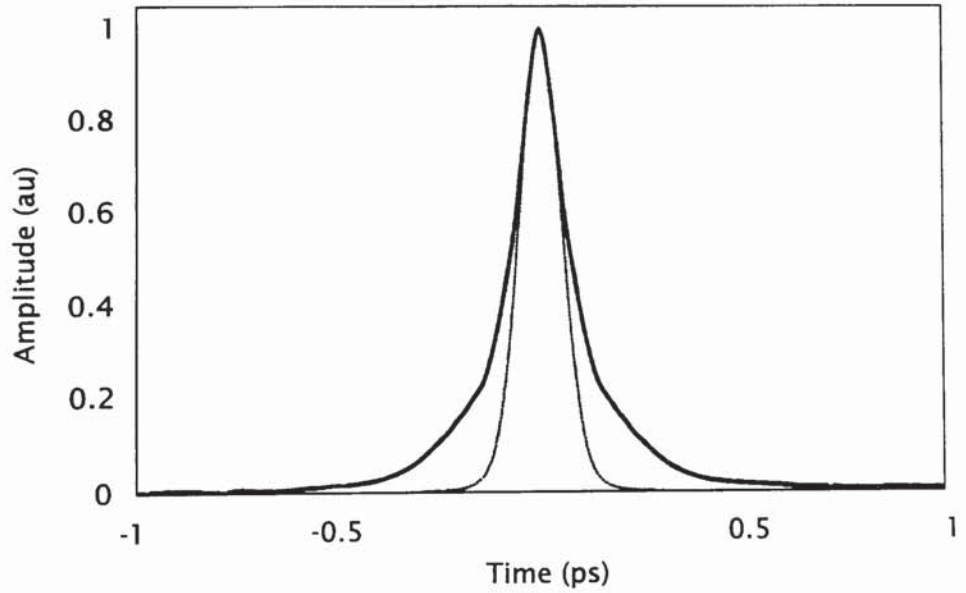

Figure 6-7 Calculated autocorrelation traces for 300fs initial pulses stretched and compressed with two identical 5mm long fibre gratings (dotted line), stretched with 170m of standard SM-28 fibre and recompressed with a linearly chirped fibre grating (solid line).

6.4 Chirped Gratings for Fibre Laser Systems

Fibre gratings are highly compatible with fibre lasers with advantages over bulk optics in compactness, simplicity and cost. Many different configurations have been proposed and demonstrated; three different arrangements are presented here. The first two sections involve gratings that are needed to provide large amounts of intracavity dispersion. Section 6.4.1 deals with the generation of high power picosecond pulses from a fibre laser containing two gratings with negative group delay dispersion. Section 6.4.2 describes how gratings centred at 1064.5nm have incorporated into a high-power neodymium soliton fibre laser. Section 6.4.3 uses chirped gratings in the form of Fabry-Perot resonators as frequency selecting elements in a ring laser operating CW at eleven simultaneous, and equally spaced, wavelengths.

6.4.1 Generation of 10nJ picosecond pulses from a modelocked fibre laser

This work was in collaboration with M Fermann of IMRA America, Inc. Fibre dispersion limits the pulse widths that can be achieved from fibre lasers. Chirped fibre gratings provide a convenient method of introducing dispersion into a cavity to overcome this limit[108]. This results in a substantial increase in the pulse energies compared to conventional soliton fibre lasers.

Two gratings were designed and fabricated to fit the requirements of the set-up shown by Figure 6-8. The gratings centred at 1555nm exhibited a reflection bandwidth of 13nm with a maximum reflectivity approaching 100%. The gratings were approximately 4mm long and therefore, from the expression $D = \frac{2Ln}{c\Delta\lambda}$ given in Chapter 2.8, they had a group delay dispersion in the region of $3.87ps^2$. The gratings were fabricated in a boron doped fibre (CIII), that had been hydrogen-loaded for seven days at 120 atmospheres pressure at room temperature.

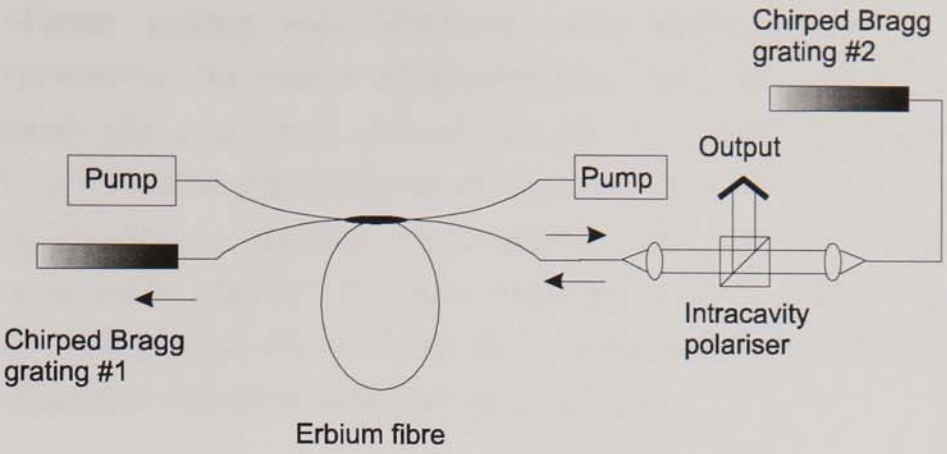

Figure 6-8 Passively modelocked fibre laser incorporating two chirped fibre gratings for pulse width control.

The gratings were incorporated into the laser shown in Figure 6-8. The fibre laser was pumped by two 980nm MOPA laser diodes that delivered up to 700mW of total launch power. An intracavity polariser was used to restrict the cavity to one polarisation and to act as a variable output coupler. The fibre laser exhibited passive modelocked operation that was initiated by applying a small perturbation to the undoped fibre and thought to be sustained by nonlinear polarisation evolution[109], where a minimum launch power of ~400mW was required. At a repetition rate of 17MHz the average modelocked power of the laser was between 100 and 170mW for pulse energies of 6 and 10nJ respectively. Assuming $sech^2$ pulses, autocorrelation traces gave pulse widths of ~4ps for the 10nJ pulses.

6.4.2 Neodymium fibre laser[110]

The work was completed in collaboration with M Hofer and M H Ober at the Technische Universität, Vienna. Since chirped fibre gratings can provide negative dispersion at wavelengths over the full transparency range of optical fibres the design of compact picosecond soliton fibre lasers becomes possible at almost any available rare earth transition.

Figure 6-9 shows the set-up of the high-power neodymium soliton laser. The Bragg grating was written into a germania doped fibre (CA3555) that has a cut-off at ~900nm. The fibre had been hydrogen-loaded for one week at 150 atmospheres pressure and room temperature. The

~12mm grating was fabricated using wavefronts with dissimilar curvatures. The centre wavelength was 1066.5nm and the reflectivity bandwidth was ~7nm. The grating was over double the usual grating length because a group delay dispersion of around $10ps^2$ over as large a bandwidth as possible was required. The increase in length was achieved by placing a 1:3 beam expander in front of the beamsplitter in the holographic set-up. From the grating parameters the group delay dispersion would be expected to be $\sim 10.14ps^2$.

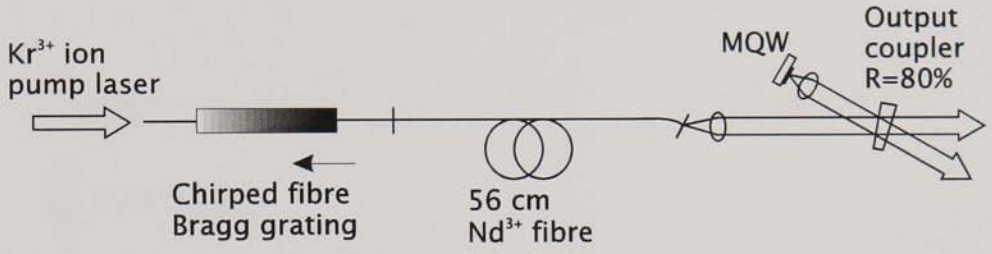

Figure 6-9 Cavity set-up of a Nd^{3+} fibre laser incorporating a chirped fibre Bragg grating for dispersion compensation.

The dispersion characteristics were measured using a white light fibre Michelson interferometer[111]. Figure 6-10 shows the interferogram and the reflectivity spectrum of the grating. From the measurement it was deduced that the grating exhibited a group delay dispersion of $-9.27 \pm 0.5ps^2$ and a third order dispersion of $-1.5 \pm 0.2ps^3$ at a wavelength of 1065nm.

The laser exhibited a CW lasing threshold of 22mW of launched power; passive modelocking occurred at 390mW of launch power. The average output power of the modelocked laser was 65mW at a repetition rate of 52MHz corresponding to a pulse energy of 1.25nJ. The laser routinely produced 6ps pulses with a time bandwidth product of 0.32, close to a bandwidth limited $sech^2$ pulse shape.

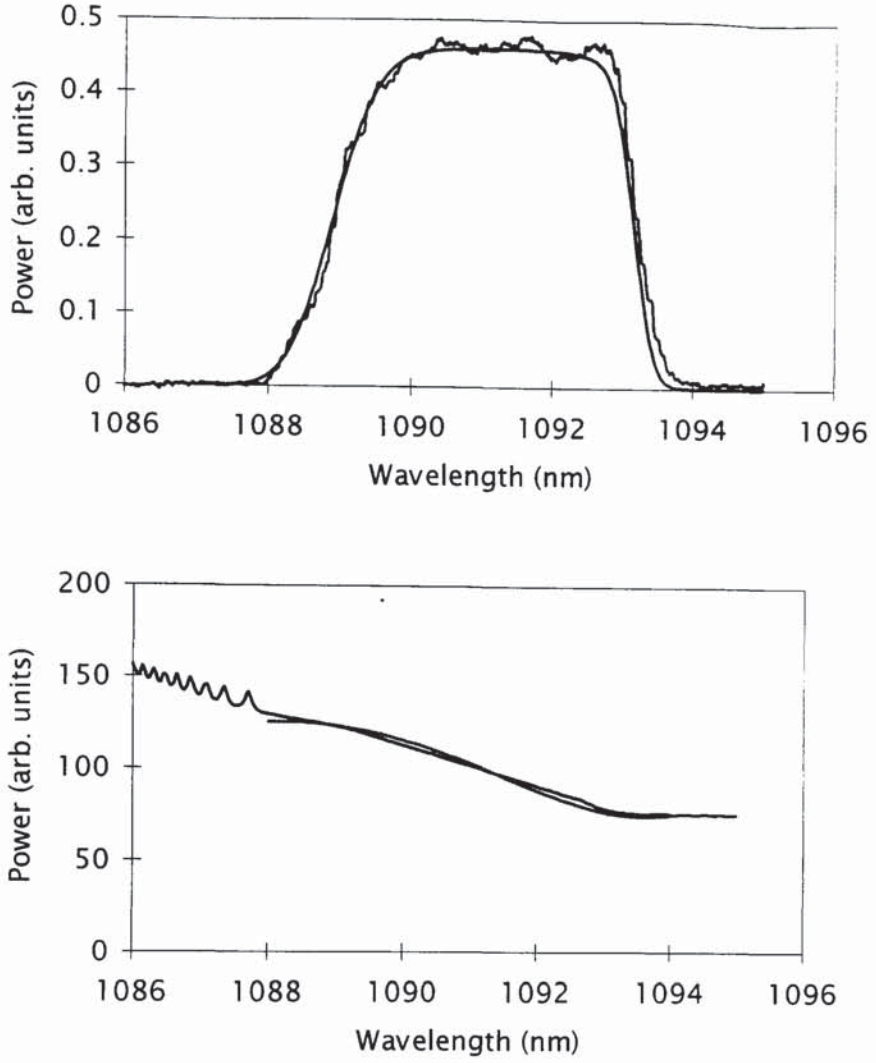

Figure 6-10 Interferogram and reflectivity of the chirped fibre grating. The solid curve is a quadratic fit to the time delay.

6.4.3 CW multi-wavelength laser

Another use for chirped gratings in laser cavities in the form of broadband resonators is as frequency selectors. In collaboration with G Town at Sydney University, chirped Bragg resonators were used as wavelength selectors in multi-wavelength lasers with the aim of demonstrating multichannel sources for wavelength division multiplexed telecommunication systems. Multi-wavelength sources have been realised using arrays of semiconductor laser chips and a feedback element like a diffraction grating[112,113,114] and similarly by using arrays of

doped fibre amplifiers. A multi-wavelength laser using a length of multimode fibre as a frequency filter in ring cavity to give four simultaneous lasing lines around 1600nm has also been demonstrated[115]. Using the fibre resonators gave more simultaneous lasing lines than had been previously demonstrated. The resonators are easy to define in terms of wavelength and line spacing giving good flexibility.

Chirped fibre Fabry-Perot resonators were designed for application in multiple wavelength sources containing a single gain medium. The ring laser configuration used is illustrated in Figure 6-11. The isolator confined the laser to unidirectional operation to avoid spatial hole burning effects. The gain medium consisted of six metres of alumino-silicate fibre doped with ~250ppm of erbium and was pumped by 300mW of power from a Ti-sapphire laser.

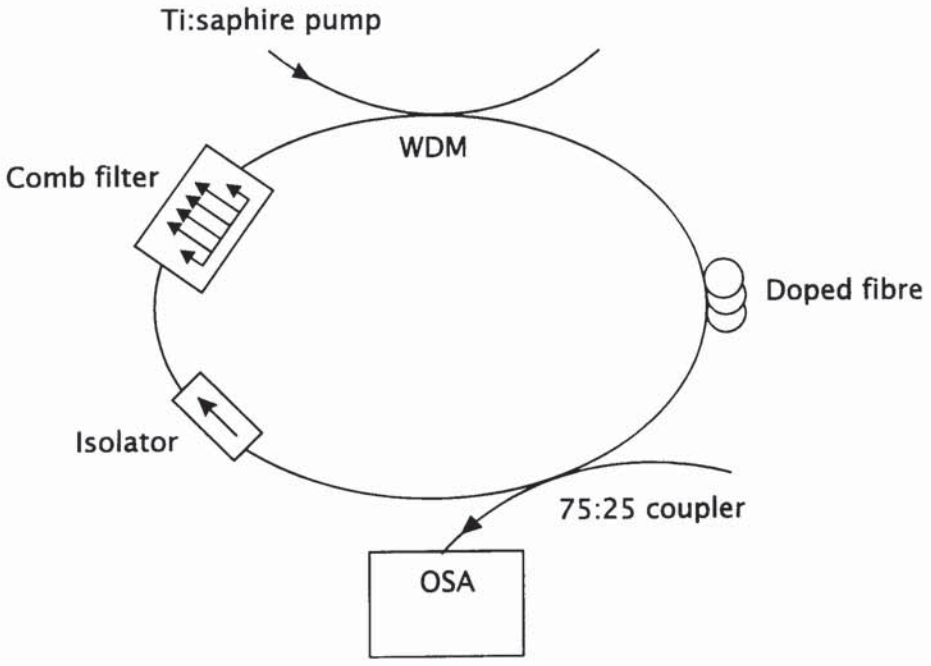

Figure 6-11 Ring laser cavity incorporating a fibre grating, resonator, comb filter.

One of the main problems with multi-wavelength operation of a single gain medium that experiences homogeneous broadening is that cross gain saturation occurs between the lasing wavelengths and they compete against each other for gain. This leads to unstable operation

but can be reduced by cooling the gain medium[116,117]. In this case the doped fibre was cooled to 77K.

The chirped Fabry-Perot resonator was combined with a 6nm tuneable filter to stop lasing outside the resonator bandwidth. A selection of different resonators were incorporated into the laser cavity. It was found that the filters with the highest finesse gave the laser lines with the highest stability and narrowest spectral widths. Figure 6-12 shows a comb of eight out of the eleven lasing lines achieved with a filter of finesse 4 and free spectral range of 0.65nm. The plot illustrates the excellent long-term stability and narrow linewidths from this laser configuration. The linewidth of the lasing lines was measured to be 0.1nm on all lines, this was the resolution limit of the optical spectrum analyser. To check that the lines were simultaneously lasing, one line was selected using a monochromator and monitored using the voltage fluctuations from an InGaAs photodetector. Typical signal-to-noise ratio for each lasing line was better than 20dB.

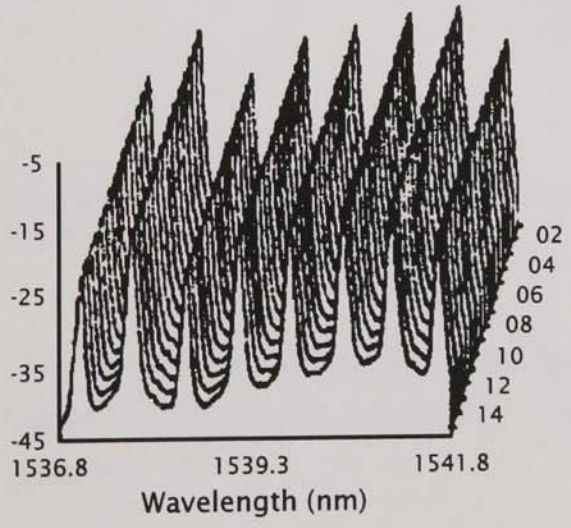

Figure 6-12 Comb of eleven lasing lines achieved with a filter of finesse 4 and free spectral range 0.65nm.

6.5 Fibre Grating-Coupler Arrangements

By writing gratings on the two arms of a coupler a wavelength selective folded Mach-Zehnder is achieved where light outside the bandwidths of the grating are separated from the reflected signal. A number of applications using fibre grating-coupler arrangements have been proposed. This work was done in collaboration with K Byron, H Rourke and T Cullen at BNR Europe Ltd.

6.5.1 Background

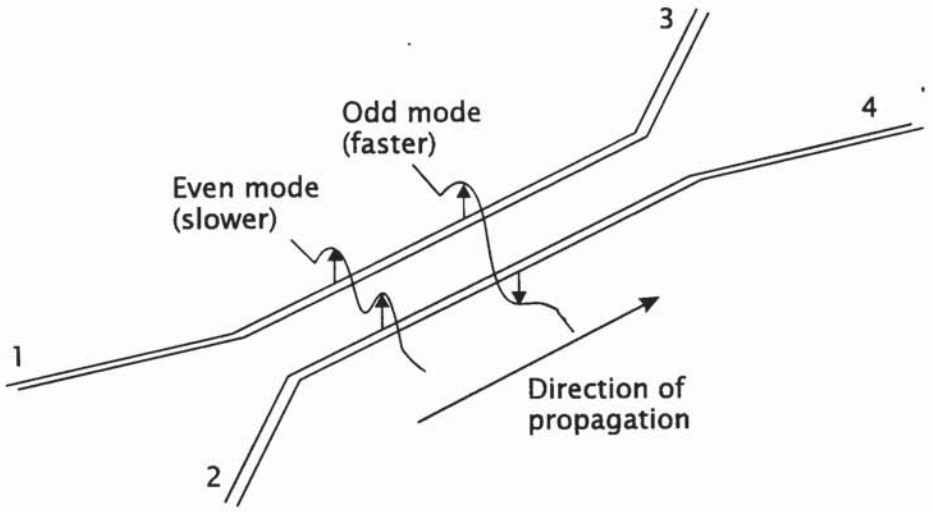

Figure 6-13 Even and odd modes in a single mode fibre coupler where arm 1 is the input arm.

The phase relationship between light in the two arms of a coupler (Figure 6-13) is well documented[118]. The phase between the two modes is given by

$$\phi = L(\beta_{even} - \beta_{odd}) = \frac{2\pi L}{\lambda}(n_{even} - n_{odd})$$

Equation 13

where β is the field propagation constant, λ is the wavelength in a vacuum of the light travelling down the fibre, and $n_{even,odd}$ are the effective refractive indices for each of the modes.

The input field E through arms 1 and 2 can be considered to have component associated fields E_1 and E_2 where

E_1=E/2+E/2=E and E_2=E/2-E/2

Equation 14

If the common phase delays due to the physical length of the coupler are neglected, exp(-jβL), the output from arms 3 and 4 can be written as

$$E_4 = \frac{E}{2} - \frac{E}{2} \cdot \exp(j\phi)$$

$$E_4 = \frac{E}{\sqrt{2}} \cdot \sqrt{1-\cos\phi} . \exp\left(j\frac{\phi}{2} - j\frac{\pi}{2} \right)$$

Equation 15

So for any coupler there will always be a π/2 phase lag between the two outputs of arms 3 and 4. This is independent of the coupling strength and the length of the coupler. The value of ϕ determines the coupling ratio. At the input of the coupler where there is no coupling, ϕ is zero. When ϕ is π/2 a 50% split ratio is achieved and when ϕ is π then 100% of the output appears in arm 4. The extra π/2 term in the expression for E_4 is important when the combination of gratings and couplers is considered.

By neglecting the common phase shift, exp(jϕ/2), the electric field in arms 3 and 4 can be written in terms of the fields in arms 1 and 2 such that

$$E_3 = aE_1 + jbE_2$$
$$E_4 = jbE_1 + aE_2$$

Equation 16

Ideally $a^2 + b^2 = 1$, where a^2 is the power coupling ratio between connected arms and b^2 is the coupling coefficient between coupled arms.

If a grating is fabricated on each of the coupler output ports (arms 3 and 4 in Figure 6-14) then light within the grating bandwidths will be reflected and pass through the coupler a second time. This arrangement

was described by Morey[119] and Bilodeau[120]. If the gratings are identically spaced from the coupler then the reflected light exits through arm 2. To understand this, the relative phases of the light in each arm must be considered. Any light that is coupled across the coupler has a $\pi/2$ phase delay. Hence light travelling down arm 4 is delayed by $\pi/2$ relative to arm 3. The distance travelled between the coupler and being reflected by the grating and then on the return journey back to the coupler is equal in both arms, so no extra phase delay is incurred.

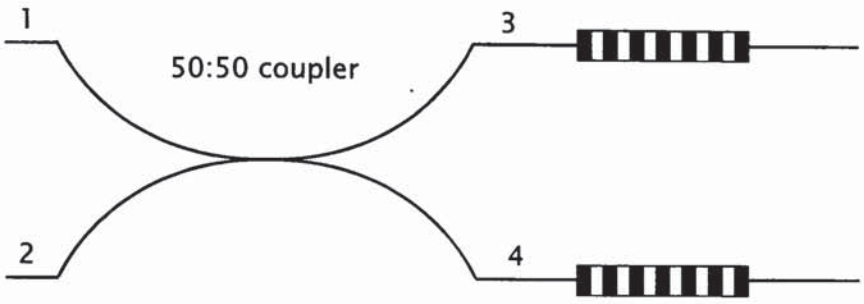

Figure 6-14 Michelson mirror - a fibre coupler with a grating on each of arms 3 and 4 at equal distances from the coupler.

The reflected light then enters the coupler for a second time. There are now two inputs, a component from arm 3 and one from arm 4. Considering the phase relative to the original wave, from light reflected from arm 3 there will be a zero phase delay into arm 1 and an added $\pi/2$ phase delay into arm 2. From arm 4, into arm 1 there is a $\pi/2$ phase delay which is added to the $\pi/2$ delay that was already experienced when passing through the coupler the first time to give a π delay, and into arm 2 there will be no added phase delay which leaves the resultant phase delay as $\pi/2$. Hence, the components in arm 1 are π out of phase and hence will interfere destructively to give zero output from that arm. The components in arm 2 are in-phase, both with a $\pi/2$ phase delay from the original input wave, and will add constructively to give a 100% output from that port.

Figure 6-15 shows a set up used to demonstrate this principle. The coupler is made of BNR Europe Ltd boron doped fibre (CIII) and mounted on a glass block to provide environmental stability. Previous to exposure the coupler was hydrogen-loaded for ten days at 100 atmospheres pressure and room temperature.

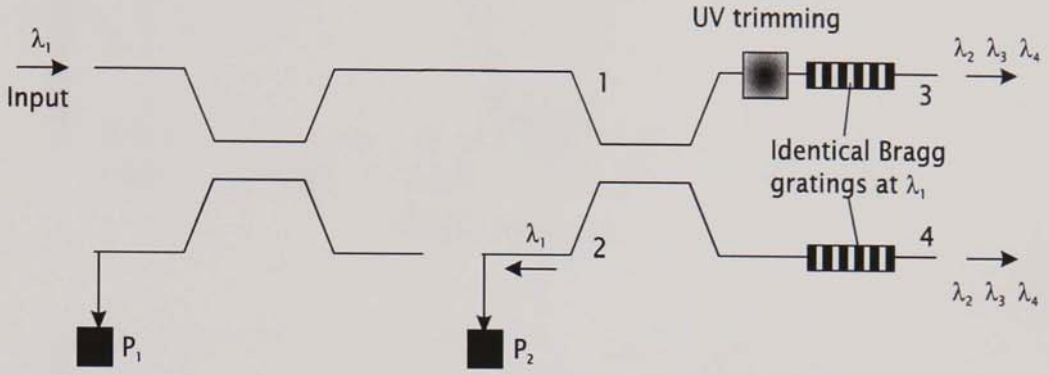

Figure 6-15 Set-up for Michelson mirror filter measurements.

Two gratings were successfully written adjacent to the fused region of a coupler. It was necessary to balance the interferometer after several days because the hydrogen diffusing out of the fibre altered the relative path lengths down each arm.

The upper graph of Figure 6-16 shows the transmission through arms 3 and 4 of the coupler, showing the profiles of both gratings. Note that there is some loss especially at the low wavelength side which could be reduced by decreasing the exposure time and/or possibly using a fibre with a higher NA. The gratings were made consecutively because this tends to give equal Bragg wavelengths for each grating. The power measured at P_2 was then monitored as one arm was UV trimmed to give minimum back reflection down the input arm. The lower graph shows the reflected signal going back down the input arm from the first and the reflection after the second grating was made. This was monitored during exposure to minimise the back reflections with the exposure times for each grating being roughly equal. The remaining sidebands are due to the larger width of the second grating.

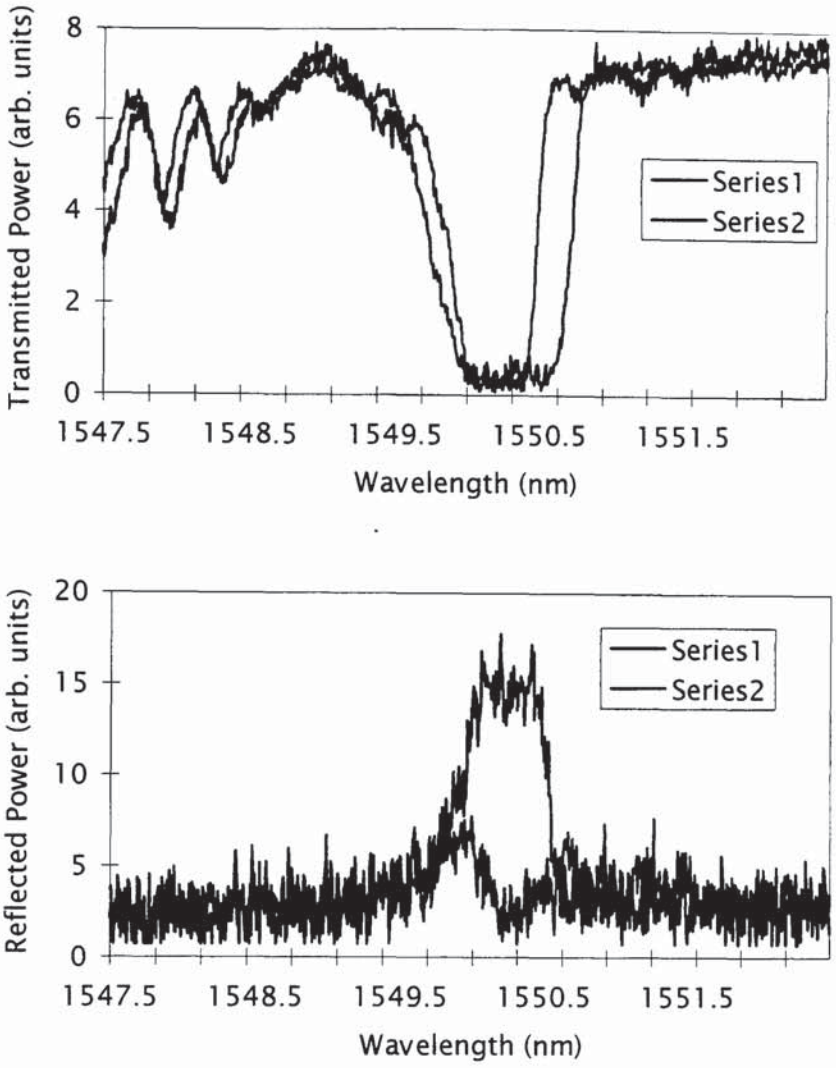

Figure 6-16 Response of a Michelson mirror. The upper trace shows the transmission profile through each arm containing a grating. The lower trace shows the reflected signal from one grating measured at P_1 and the final output at P_1 after the second grating had been fabricated.

Small errors in the positioning of the gratings can be compensated for by UV trimming the fibre in front of one of the gratings. A change in refractive index of ~1.3×10^{-4} over a 3mm length is required to tune through a phase change of π for gratings at 1550nm. UV trimming on one arm of the device produces a variable reflectivity depending on the relative phase between light reflected from the gratings in ports 3 and 4 of the coupler. This is demonstrated experimentally. The power at P_1 and P_2 of Figure 6-15 were measured. For 100% reflecting gratings and exactly 50:50 couplers then $P_2+2P_1=100\%$ of the reflected power. Arm 3

of the coupler was then UV trimmed in front of the grating whilst the power at P_1 and P_2 were continuously monitored. Figure 6-17 shows the power variation recorded at the two places. A cyclic process is clearly evident and indicates how the reflectivity of the device changes as the path length of one arm is altered by a localised change in the refractive index.

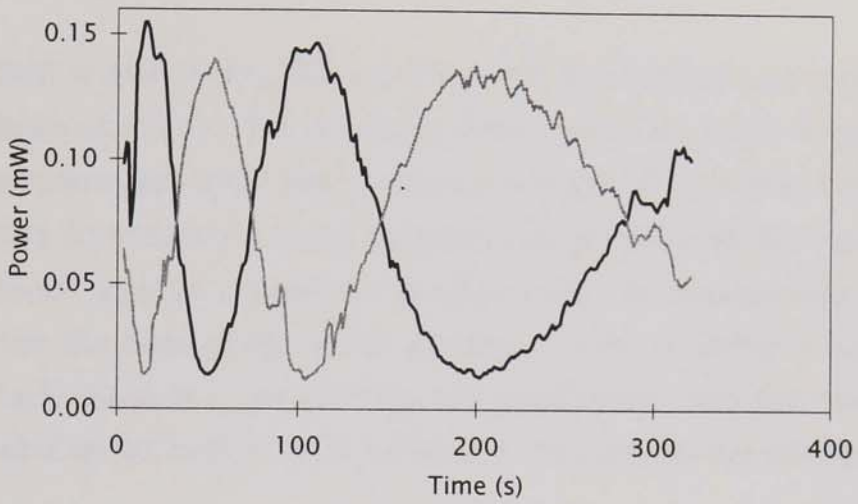

Figure 6-17 Power variation of reflected signals in arms 1 (grey) and 2 (black) of the coiupler as the device is UV trimmed.

6.5.1.1 Mach-Zehnder device

The coupler-grating idea can be taken one step further by adding a second coupler on the other side of the gratings. This was first demonstrated in planar waveguide structures[121] and later extended to fibre devices[122,123]. The Mach-Zehnder devices used were fabricated at BNR Europe Ltd. The coupling sections are only centimetres apart and the path lengths are equal along the two arms to an accuracy of several tenths of a micron. The devices were bonded onto a glass substrate for stability and hydrogenated before the gratings were written in the central region. UV trimming was used to equalise the path lengths.

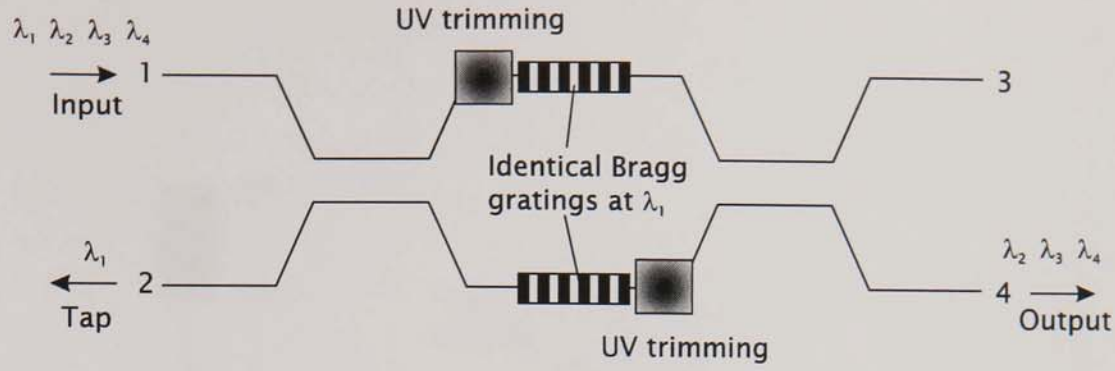

Figure 6-18 Mach-Zehnder filter

Light is split by the first coupler with the coupled arm acquiring a phase delay of $\pi/2$. At the second coupler, since the path lengths inbetween couplers are equal, interference conditions dictate that 100% of the light exits from arm 4, i.e. the diagonal port across from the input. Hence, the device acts as a balanced Mach-Zehnder in transmission. In reflection over the bandwidth of the gratings it acts as either a balanced folded Mach-Zehnder if the gratings are equidistant from the coupler, or as an unbalanced folded Mach-Zehnder if the gratings are not equidistant.

6.5.2 Fibre laser optimisation with a variable reflectivity mirror

Using the fibre grating Michelson mirror effectively combines the properties of a mirror and a bandstop filter in an all-fibre device whilst causing no extra losses to the cavity. Fibre lasers incorporating fibre Bragg gratings were first reported in 1990 by Kashyap *et al*[124] and have since been frequently applied. In these situations, the grating provides a convenient integrated mirror which avoids the need to use bulk optical mirrors. However, in common with other laser systems the output of the laser has a broadband background of spontaneous emission and in sources used for optical communication this can lead to system penalties. The Michelson-grating arrangement, shown in Figure 6-19, can be used as a laser output coupler/reflector to separate the lasing wavelength from the broadband noise. Within the bandwidth of the two gratings, light is reflected down either of arms 1 and 2. Outside the bandwidth of the gratings the background fluorescence noise is transmitted through arms 3 and 4.

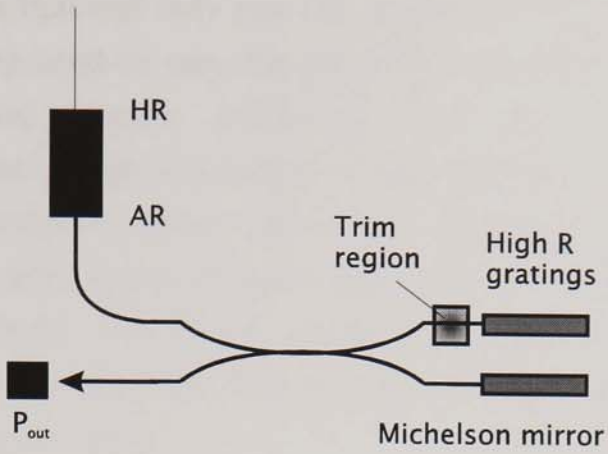

Figure 6-19 Laser optimisation using a Michelson mirror.

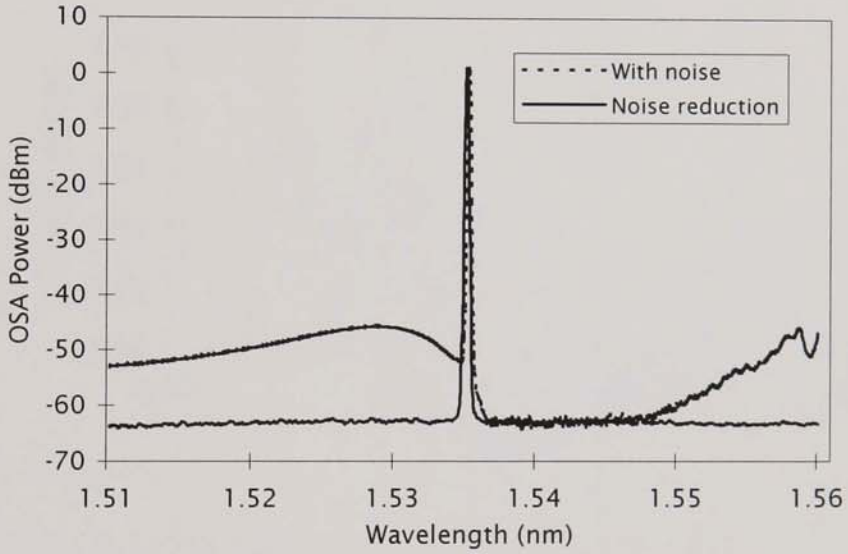

Figure 6-20 Noise reduction using a Michelson-grating device as a laser output coupler/reflector.

Figure 6-20 shows the output spectrum of an erbium fibre laser constructed in this way. One trace shows the output spectrum through the Michelson mirror end of the cavity and there is very little noise outside the lasing wavelength. The other trace is the output through the opposite end of the cavity and shows the ASE noise that would normally be seen from a fibre laser. Superimposed on this is the loss spectrum due to the profile of the grating. The total reduction in noise is at least 20dB.

The ability to introduce multiple λ/2 changes in the optical path length means that not only can this cycling of the power reflected from each port be used to vary the power output of any given laser system with different output reflectors, but also that there is enough photosensitivity in the fibre to then bias the same device in order to give the optimum output. Figure 6-21 shows how the output power of the laser varies as one of the coupler arms is UV trimmed to cycle the device reflectivity. The power variation is definitely periodic but is not as smooth as expected. This is possible due to some resonances occurring within the cavity.

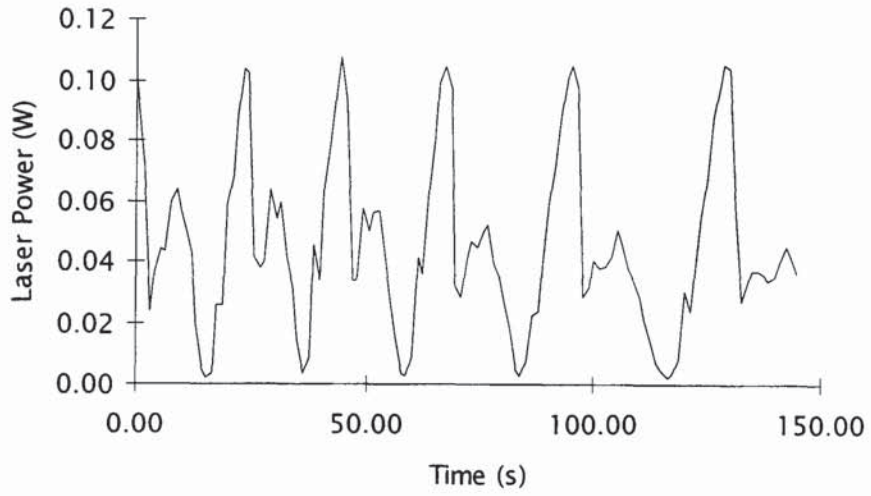

Figure 6-21 Cyclic power variation of laser as UV trim.

6.5.3 Gain clamping

The gain of an erbium fibre amplifier depends on the pump power and the mean input signal power. This introduces crosstalk and instability into a system. If the gain can be stabilised in some way then higher signal powers can be used and the systems specifications are simplified. Various approaches can be used to limit the gain variation, and introducing Bragg gratings into the amplifier so that lasing occurs may provide a passive solution. A single narrow bandwidth lasing wavelength in a homogeneously broadened gain media clamps the population

inversion over the emission bandwidth and so defines the gain at all other bandwidths.

There have been several reported applications of fibre Bragg gratings to produce gain clamped erbium doped fibre amplifiers[125,126,127]. Delavaque[125] used 1480nm Bragg gratings at both ends of an amplifier to induce lasing action. Beyond the threshold of laser action the gain across the rest of the erbium fluorescence bandwidth remained constant and independent of pump power. Massicott[127] used a similar arrangement but substituted 1520nm gratings and found that a control laser closer to the gain peak gave better gain stability. It was found that a Mach-Zehnder device could also be used at the end of the amplifier to provide both a feedback element at the end of the amplifier to initiate lasing at a specified wavelength and as a WDM element to separate the lasing wavelength from the signal wavelength with minimal loss.

Because of the availability of the Mach-Zehnder device the initial study was limited to low gain systems where the induced lasing action was ~1558nm. The maximum gain achieved on clamping is dependent on, and increases with, the lasing threshold and would therefore be higher if the amplifier was made to lase at a wavelength well away from the gain peak. Hence, ideally this should be repeated using a grating at 1520nm, allowing an amplifier with much greater gain to be demonstrated.

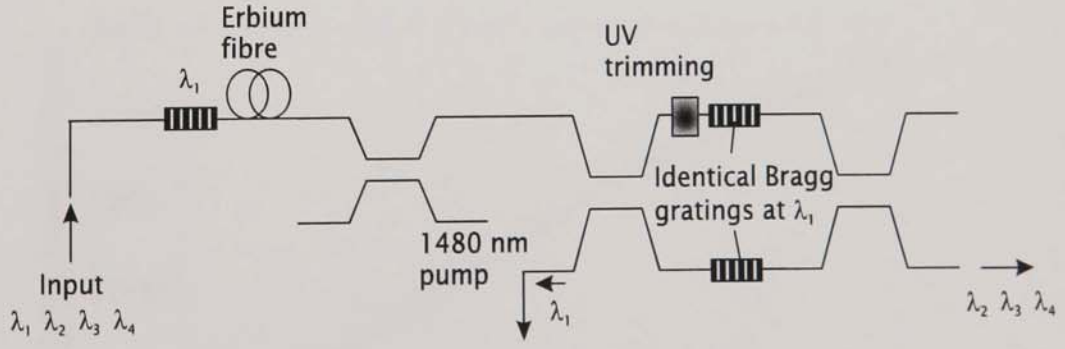

Figure 6-22 Gain clamping with a Mach-Zehnder device.

Figure 6-22 shows the experimental arrangement initially used to demonstrate gain clamping. Gratings of peak response at 1558nm were written holographically onto the centre of the Mach-Zehnder and the

arms were balanced by post fabrication UV exposure. A modulation of 100kHz was imposed on the signal wavelengths so that, using a lock-in amplifier, the signal could be distinguished from the pump and induced lasing power components. Figure 6-23 shows the signal power output measured for signals at 1530nm, 1540nm and 1550nm. Figure 6-24 shows how without gain clamping the signal amplification continues to rise as the pump power for the amplifier increases. There is a slight curve on the signal output of the amplifier at higher currents. This is due to the pump laser characteristic, see Figure 6-25.

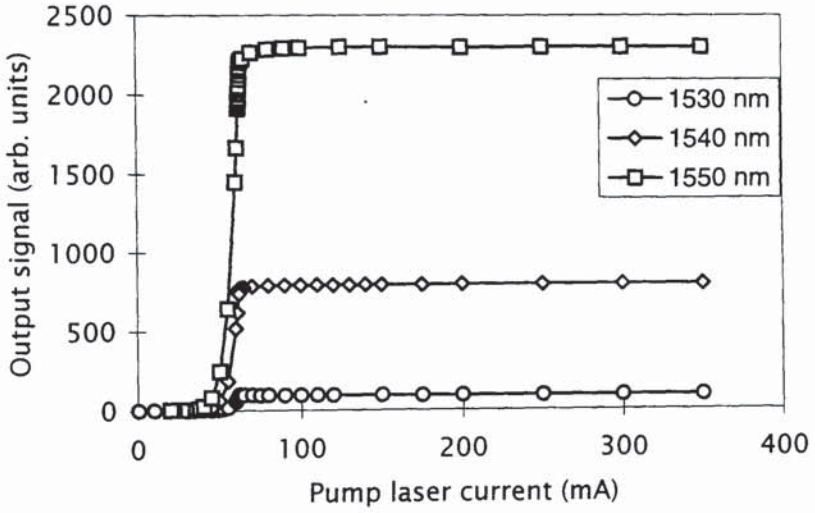

Figure 6-23 Signal powers measured for 1530, 1540 and 1550nm.

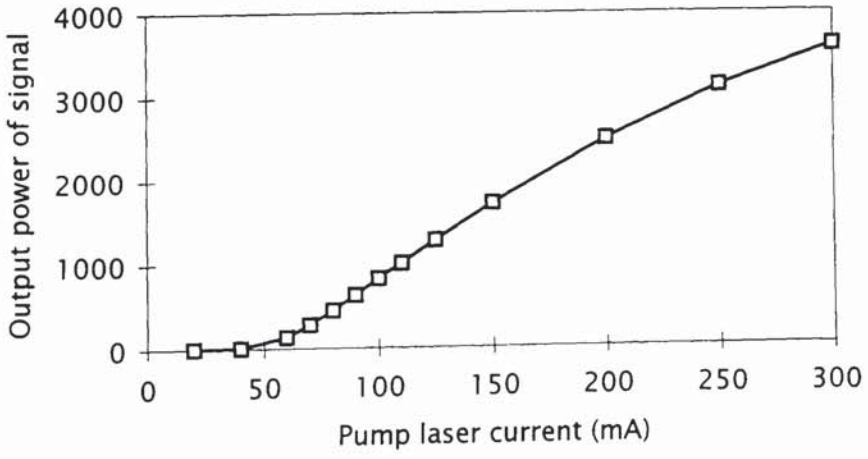

Figure 6-24 Signal output with no gain clamping.

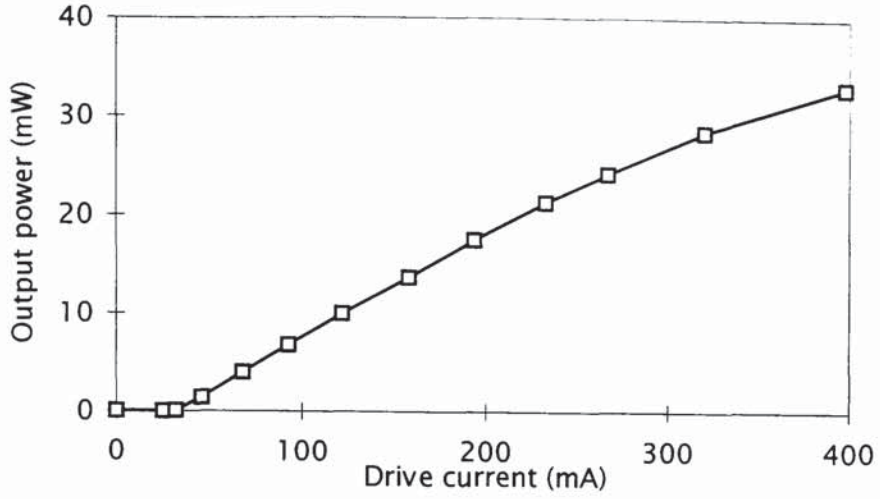

Figure 6-25 Pump laser power variation with increasing current.

Using this set-up it was also possible to demonstrate a change in the clamped amplifier gain by tuning a single grating so that its peak wavelength no longer coincided with that of the Mach-Zehnder gratings; this alters the feedback and hence also the lasing threshold and the level of gain clamping. In Figure 6-26 two levels of gain clamping can be seen, corresponding to the grating being subject to zero strain and then stretched in length by 0.2%. By straining the grating it was possible to continuously alter the gain level by up to 3dB.

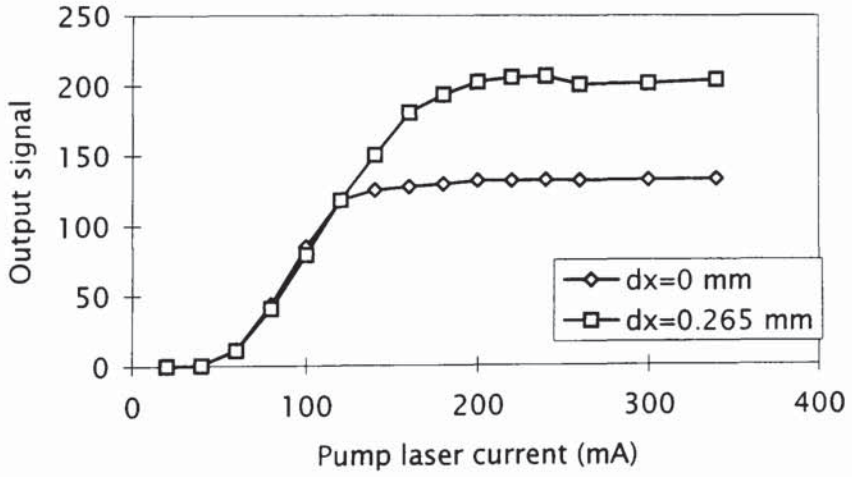

Figure 6-26 Detuning a grating to change the amplifier gain.

7. Conclusions

This thesis has covered the fabrication and application of uniform-period and chirped fibre Bragg gratings. The gratings were fabricated using holographic interferometric techniques. From the study of uniform-period gratings it was found that gratings increase in strength during an exposure up to a maximum reflectivity and thereafter they decay; also, the maximum reflectivity attained has been shown to be power dependent. These results are consistent with other published work. Hydrogen-loading was found to significantly enhance the photosensitivity of germania doped fibres, thereby substantially reducing the exposure times and producing strong, ~100% reflecting gratings.

The work on the fabrication of chirped gratings was highly successful. Three different fabrication techniques were developed, including the first direct-write technique for fabricating chirped fibre gratings to be published. The technique of using the interference between two beams with dissimilar wavefront curvatures has been extensively used to provide a wide range of gratings. Three different optical variants of within this technique were used, providing the capability to fabricate chirped gratings varying from those with bandwidths of 180nm, to those with small to medium bandwidths and linear chirp profiles, to those with narrow bandwidth quadratic chirped profiles.

Once the basic problems of chirped fibre grating fabrication had been overcome, two broad areas of application were pursued. The first of these sought to determine whether or not chirped gratings could be concatenated to fabricate more complicated structures: this led to the resonator work described in Chapter 5. For the first time it was shown that Fabry-Perot and Moiré resonators could be successfully fabricated using chirped gratings. This overcame the limitation of being able to fabricate only devices that had both a narrow passband and a narrow stopband and, consequently, increased the range of possible applications for this technology. The second broad area pursued was in exploring applications where gratings could be used to replace bulk

optic components, concentrating on applications that took advantage of the attributes given by the fabrication techniques available, namely, the extensive wavelength and dispersion flexibility, the smooth response profiles achievable, and, where necessary, the ease with which, relatively accurately, a matched pair of gratings could be fabricated.

The identification of relevant applications led to the first published demonstrations of all-fibre grating dispersion compensation and femtosecond chirped pulse amplification. Chirped gratings were used to provide dispersion in modelocked lasers. Chirped resonators were inserted into a ring laser to produce a comb of eleven simultaneously lasing wavelengths, the resonator ensuring that the lasing lines were evenly spaced and stable in terms of wavelength. Finally, gratings were combined with couplers and fibre Mach-Zehnder interferometers to investigate novel applications. It was shown that these devices can be used as variable output couplers for laser cavities enabling the cavity optimisation. The devices also act as filters for the suppression of ASE noise. The gain clamping of amplifiers was also demonstrated in a configuration that allowed the clamping level to be set by varying the feedback, at the lasing wavelength, into the amplifier.

Future work should include further characterisation of the relationship between power, fibre-type and refractive index change. Further work would be desirable on the fabrication and applications of quadratic chirped gratings. The origins of, and limits imposed by, loss in resonating structures needs further consideration. There remain issues surrounding the lifetime of gratings especially when high optical powers are involved. However, the largest area of future work will probably be in the identification of new applications and the fabrication of relevant gratings.

In addition to the applications mentioned above, it seems highly probable the gratings will be used for dispersion compensation in high-bit rate systems, for control and noise suppression in amplifiers, and for sensor arrays. The incorporation of gratings into real systems will require further work on the packaging of gratings.

8. Publications resulting from this work

1. K C Byron, K Sugden, T Bricheno, I Bennion, 'Fabrication of chirped Bragg gratings in photosensitive fibre', *Electronics Letters*, **29**, 1659-1660, 1993.

2. K Sugden, I Bennion, A Molony, N Copner, 'Chirped gratings produced in photosensitive optical fibres by fibre deformation during exposure', *Electronics Letters*, **30**, 440-441, 1994.

3. K.Sugden, I.Bennion, 'Fabrication and properties of chirped fibre gratings', *IOP topical meeting* on In-fibre Bragg Gratings and Special Fibres, London, May 1994.

4. M Farries, D Reid, M Goodwin, K Sugden, A Molony, I Bennion, 'The fabrication of chirped fibre optic Bragg gratings with 144nm reflection bandwidths', *IOP topical meeting* on In-fibre Bragg Gratings and Special Fibres, London, May 1994.

5. M C Farries, K Sugden, D C J Reid, I Bennion, A Molony, M J Goodwin, 'Very broad reflection bandwidth (44nm) chirped fibre gratings and narrow bandpass filters produced by the use of an amplitude mask', *Electronics Letters*, **30**, 891-892, 1994.

6. J A R Williams, I Bennion, K Sugden, N J Doran, 'Fibre dispersion compensation using a chirped in-fiber Bragg grating', *Electronics Letters*, **30**, 985-986, 1994.

7. K Sugden, I Bennion, A Molony, M C Farries, D C J Reid, M J Goodwin. 'Fabrication and properties of chirped fibre gratings with reflection bandwidths exceeding 50nm and narrow bandpass fibre grating filters', *CLEO Europe*, Amsterdam, Netherlands, *Technical Digest*, 230-231, August 1994.

8. G Town, K Sugden, J Williams, I Bennion, S Poole, 'Wide-band Fabry-Perot-like filters in optical fibre', *IEEE Lasers and Electro-Optics Society Annual Meeting (LEOS'94)*, Boston, MA, Technical Digest, 142-144, November 1994.

9. G E Town, K Sugden, J A R Williams, I Bennion, S B Poole, 'Wide-band Fabry-Perot-like filters in optical fibre', *IEEE Photonics Technology Letters*, **17**, 78-80, 1994.

10. K Byron, H Rourke, P Foote, M Goodwin, C Ragdale, M Gower, S Mihailov, I Bennion, K Sugden, L Zhang, P Dyer, R Farley, F Payne, 'Fabrication of fibre grating structures and applications in systems', *IEE Colloquium*, DTI Optoelectronic Systems LINK Programme, London, paper 4, June 1994.

11. G Town, K Sugden, J Williams, I Bennion, S Poole, 'In-fibre broad-band Fabry-Perot filters', 19th Australian Conference on Optical fibre Technology (*ACOFT '94)*, Melbourne, December 1994.

12. K Sugden, L Zhang, I Bennion, G E Town, 'Efficient fibre grating transmission filters', *IEE Colloquium*, Optical Fibre Gratings and their Applications, London, 1995.

13. J A R Williams, K Sugden, L Zhang, I Bennion, N J Doran, 'In-fibre grating systems for pulse compression and complete dispersion compensation', *IEE Colloquium*, Optical Fibre Gratings and their Applications, London, January 1995.

14. M C Farries, D C J Reid, M J Goodwin, K Sugden, I Bennion. 'Fabrication and performance of packaged fibre gratings for telecommunications', *IEE Colloquium*, Optical Fibre Gratings and their Applications, London, January 1995.

15. M E Fermann, A Galvanauskas, D Harter, K Sugden, I Bennion, 'Compact all-fibre femtosecond-pulse amplification circuit', *Topical Meeting on Advanced Solid State Lasers (ASSIL'95)*, Memphis, Tennessee, 1995.

16. A Galvanauskas, M E Fermann, D Harter, K Sugden, I Bennion, 'All-fibre femtosecond pulse amplification circuit using chirped Bragg gratings', *Applied Physics Letters*, **66**, 1053-1055, 1995.

17. M E Fermann, K Sugden, I Bennion, 'High-power picosecond soliton fibre lasers using chirped fibre Bragg gratings', *Conf on Lasers and*

Electro-optics (CLEO'95), Baltimore, Maryland, Technical Digest, 51-52, May 1995.

18. M E Fermann, K Sugden, I Bennion, 'High power soliton fibre laser based on pulse width control with chirped fibre Bragg gratings', *Optics Letters*, **20**, 172-174, 1995.

19. M E Fermann, K Sugden, I Bennion, 'Generation of 10 nJ picosecond pulses from a modelocked fibre laser', *Electronics Letters*, **31**, 194-195, 1995.

20. J Chow, G Town, B Eggleton, M Ibsen, K Sugden, I Bennion, 'Multiwavelength operation of an erbium-doped fibre laser by using in-fibre comb filters', *Conf on Lasers and Electro-optics (CLEO'95)*, Baltimore, Maryland, Technical Digest, 8-9, May 1995.

21. A Galvanauskas, M E Fermann, D Harter, K Sugden, I Bennion, 'Use of in-fibre chirped Bragg gratings in all-fibre femtosecond-pulse amplification circuit', *Conf on Optical Fibre Communications (OFC'95)*, San Diego, California, Technical Digest, MG2, February 1995.

22. L Zhang, K Sugden, I Bennion, A Molony, 'Wide stopband chirped fibre Moiré grating transmission filters', *Electronics Letters*, **31**, 477-478, 1995.

23. L Zhang, K Sugden, I Bennion, 'Chirped fibre-Moiré-grating transmission filters', *Conf on Lasers and Electro-optics (CLEO'95)*, Baltimore, Maryland, Technical Digest, 29-30, May 1995.

24. J Chow, G Town, M Ibsen, B Eggleton, K Sugden, I Bennion, 'Multiwavlength operation of an erbium-doped fibre laser using in-fibre comb-filters', *Proc 10th International Conf on Integrated Optics and Optical Fibre Communications (IOOC'95)*, Hong Kong, June 1995.

25. M E Fermann, K Sugden, I Bennion, 'Environmentally stable high power soliton fibre lasers using chirped fiber Bragg gratings', *Optics Letters*, **20**, 1625-1627, 1995.

26. M Hofer, M H Ober, R Hofer, M E Fermann, G Sucha, D Harter, K Sugden, I Bennion, C A C Mendonca, T H Chiu. 'High power neodymium

soliton fibre laser using a chirped fiber grating', *Optics Letters*, **20**, 1701-1703, 1995.

27. L Zhang, K Sugden, J A R Williams, I Bennion, 'In-fibre transmission filters with broad stopbands using chirped Bragg gratings', Topical Meeting on Photosensitivity and Quadratic Nonlinearity in Glass Waveguides: Fundamentals and Applications *(PQNGW'95)*, Portland, Oregon, Technical Digest, 132-135, September 1995.

28. K Sugden, L Zhang, J Williams, I Bennion, 'Dissimilar wavefront technique for linear and quadratic chirps' Topical Meeting on Photosensitivity and Quadratic Nonlinearity in Glass Waveguides: Fundamentals and Applications *(PQNGW'95)*, Portland, Oregon, Technical Digest, 136-139, September 1995.

29. K Sugden, I Bennion, K Byron, H Rourke, 'Grating Michelson mirrors for optimised fibre laser performance' Topical Meeting on Photosensitivity and Quadratic Nonlinearity in Glass Waveguides: Fundamentals and Applications *(PQNGW'95)*, Portland, Oregon, Technical Digest, 261-264, September 1995.

30. L Zhang, K Sugden, J A R Williams, I Bennion, D C J Reid, C M Ragdale, 'Post-fabrication exposure of gap-type bandpass filters in broadly chirped fibre gratings', *Optics Letters,* **20**, 1927-1929, 1995.

31. I Bennion, J A R Williams, L Zhang, K Sugden, N J Doran, 'UV-written in-fibre Bragg gratings', *Opt Quantum Electronics*, **28**, 93-135, 1996.

32. J Chow, G Town, B Eggleton, M Ibsen, K Sugden, I Bennion, 'Multiwavlength operation in an erbium-doped fibre laser using in-fibre comb-filters', *Photonics Technology Letters*, **8**, 60-62, 1996.

9. References

[1] G Meltz, W W Morey, W H Glen, 'Formation of Bragg gratings in optical fibres by a transverse holographic method', *Opt Lett*, **14**, 823-825, 1989.

[2] F Ouellette, 'All-fibre filter for efficient dispersion compensation', *Opt Lett*, **16**, 303-305, 1991.

[3] R M Jopson, A H Gnauck, R M Derosier, 'Compensation of fibre chromatic dispersion by spectral inversion.', *Electron Lett*, **29**, 576-578, 1993.

[4] H G Winful, 'Pulse compression in optical fibre filters', Appl Phys Lett, **46**, 527-529, 1985.

[5] J E Roman, K A Winnick, 'Waveguide grating filters for dispersion compensation and pulse compression', *IEEE J Quantum Electron*, **29**, 975-982, 1993.

[6] F Ouellette, 'Limits of chirped pulse compression with an unchirped Bragg grating filter', *Appl Opt*, **29**, 4826-4829, 1991,

[7] L T Blair, S A Cassidy, 'Wavelength division multiplexed sensor network using Bragg fibre gratings', *Electron Lett*, **28**, 1734-1735, 1992.

[8] I M I Habbab, A A M Saleh, N Frigo, G E Bodeep, 'Noise reduction in long-haul lightwave all amplifier systems', *J Lightwave Technol*, **10**, 1281-1289, 1992.

[9] M Farries, C M Ragdale, D C J Reid, 'Broadband chirped fibre Bragg filters for pump rejection and recycling in erbium doped fibre amplifiers', *Electron Lett*, **28**, 487-489, 1992.

[10] R Kashyap, R Wyatt, R J Campbell, 'Wideband gain flattened erbium fibre amplifier using photosensitive fibre blazed grating', *Electron Lett*, **29**, 154-156, 1993.

[11] R P Davey, R P E Flemming, K Smith, R Kashyap, J P Armitage, 'Mode-locked erbium fibre laser with wavelength selection by means of fibre Bragg grating reflector', *Electron Lett*, **27**, 2087-2089, 1991.

[12] G G Ball, W W Morey, 'Efficient integrated Nd^{3+} fibre laser', *IEEE Photon Technol Lett*, **3**, 1077-1078, 1991.

[13] I M Jauncey, L Reekie, R J Mears, D N Payne, C J Rowe, D C J Reid, I Bennion, 'Narrow-linewidth fibre laser with integral fibre grating', *Electron Lett*, **22**, 987-988, 1986.

[14] G Meltz, W W Morey, 'Design and performance of bi-directional fibre Bragg grating taps', *Conf on Optical Fibre Communication (OFC'91)*, San Diego, California, Tech Dig, **44**, 1991.

[15] K O Hill, Y Fuji, D C Johnson, B S Kawasaki, 'Photosensitivity in optical fibre waveguides : application to reflection filter fabrication', *Appl Phys Lett*, **32**, 647-649, 1978.

[16] B S Kawasaki, K O Hill, D C Johnson, Y Fujii, 'Narrow-band Bragg reflectors in optical fibres', *Opt Lett*, **3**, 66-68, 1978

[17] R Kashyap, J R Armitage, R Wyatt, S T Davey, D L Williams, 'All-fibre narrowband reflection gratings at 1500 nm,' *Electron Lett*, **26**, 730-731, 1990.

[18] H Patrick, S L Gilbert, 'Growth of Bragg gratings produced by continuous wave ultraviolet light in optical fibres', *Opt Lett*, **18**, 1484-1486, 1993.

[19] B J Eggleton, P A Krug, L Polardian, K A Ahmed, H-F Liu, 'Experimental demonstration of compression of dispersed optical pulses by reflection from self-chirped optical Bragg gratings', *Opt Lett*, **19**, 877-879, 1994.

[20] Q Zhang, D A Brown, L Reinhart, T F Morse, 'Simple prism-based scheme for fabricating Bragg gratings in optical fibres', *Opt Lett*, **19**, 2030-2032, 1994.

[21] I Bennion, D C J Reid, C J Rowe, W J Stewart, 'High-reflectivity monomode-fibre grating filters', *Electron Lett*, **22**, 341-343, 1986.

[22] J Buus, D J Robbins, C M Ragdale, D C J Reid, 'Transmission characteristics of fibre gratings', *IEE Proceedings*, **138**, 155-159, 1991.

[23] K O Hill, B Malo, F Bilodeau, D C Johnson, J Albert, 'Bragg gratings fabricated in monomode photosensitive optical fibre by UV exposure through a phase mask', *Appl Phys Lett*, **62**, 1035-1037, 1993.

[24] R Kashyap, J R Armitage, R J Campbell, D L Williams, G D Maxwell, B J Ainslie, C A Millar, 'Light-sensitive optical fibres and planar waveguides', *BT Technol J*, **11**, 1993.

[25] D Z Anderson, V Mizrahi, T Erdogan, A E White, 'Production of in-fibre gratings using a diffractive optical element', *Electron Lett*, **29**, 566-568, 1993.

[26] J Martin, F Ouellette, 'Novel writing technique of long and highly reflective in-fibre gratings', *Electron Lett*, **30**, 811-812, 1994.

[27] H N Rourke, S R Baker, K C Byron, R S Baulcomb, S M Ojha, S Clements, 'Fabrication and characterisation of long, narrowband fibre gratings by phase mask scanning', *Electron Lett*, **30**, 1341-1342, 1994.

[28] R J Campbell, R Kashyap, 'Spectral profile and multiplexing of Bragg gratings in photosensitive fibre', *Opt Lett*, **16**, 898-900, 1991.

[29] Q Zhang, D A Brown, L Reinhart, T F Morse, J Q Wang, G Xiao, 'Tuning Bragg wavelength by writing gratings on pre-strained fibres', *IEEE Photon Technol Lett*, **6**, 839-341, 1994.

[30] J D Proshaska, E Snitzer, S Rishton, V Boegli, 'Magnification of mask fabricated fibre Bragg gratings', *Electron Lett*, **29**, 1614-1615, 1993.

[31] B Malo, K O Hill, F Bilodeau, D C Johnson, J Albert, 'Point-by point fabrication of micro-Bragg gratings in photosensitive fibre using single excimer pulse refractive index modification techniques', *Electron Lett*, **29**, 1668-1669, 1993.

[32] S J Mihailov, M C Gower, 'Recording of efficient high-order Bragg reflectors in optical fibres by mask image projection and single pulse exposure with an excimer laser', *Electron Lett*, **30**, 707-709, 1994.

[33] A C Livarnos, A Katzir, A Yariv, 'Fabrication of grating structures with variable period', *Opt Commun*, **20**, 179-182, 1977.

[34] H Kogelnik, 'Filter response of non-uniform almost-periodic structures', *Bell Syst Techn J*, **55**, 109-127, 1976.

[35] M C Farries, K Sugden, D C J Reid, I Bennion, A Molony, M J Goodwin 'Very broad reflection bandwidth (44nm) chirped fibre gratings and narrow bandpass filters produced by the use of an amplitude mask', *Electron Lett*, **30**, 891-892, 1994.

[36] K Sugden, I Bennion, A Molony, N Copner, 'Chirped gratings produced in photosensitive optical fibres by fibre deformation during exposure', *Electron Lett*, **30**, 440-441, 1994.

[37] P C Hill, B J Eggleton, 'Strain gradient chirp of fibre Bragg gratings', *Electron Lett*, **30**, 1172-1174, 1994.

[38] K C Byron, K Sugden, T Bricheno, I Bennion, 'Fabrication of chirped gratings written holographically in optical fibre tapers', *Electron Lett*, **29**, 1659-1660, 1993.

[39] K O Hill, F Bilodeau, B Malo, T Kitagawa, S Theriault, D C Johnson, J Albert, 'Aperiodic in-fibre Bragg gratings for optical fibre dispersion compensation', *Conf on Optical Fibre Communication (OFC'94)*, San Diego, California, *Tech Dig*, PD2-1, 335, 1994.

[40] R Kashyap, S V Chernikov, P F Mckee, J R Taylor, '30ps chromatic dispersion compensation of 400fs pulses at 100Gbit/s in optical fibre using an all fibre photoinduced chirped reflection grating', *Electron Lett*, **30**, 1078-1080, 1994.

[41] K Sugden, I Bennion, A Molony, M C Farries, D C J Reid, M J Goodwin. 'Fabrication and properties of chirped fibre gratings with reflection bandwidths exceeding 50nm and narrow bandpass fibre grating filters', *Technical Digest CLEO Europe '94*, CWF57, 230-231, 1994.

[42] D Garthe, R E Epworth, W S Lee, A Hadjifotiou, C P Chew, T Bricheno, A Fielding, H N Rourke, S R Baker, K C Byron, R S Baulcomb, S M Ohja, S Clements, 'Adjustable dispersion equaliser for 10 and 20Gbit/s over distances up to 160km', *Electron Lett*, **30**, 2159-2160, 1994.

[43] M Le Blanc, S Y Huang, M M Ohn, R M Measures, 'Tuneable chirping of a fibre Bragg grating using a tapered cantilever bed', *Electron Lett*, **30**, 2163-2165, 1994.

[44] K O Hill, F Bilodeau, B Malo, T Kitagawa, S Theriault, D C Johnson, J Albert, K Takiguchi, 'Chirped in-fibre Bragg gratings for compensation of optical-fibre dispersion', *Opt Lett*, **19**, 1314-1316, 1994.

[45] A Yariv, 'Coupled-mode theory for guided-wave optics', *IEEE J Quantum Electron*, QE-9, 919-933, 1973.

[46] D K W Lamb, B K Garside, 'Characterisation of single-mode optical fibre filters', *Appl Opt*, **20**, 440-445, 1981.

[47] K O Hill, 'Aperiodic distributed-parameter waveguides for integrated optics', *Appl Opt*, **13**, 1853-1856,1974.

[48] M Matsuhara, K O Hill, 'Optical-waveguide band rejection filters: design', *Appl Opt*, **13**, 2886-2888, 1974.

[49] M Matsuhara, K O Hill, A Wantanabe, 'Optical-waveguide filters: synthesis', *J Opt Soc Amer*, **65**, 804-809, 1975.

[50] B-G Kim, E Garmire, 'Comparison between the matric method and the coupled-wave method in the analysis of Bragg reflector structures', *J Opt Soc Amer A*, **9**, 132-136, 1992.

[51] J Hong, W Huang, T Makino, 'On the transfer matrix method for distributed-feedback waveguide devices', *J Lightwave Technol*, **10**, 1860-1868, 1992.

[52] D K Lamb, K O Hill, 'Dispersion cancellation using optical-fibre filters', *Opt Lett*, **7**, 291-293, 1982.

[53] F Ouellette, 'Dispersion cancellation using linearly chirped Bragg grating filters in optical waveguides', *Opt Lett*, **12**, 847-849, 1987.

[54] D L Hetherington, R K Kostuk, M C Gupta, 'Dispersion compensation for an integrated optic grating utilising a transmission volume hologram', *Appl Opt*, **32**, 303-307, 1993.

[55] J M Yeun, 'Ultraviolet absorption studies of germania silicate glasses', *Appl Opt*, **21**, 136, 1982.

[56] R M Atkins, V Mizrahi, T Erdogan, '248nm induced vacuum UV spectral changes in optical fibre preform cores: Support for a colour centre model of photosensitivity', *Electron Lett*, **29**, 385-386, 1993.

[57] R M Atkins, V Mizrahi, 'Observation of changes in UV absorption bands of single mode germanosilicate core optical fibres on writing and thermally erasing refractive index gratings', *Electron Lett*, **28**, 1743-1744, 1992.

[58] D P Hand, P St J Russell, 'Photoinduced refractive-index changes in germanosilicated fibres', *Opt Lett*, **15**, 102-104, 1990.

[59] D L Williams, S T Davey, R Kashyap, J R Armitage, B J Ainslie, 'Direct observation of UV induced bleaching of 240nm absorption band in photosensitive germanosilicate glass fibres', *Electron Lett*, **28**, 369-370, 1990.

[60] K D Simmons, S LaRochelle, V Mizrahi, G I Stegeman, D L Grinscom, 'Correlation of defect centres with a wavelength-dependent photosensitive response in germania-doped silica optical fibres', *Opt Lett*, **16**, 141-143, 1991.

[61] T E Tsai, C G Askins, E J Friebele, 'Photoinduced grating and intensity dependence of defect generation in Ge-doped silica optical fibre', *Appl Phys Lett*, **61**, 390-392, 1992.

[62] T E Tsai, E J Friebele, D L Griscom, 'Thermal stability of photoinduced gratings and paramagnetic centres in Ge- and Ge/P-doped silica optical fibres', *Opt Lett*, **18**, 935-937, 1993.

[63] W X Xie, P Niay, P Bernage, M Douay, J F Byron, T Georges, M Monerie, B Poumellec, 'Experimental evidence of two types of photorefractive effects occurring during photoinscriptions of Bragg gratings within germanosilicate fibres', *Opt Commun*, **104**, 185-195, 1993.

[64] P Cordier, J C Doukhan, E Fertein, P Bernage, P Niay, J F Bayon, T Georges, 'TEM characterisation of structural changes in glass associated to Bragg grating inscription in a germanosilicate optical fibre preform', *Opt Commun*, **111**, 269-275, 1994.

[65] P Niay, P Bernage, S Legoubin, M Douay, W X Xie, J F Byron, T Georges, M Monerie, B Poumellec, 'Behaviour of spectral transmissions of Bragg gratings written in germania-doped fibre: writing and erasing experiments using pulsed or cw uv exposure', *Opt Commun*, **113**, 176-192, 1994.

[66] J P Bernardin, N M Lawandy, 'Dynamics of the formation of Bragg gratings in germanosilicate optical fibres', *Opt Commun*, **79**, 194-195, 1990.

[67] K S Chiang, M G Sceats, D Wong, 'Ultraviolet photolytic-induced changes in optical fibres: the thermal expansion coefficient', *Opt Lett*, **18**, 965-967, 1993.

[68] G D Maxwell, B J Ainslie, D L Williams, R Kashyap, 'UV written 13dB reflection filters in hydrogenated low loss planar silica waveguides', *Electron Lett*, **29**, 425-426, 1993.

[69] P J Lemaire, 'Enhanced UV photosensitivity in fibres and waveguides by high-pressure hydrogen loading', *Conf on Optical Fibre Communication (OFC'95)*, San Diego, California, Tech Dig, WN5, 162-163, 1995.

[70] F Bilodeau, D C Johnson, B Malo, K A Vineberg, K O Hill, 'Ultraviolet light photosensivity in Er^{3+}-Ge doped optical fibre,' *Opt Lett*, **15**, 1138-1140, 1990.

[71] M M Broer, R L Cone, J R Simpson, 'Ultraviolet-induced distributed feedback gratings in Ce^{3+} doped silica optical fibres,' *Opt Lett*, **16**, 1381-1382, 1991.

[72] K O Hill, B Malo, F Bilodeau, D C Johnson, T F Morse, A Kilian, L Reinhart, O Kyunghwan, 'Photosensitivity in Eu^{2+}:Al_2O_3-doped-core fibre: Preliminary results and application to mode convertors,' *Conf on Optical Fibre Communications (OFC'91)*, San Diego, California, Tech Dig, 14-17, PD3-1, 1991.

[73] T A Strasser, A E White, M F Yan, P J Lemaire, T Erdogan, 'Strong Bragg phase gratings in phosphorus-doped fibre induced by ArF excimer radiation', *Conf on Optical Fibre Communication (OFC'95)*, San Diego, California, Tech Dig, 159-160, 1995.

[74] J R Armitage, 'Fibre Bragg reflectors written at 262nm using a frequency quadrupled diode-pumped Nd^{3+}:YLF laser', *Electron Lett*, **29**, 1181-1183, 1993.

[75] E Fertein, S Legoubin, M Douay, S Canon, P Bernage, P Niay, F Bayon, T Georges, 'Shifts in the resonance wavelengths of Bragg gratings during writing or bleaching experiments by UV illumination within the gemanosilicate optical fibres', *Electron Lett*, **27**, 1838-1839, 1991.

[76] D L Williams, B J Ainslie, R Kashyap, G Sherlock, R P Smith, J V Collins, 'Temperature stable 1.3mm laser with Bragg fibre grating external cavity for access networks', *European Conf on Optical Communications (ECOC'93)*, **2**, 202, 1993.

[77] D L Williams, B J Ainslie, R Kashyap, G D Maxwell, J R Armitage, R J Campbell, R Wyatt, 'Photosensitive index changes in germania doped silica glass fibres and waveguides', *Photosensitivity and Self-Organisation in Optical Fibres and Waveguides*: Ed F Ouellette, SPIE, **2044**, 55-68, 1993.

[78] T Erdogan, V Mizrahi, 'Decay of UV induced fibre Bragg gratings', *Conf on Optical Fibre ommunication (OFC'94), San Diego, California, Tech Dig*, **50**, 1994.

[79] T Erdogan, V Mizrahi, P J Lemaire, D Monroe, 'Decay of ultraviolet-induced Bragg gratings', *J Appl Phys*, **76**, 73-80, 1994.

[80] M Douay, E Fertain, W X Xie, P Bernage, P Niay, J F Bayon, T Georges, 'Thermal hysteresis of Bragg wavelengths of intra-core fibre gratings', *IEEE Photon Technol Lett*, **5**, 1331-1334, 1993.

[81] J-L Archambault, L Reekie, P St Russell, '100% reflectivity Bragg reflectors produced in optical fibres by single excimer laser pulses', *Electron Lett*, **29**, 453-455, 1993.

[82] V Mizrahi, J E Sipe, 'Optical properties of photosensitive fibre phase gratings', *J Lightwave Technol*, **11**, 1513-1517, 1993.

[83] I Camilibel, D A Pinnow, F W Dabby, 'Optical ageing characteristics of borosilicate clad fused silica core fibre optical waveguides', *Appl Phys Lett*, **26**, 185-187, 1975.

[84] P J Lemaire, 'Material aspects of photosensitivity in hydrogen loaded glasses', *Mini-symposium on Novel Optical Effect in Glasses*, The Rank Prize Funds, Cumbria, UK, 1995.

[85] V Mizrahi, S LaRochelle, G I Stegeman, 'Physics of photosensitive-grating formation in optical fibres', *Phys Rev A*, **43**, 433-438, 1991.

[86] L Dong, J L Archambault, L Reekie, P St J Russell, 'A study of UV photosensitivity in germanosilicate preforms and fibres', *IEE Colloquium on optical fibre gratings and their applications*, London, UK, 1995.

[87] B Malo, J Albert, KO Hill, F Bilodeau, DC Johnson, 'Effective index drift from molecular hydrogen diffusion in hydrogen-loaded optical fibre gratings and its effect on Bragg grating fabrication', *Electron Lett*, **30**, 442-444, 1994.

[88] K Sugden, L Zhang, J Williams, I Bennion, 'Dissimilar wavefront technique for linear and quadratic chirps', Conf on Photosensitivity and Quadratic Nonlinearity in Glass Waveguides (*PQNGW'95)*, OSA, Portland, Oregon, Tech Dig, **22**, 136-139, 1995.

[89] J A R Williams, N J Doran, I Bennion, 'Cubic and quadratic dispersion compensation using in-fibre Bragg gratings', *Topical Meeting in Integrated Photonics Research*, OSA, DanaPont, California, Techn Digest, IFD4, February 1995.

[90] U Erikson, P Blixt, J A Tellefsen Jr, 'Design of fibre gratings for total dispersion compensation', *Opt Lett*, **19**, 1028-1030, 1994.

[91] J A R Williams, I Bennion, N J Doran, 'The design of in-fibre Bragg grating systems for cubic and quadratic dispersion compensation', Opt Commun, 116, 62-66, 1995

[92] L F Mollenauer, E Lichtman, M J Neubelt, G T Harvey, 'Demonstration, using sliding-frequency guiding filters, of error-free soliton transmission over more than 20mm at 10GBit/s, single channel, and over more than 13mm at 20GBit/s in a two-channel WDM,' *Electron Lett*, **29**, 910-911, 1993.

[93] G T Harvey, L F Mollenauer, 'Harmonically mode-locked fibre ring laser with an internal Fabry-Perot stabiliser for soliton transmission,' *Opt Lett*, **18**, 107-109, 1993.

[94] M Romagnoli, S Wabnitz, P Franco, M Midrio, F Fontana, G Town, 'Tuneable erbium-ytterbium fibre sliding frequency soliton laser,' *J Opt Soc Amer B*, 12, 72-86, 1995.

[95] W W Morey, T J Bailey, W H Glenn, G Meltz, "Fibre Fabry-Perot interferometer using side exposed fibre Bragg gratings", *Conf on Optical Fibre Communication (OFC'92)*, San Jose, California, Tech Dig, 96, 1992.

[96] L Zhang, K Sugden, I Bennion, A Molony, 'Wide stopband chirped fibre Moiré grating transmission filters', *Electron Lett*, **31**, 477-478, 1995

[97] L Zhang, K Sugden, I Bennion, 'Chirped fibre-Moiré-grating transmission filters', Conf on (CLEO'95), Tech Dig, CMG2, 1995.

[98] V Mizrahi, T Erdogan, D J Digiovanni, P J Lemaire, S G Kosinski, T A Strasser, A E White, 'Fibre-grating transmission filters for use in an all-fibre demultiplexer', *Conf on Optical Fibre Communications (OFC'94)*, San Jose, California, Techn Dig, 52-53, 1994.

[99] L Zhang, K Sugden, J A R Williams, I Bennion, 'In-fibre transmission filters with broad stopbands using chirped Bragg gratings', *Conf on Photosensitivity and Quadratic Nonlinearity in Glass Waveguides, (PQNGW'95)*, Techn Dig, **22**, 132-135, 1995.

[100] D C J Reid, C M Ragdale, I Bennion, D J Robbins, J Buus, W J Stewart, "Phase-shifted Moiré grating fibre resonators', *Electron Lett*, **26**, 10-12, 1990.

[101] S Legoubin, E Fertein, M Douay, P Bernage, P Niay, F Bayon, T Georges, "Formation of Moiré grating in core of germanosilicate fibre by transverse holographic double exposure method", *Electron Lett*, **27**, 1945-1946, 1991.

[102] J A R Williams, I Bennion, K Sugden, N J Doran, 'Fibre dispersion compensation using a chirped in-fibre Bragg grating', *Electron Lett*, **30**, 12, 985-986, 1994.

[103] A Galvanauskas, M E Fermann, D Harter, K Sugden, I Bennion, 'All-fibre femtosecond pulse amplification circuit using chirped Bragg gratings', *Appl Phys Lett*, **66**, 9, 1053-1055, 1995.

[104] A Galvanauskas, M E Fermann, D Harter, 'High-power amplification of femtosecond optical pulses in a diode-pumped fibre system', *Opt Lett*, **19**, 16, 1201-1203, 1994.

[105] D Strickland, G Mourou, 'Compression of amplified chirped optical pulses', *Opt Commun*, **55**, 447-449, 1985.

[106] M E Fermann, A Galvanauskas, D Harter, 'All-fibre source of 100-nJ subpicosecond pulses', *Appl Phys Lett*, **64**, 11, 1315-1317, 1994.

[107] A Galvanauskas, M E Fermann, P Blixt, J A Tellefsen, D Harter, 'Hybrid diode-laser fibre-amplifier source of high energy ultrashort pulses', *Opt Lett*, **19**, 1043, 1994.

[108] M E Fermann, K Sugden, I Bennion, 'Generation of 10nJ picosecond pulses from a modelocked fibre laser', *Electron Lett*, **31**,194-195, 1995.

[109] M Hofer, M E Fermann, F Haberl, M H Ober, A J Schmidt, 'Modelocking with cross-phase and self-phase modulation', *Opt Lett*, **16**, 502-504, 1991.

[110] M Hofer, M H Ober, R Hofer, M E Fermann, G Sucha, D Harter, K Sugden, I Bennion, C A C Mendonca, T H Chiu, 'High-power neodymium soliton fibre laser that uses a chirped fibre grating', *Opt Lett*, **20**, 16, 1701-1703, 1995.

[111] W H Know, N M Pearson, K D Li, C A Hirlimann, *Opt Lett*, **13**, 574, 1988.

[112] I H White, 'A multichannel grating cavity laser for wavelength division multiplexing applications,' *IEEE J Lightwave Technol*, **9**, 7, 93, 1991.

[113] M C Farries, A C Carter, G G Jones, I Bennion, 'Tuneable multiwavelength laser with single fibre output,' *Electron Lett*, **27**, 1498-1499, 1991.

[114] M Zirngibl, C H Joyner, '12 frequency WDM laser based on a transmissive waveguide grating router,' *Electron Lett*, **30**, 9, 701-702, 1994.

[115] A J Poustie, N Finlayson, 'Multi-wavelength fibre laser using a spatial mode beating filter', *Opt Lett*, **19**, 10, 716-718, 1994.

[116] E L Goldstein, L Eskilden, V da Silva, M Andrejco, Y Silberberg, 'Suppression of dynamic cross-saturation in multiwavelength lightwave networks with inhomogeneously broadened amplifiers,' *IEEE Photon Technol Lett*, **5**, 8, 937-938, 1993.

[117] A -M Brianon, B Jacquier, J -C Gacon, C Le Sergent, J -F Marcerou, 'Inhomogeneous line broadening of optical transitions in Nd^{3+} and Er^{3+} doped preforms and fibres,' *Proc SPIE, Fibre Laser Sources and Amp*, **1373**, 1990.

[118] C Hentschel, 'Fibre Optics Handbook', Hewlett-Packard GmbH, 1988.

[119] W W Morey. 'Tuneable narrow-line bandpass filter using fibre gratings', *Opt Fibre Conf*, OFC'91, San Diego, California, post deadline paper PD20-1, February, 1991.

[120] F Bilodeau, K O Hill, B Malo, D C Johnson, J Albert, 'High-return loss narrowband all-fibre bandpass Bragg transmission filter', *IEEE Photon Technol Lett*, **6**, 1, 80-82, 1994.

[121] R Kashyap, G D Maxwell, B J Ainslie, 'Laser trimmed four-port bandpass filter fabricated in single mode photosensitive fibre', *IEEE Photon Technol Lett*, **5**, 191-194, 1993.

[122] F Bilodeau, B Malo, D C Johnson, J Albert, S Thériault, K O Hill, 'High-performance wavelength-division multiplexing/demultiplexing device using an all-fibre Mach-Zehnder interferometer and photoinduced Bragg gratings', *OFC'95, Technical Digest*, paper WI1. 130-131, 1995.

[123] T C Cullen, H N Rourke, C P Chew, S R Baker, T Bricheno, K C Byron, A Fielding, 'Compact all-fibre wavelength drop and insert filter', *Electron Lett*, **30**, 25, 2160-2161, 1994.

[124] R Kashyap, J R Armitage, R Wyatt, S T Davey, D L Williams, 'All-fibre narrowband reflection gratings at 1550nm', *Electron Lett*, 26, 11, 730, 1990.

[125] E Delevaque, T Georges, J F Bayon, M Monerie, P Niay, P Berage, 'Gain control in erbium-doped amplifiers by lasing at 1480nm with photoinduced Bragg gratings written on the fibre ends', *Electron Lett*, **12**, 1112-1113, 1993.

[126] M Zirngibl, 'Gain control in erbium-doped fibre amplifiers by an all-optical feedback loop', *Electron Lett*, **7**, 560-561, 1991.

[127] J F Massicott, S D Willson, R Wyatt, J R Armitage, R Kashyap, D Williams, R A Lobett, '1480nm pumped erbium doped fibre amplifier with all optical automatic gain control', *Electron Lett*, **30**, 12, 962-965, 1994.